COMPUTATIONAL MODELLING OF PATTERN FORMATION BY MYXOBACTERIA

COMPUTATIONAL MODELLING OF PATTERN FORMATION BY MYXOBACTERIA

Proefschrift

ter verkrijging van de graad van doctor
aan de Technische Universiteit Delft,
op gezag van de Rector Magnificus prof. ir. K. C. A. M. Luyben,
voorzitter van het College voor Promoties,
in het openbaar te verdedigen op woensdag 15 januari 2014 om 12:30 uur

door

Albertas JANULEVICIUS

master in biophysics, Vilnius University
geboren te Vilnius, Litouwen.

Dit proefschrift is goedgekeurd door de promotor:

Prof. dr. ir. M.C.M. van Loosdrecht

Copromotor: Dr. ir. C. Picioreanu

Samenstelling promotiecommissie:

Rector Magnificus,	voorzitter
Prof. dr. ir. M.C.M. van Loosdrecht,	Technische Universiteit Delft, promotor
Dr. ir. C. Picioreanu,	Technische Universiteit Delft, copromotor
Prof. dr. G.P. van Wezel,	Universiteit Leiden
Prof. dr. ir. J.J. Heijnen,	Technische Universiteit Delft
Prof. dr. C. Dekker,	Technische Universiteit Delft
Dr. J.A. Kaandorp,	Universiteit van Amsterdam
Dr. D. Whitworth,	Aberystwyth University
Prof. dr. ir. L. van der Wielen,	Technische Universiteit Delft, reservelid

This study was funded by the Netherlands Organization for Scientific Research (NWO VIDI grant No. 864-06-003).

ISBN 978-94-6259-034-2

An electronic version of this dissertation is available at
http://repository.tudelft.nl/.

Contents

NOTATION LIST

Symbol	Definition
B	Cell bending stiffness
C	Alignment of a population
C_{t2}	Orientational stability of cells in a two-cell collision
C_j^{a}	Orientation autocorrelation function of bacterium j
d_{e}	Largest distance of direct contact between particles in a 3D model
d_{g}	Maximum adhesion distance
$\boldsymbol{F}_i^{\mathrm{s}}$	Pseudo surface tension force on particle i
$\boldsymbol{F}_i^{\mathrm{r}}$	Substratum reaction force on particle i
$\boldsymbol{F}_{\mathrm{H}}^{\mathrm{g,n}}$	Guiding force on head particle in the direction normal to bacterial body
$\boldsymbol{F}_{\mathrm{H}}^{\mathrm{g,n}}$	Guiding force on head particle in the direction tangent to bacterial body
$\boldsymbol{F}_{\mathrm{T}}^{\mathrm{g,n}}$	Guiding force on tail particle in the direction normal to bacterial body
$\boldsymbol{F}_{\mathrm{T}}^{\mathrm{g,t}}$	Guiding force on tail particle in the direction tangent to bacterial body
$\boldsymbol{F}_{\mathrm{H}}$	Guiding force on head particle
$\boldsymbol{F}_{\mathrm{T}}$	Guiding force on tail particle
$F_{\mathrm{max}}^{\mathrm{g}}$	Maximum guiding force
$\boldsymbol{F}_i^{\mathrm{l},j}$	Force acting on a particle i by linear spring j
$\boldsymbol{F}_i^{\mathrm{a},j}$	Force acting on a particle i by angular spring j
$\boldsymbol{F}_i^{\mathrm{e}}$	Engine force on particle i
F^{e}	Engine force magnitude per cell
$\boldsymbol{F}_i$	Total force acting on particle i
$\boldsymbol{F}_{ij}^{\mathrm{c}}$	Collision force on particle i of bacterium j
$\boldsymbol{F}_i^{\mathrm{d,t}}$	Drag force on particle i in the direction tangent to bacterial body
$\boldsymbol{F}_i^{\mathrm{d,n}}$	Drag force on particle i in the direction normal to bacterial body
F_{c}	Critical lateral restriction force
k^{s}	Pseudo surface tension force scaling factor
k^{r}	Substratum reaction spring stiffness
k^{a}	Anglular spring stiffness
k^{l}	Linear spring stiffness
k^{e}	Engine direction property (1 or –1)
k^{g}	Guiding force constant
k^{c}	Collision stiffness

l_0	Equilibrium length of linear spring
$\boldsymbol{l}_i$	Linear spring vector
L	Bacterium length
N	Number of particles in a bacterium
$\hat{\boldsymbol{n}}_i$	Normal to bacterial body at position $\boldsymbol{r}_i$
$\hat{\boldsymbol{n}}_{1i}$, $\hat{\boldsymbol{n}}_{2i}$	Normal and binormal to bacterial body at position $\boldsymbol{r}_i$ in 3D model
$\boldsymbol{o}_j$	Orientation of bacterium j
$\boldsymbol{Q}_{ij}$	i-th line segment of bacterium j
$\boldsymbol{r}_i$	Position of particle i
$\boldsymbol{\tau}_i^{\mathrm{a},j}$	Torque produced by angular spring j on particle i
$\hat{\boldsymbol{t}}_i$	Tangent to bacterial body at position $\boldsymbol{r}_i$
T_{R}	Cell reversal period
v_{b}	Speed of bacterial gliding
$\boldsymbol{v}_i$	Velocity of particle i
$\boldsymbol{v}_i^{\mathrm{f}}$	Terminal (final) velocity of particle i
W	Bacterium width
$\hat{\boldsymbol{z}}$	Unit vector in vertical (+z) direction
α_{c}	Critical angle for lateral restriction
α_i	Angle between linear springs i and $i+1$
ζ^{t}	Drag coefficient in the direction tangent to bacterial body
ζ^{n}	Drag coefficient in the direction normal to bacterial body
θ	Angle between orientations of two cells
ω	Angular speed of a circular aggregate

1

INTRODUCTION

1.1. MYXOBACTERIA

1.1.1. WHAT ARE THE MYXOBACTERIA?

The myxobacteria are gram-negative, rod shaped bacteria, belonging to the Delta branch of Proteobacteria, order Myxococcales. Myxobacteria are remarkable for their complex life cycle: in vegetative state, when nutrients are available, myxobacteria cooperatively swarm on a solid surface and feed. When exposed to starvation conditions, myxobacteria exhibit multicellular morphogenesis: 10^5–10^6 cells aggregate and form a fruiting body [1]. Witin a fruiting body, vegetative cells differentiate into desiccation-resistant spores, that are able to survive unfavorable environmental conditions. The name of myxobacteria originates from Greek word *myxa*, meaning slime, mucus, and shows their ability to secrete polysaccharide slime. Different aspects of myxobacteria motility and development are covered in a number of excellent reviews [2–6]. Due to their unique life cycle, myxobacteria often serve as relatively simple model organism to study multicellular development and morphogenesis (Figure 1.1).

Currently, there are about 50 known myxobacteria species, classified into 17 genera. Myxobacteria are mostly found in topsoil, decaying organic material, dung of animals, rotting wood, bark of dead and living trees [7]. Myxobacteria are mesophiles, usually have low salt tolerance and are very sensitive to desiccation in vegetative state [1]. Almost all known myxobacteria are strictly aerobic organotrophs that degrade insoluble macromolecules by secreting hydrolytic exoenzymes. Myxobacteria can be divided into two metabolic groups : i) cellulolytic (decomposing celulose), e.g. *Sorangium cellulosum* ii) proteolytic (hydrolyze proteins) - the majority of the species, e.g. *Myxococcus xanthus*, the most studied myxobacterium [3]. In nature this group feeds on other microorganisms by secreting hydrolytic exoenzymes that are very effective in killing and decomposing other bacteria and yeast. Due to these qualities, myxobacteria have been often called micropredators. However, they do not depend on living organisms and may

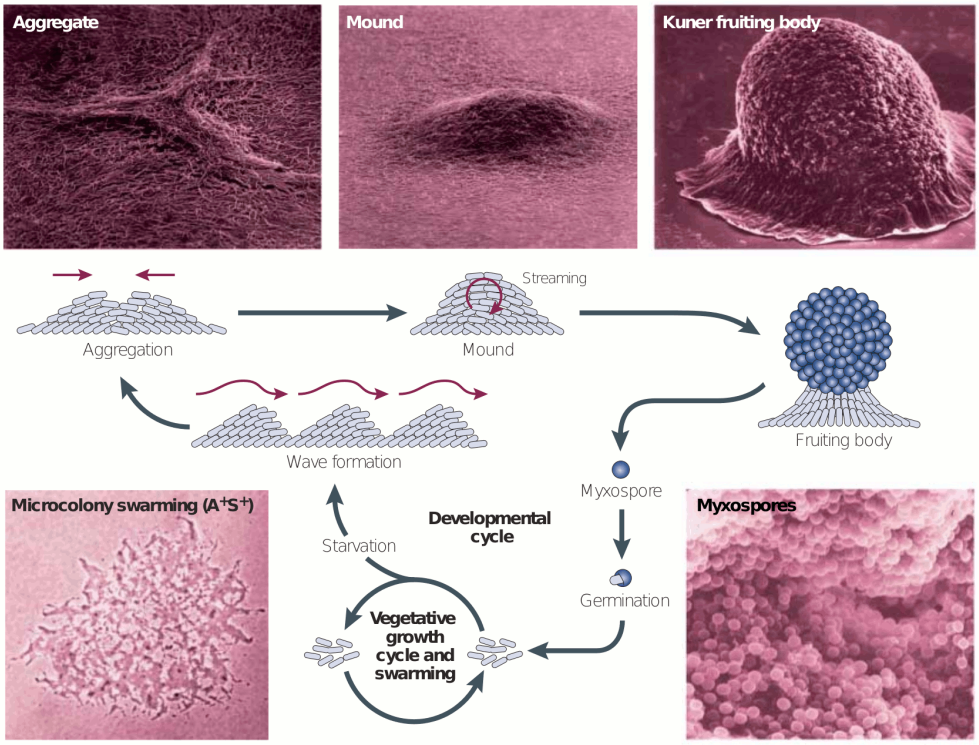

Figure 1.1: Life cycle of *Myxococcus xanthus*, the most studied myxobacterium. Reproduced with permission from Kaiser [5].

as well be considered scavengers. Myxobacteria feed in large groups, thin spreading and migrating colonies called swarms. A myxobacterium cell is thought to benefit from feeding with the community, because more efficient use of enzymes can be achieved by minimizing the loss by diffusion [1]. Due to this collective feeding, groups of myxobacteria have also been called “wolf packs” [8]. It has been experimentally shown that *M. xanthus* cell can show measurable growth on casein only above a certain cell density [9], while being able to grow on hydrolyzed casein at low cell densities. Fruiting body formation can be also explained by the need of myxbacteria cells to live within a community. Fruiting bodies may be a mechanism that evolved to ensure that when spores germinate upon favorable environmental conditions, cell density is large enough for cells to begin feeding efficiently. Besides being a model organism for multicellular organization and morphonegesis, myxobacteria also receive a lot of attention due to their ability to secrete a large number of secondary metabolites, for example growth inhibitors. Most of them are thought to inhibit eukaryotic competitors, like fungi and protozoa. Growth inhibitors produced by myxobacteria are thought to help defend their niche because the myxobacterial colonies are effectively stationary [1].

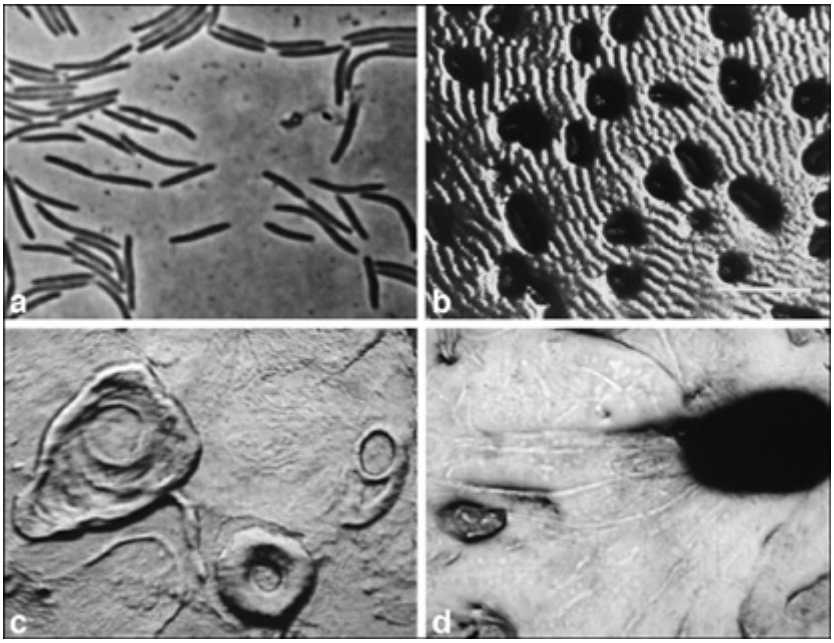

Figure 1.2: Patterns arising in developing myxobacteria population. (a) Individual rod shaped cells. (b) Travelling waves (ripples). (c). Circular and spiral aggregates. (d). Streams travelling into cell aggregates. Reproduced with permission from Dworkin [15].

1.1.2. MOTILITY OF MYXOBACTERIA

Vegetative myxobacteria are rod-shaped, typically 3–6 µm long and 0.7–1 µm wide (Figure 1.2A) [3]. Myxobacteria cells move on a substratum by gliding, which is defined as the movement of a bacterium on a solid surface in the direction of the long axis of the cell without the aid of flagella [10]. Gliding speed of myxobacteria is typically between 1–13 µm·min^{-1} [11–13]. It has been estimated that in a vegetative swarm, 90% of swarm expansion comes from cell movement and only 10% from cell growth [11]. There appears to be two morphological cell types of myxobacteria: slender flexible rods with tapering ends and cylindrical more rigid rods with rounded ends [3]. Myxobacteria cell flexibility is easily noticeable in experiments where the leading pole of the cell is fixed and unable to move [14]. In such conditions, *M. xanthus* cells exhibit snake-like, flailing motions. The importance of different cell morphologies, apparent flexibilities and their role in myxobacterial life cycle is not known. Myxobacteria glide on the surface approximately 1000 times slower than the speed of flagellated bacteria. It has been speculated that myxobacteria employ slow motility systems in order not to outrun their own endogenously secreted enzymes and antibiotics, and rely on insect, bird or bat vectors for efficient fruiting body and spore transport [4]. Furthermore, flagella require liquid medium and might not be useful in relatively dry soil environment.

Myxobacterial cells periodically reverse the direction of gliding, i.e. the leading pole

after the reversal becomes the trailing pole [16]. Cell reversal period in vegetative swarms is 7–10 min, but reversal period is considerably increased during the course of fruiting body development, so that cells at the final stages of fruiting body development move essentially unidirectionally [12, 17]. At low cell densities, single cells or cell groups are often seen to follow slime trails laid by other cells [18]. Slime might play a role in guiding cells [2], but the exact role of slime trails in organizing cell movement is not known. Further, *M. xanthus* swarms have been shown to move towards groups of other bacteria or inanimate objects, like glass beads [19]. The mechanism of this behaviour still remains a mystery. This phenomenon might be related to elasticotaxis, a tendency of cells to travel along the mechanical stress lines in the agar [20].

Genetic studies have shown that *Myxococcus xanthus* possesses two distinct motility systems (Figure 1.3) [21]. One type of motility, S motility (for "Social"), is responsible for cells moving in groups and works only when cells are within one cell length from each other [11]. S motility is powered by the extension, adhesion and retraction of type IV pili from the leading pole of the cell [22], similarly to twiching motility found in *Pseudomonas*. Type IV pili (also called fimbriae), are 5–8 nm wide and are roughly one cell length. An extended pilus attaches to cell surface extensions, fibrils, or on other cells and thus mediate group movement [23]. The other motility type, A motility ("Adventurous") allows the movement of single cells. A motility is not completely understood. Two dominant hypotheses for A motility suggest that it might be powered by extrusion of slime from the rear of the cell (the "slime gun" model, Wolgemuth *et al.* [24]) or alternatively, by focal adhesion complexes that are fixed to the substratum along the whole length of the cell [25], similar to focal adhesions of eukaryotic cells [26]. Recently, a helical rotor model of A motility has emerged, where motor proteins move on a cytoskeletal helix and create cell surface waves that push the cell forward [4]. Mutants with both motility systems defective (A-S-) are non-motile.

1.1.3. FRUITING BODIES

Myxobacterial fruiting bodies can measure 10–1000 µm and many can be seen with the naked eye [3]. The shape, size and color of fruiting bodies can vary depending on the species (Figure 1.4). Simplest fruiting bodies are just mounds of slime, while other species form one or many sporangioles, structures with a well-defined wall. The sporangioles can be located on a substratum or raised on slime stalks that can have elaborated tree-like structure. Spores inside fruiting bodies are desiccation resistant and can be kept for 25 years [1].

The mechanisms of fruiting body formation in myxobacteria are not well understood. The fascinating aspect of this process is that a large number of cells move collectively and organize themselves into well defined structures. The process of fruiting begins in the center of a swarm and then expands to the peripheral regions [3]. A homogeneous cell population begins to aggregate, forming spiral cell aggregates (Figure 1.2C), that can develop into a fruiting body or disperse [28]. During the aggregation process distinctive cell movement patterns appear in the population. Streams of cells move into aggregation centers (Figure 1.2D) [6] and travelling waves (ripples) form between the

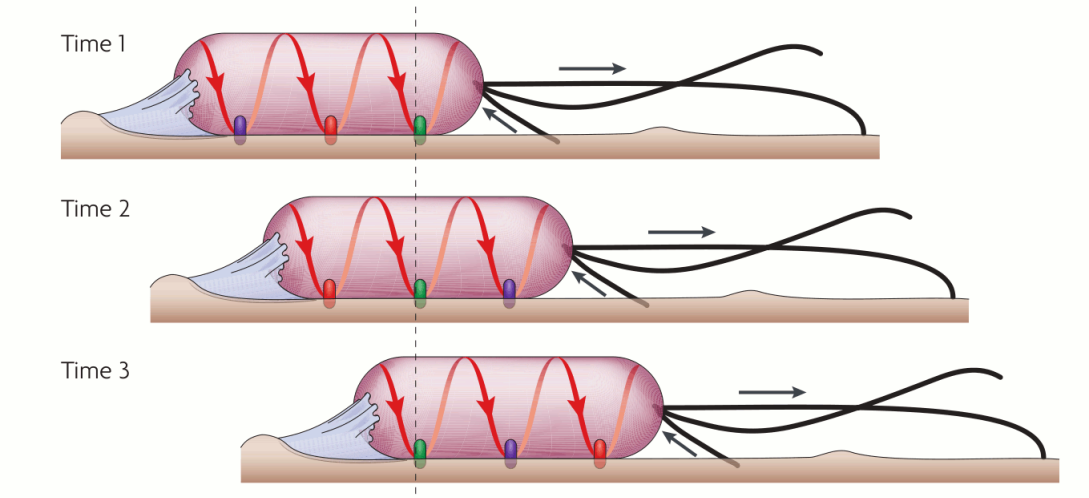

Figure 1.3: Motility systems of *M. xanthus*. Reproduced with permission from Zusman *et al.* [27].

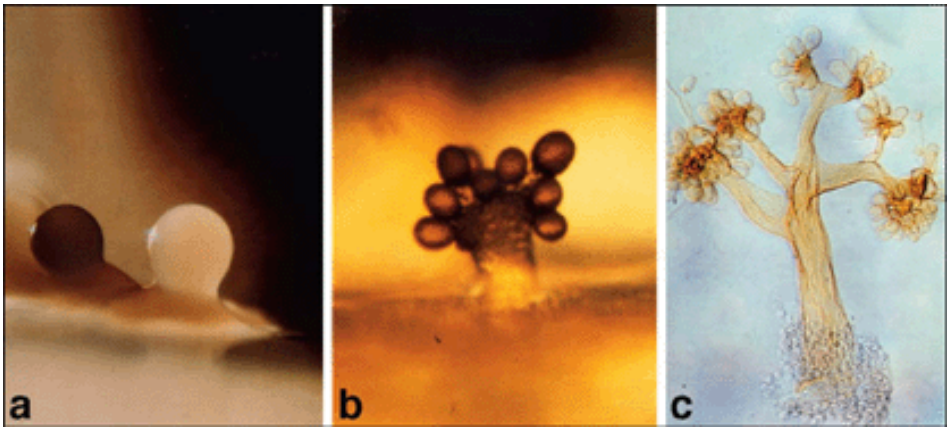

Figure 1.4: Fruiting bodies of myxobacteria. Each fruiting body measures several hundred micrometers. (a) *Myxococcus fulvus* (b) *Stigmatella aurantiaca* (c) *Chondromyces crocatus*. Reproduced with permission from Dworkin [15].

aggregates (Figure 1.2B) [29]. Interestingly, two species with similar tree-shaped fruiting bodies, *Chondromyces* and *Stigmatella aurantiaca*, exhibit a different developmental path. In *Chondromyces*, an undifferentiated cell mass secretes slime stalk, raising the cells upwards. The formation of sporangioles takes place afterwards. In *S. aurantiaca*, a mass of cells form a structure of the shape and size of the final fruiting body and later the cells withdraw from the stalk and sporangioles mature [3].

1.2. MODELING STUDIES

A number of modelling studies addressed different aspects of myxobacterial development, both at cell and at population scales.

1.2.1. MODELING APPROACHES AND GOALS

Population models attempt to simulate cell movement patterns arising in large myxobacteria populations. Simplest myxobacteria fruiting bodies (mounds of *M. xanthus*) contain 10^5 cells, and multiple fruiting bodies form in a starving swarm. Simulating movement of a large number of individual cells presents a formidable computational challenge. The models simulating large myxobacteria populations can be divided into **continuum (mean-field)** models and **individual-based** models. Continuum models do not take into account properties of each individual cell, but averages them at a particular point in space and time. This reduces the number of degrees of freedom in the model (i.e. the number of variables) and therefore reduces the precision with which the system is described. The advantage of this approach is that it allows for greater computational efficiency and thus for simulation of larger populations of cells. An example of the continuum model is the study showing that an intracellular clock with a refractory period could result in travelling wave (rippling) patterns in a population of aligned myxobacteria [30]. In this model, a cell is assumed to have an internal clock. Its speed of advance depends on the number of collisions between cells, which is proportional to cell population density. When the clock reaches a critical value, a cell reverses direction and the cell goes through a refractory period, during which a cell is insensitive to collisions with other cells, i.e. intracellular clock of a cell does not speed up if the cell collides with other cells. The model is formulated in terms of continuous cell density function that depends on spatial and time coordinates, and the position (phase) of the intracellular clock. The simulation process involves the numerical solution of a partial differential equation. Using a similar idea of a cell density function, Gallegos *et al.* [31] modelled how swarm spreading rate depends on effective diffusion of bacteria and nutrient concentration and found it to be in good agreement with experimental results.

Individual-based approaches consider the properties of each individual cell. This allows for a more accurate representation of the system under study, but is more computationally intensive, due to the need to simulate large number of cells. In general, such models can be divided into **lattice-based** [32–35] and **off-lattice** node-based Monte-Carlo models [13, 36, 37]. In lattice-based models, space is discrete, and each cell can occupy one or more lattice sites. Rules are introduced to describe how each cell changes

its position on the lattice. Some of these studies reproduce the rippling behavior of myxobacteria based on refractory period of a reversing cell [32, 38, 39]. Other studies are able to simulate the formation of streams and cell aggregates with the assumption that cells tend to turn towards other cells in the neighborhood [33–35]. In an off-lattice based model, space is continuous; cells are modeled as a set of connected nodes. During the Monte-Carlo simulation process, nodes change their position stochastically and the new system configuration is accepted or rejected based on how total system energy changes. **Cellular Potts** models are defined on a lattice but use energy-based approach [40, 41]. In these models, a cell can occupy multiple lattice sites and cellular flexibility and complex cell configurations can be accounted for. For example, Starruß *et al.* [40] showed that cell flexibility can affect cell clustering behaviour in a low-density population. Finally, there is a large group of models that study movement patterns of more general systems of self-propelled particles or rods and does not consider myxobacteria in particular [42, 43].

Other types of modelling studies consider the processes inside the myxobacterium cell. The study of Nan et al. models the mechanics of helical rotor distributed motility engine [44]. Igoshin et al. studied the molecular signaling network of Frz chemosensory system and demonstrated that it can potentially work as a biochemical oscillator ("Frizilator") to form an intracellular clock that is required for traveling wave formation in their former study [45].

1.2.2. DISCUSSION OF MODELING APPROACHES

Cellular Potts models simulate the mechanical effects of myxobacteria interactions well, but are computationally expensive. Node-based Monte Carlo models use 3–5 nodes per cell, which, given the observed myxobacteria cell flexibility and ability to bend it into complex configurations, might not be a realistic representation of a cell from a mechanical point of view. In addition, the important parameters used in the aforementioned simulations (such as cell bending stiffness) were either not studied or not correlated with experimentally measurable parameters. Lattice-based models simulate some aspects of interaction between moving myxobacteria cells, but do not account for cell flexibility, nor do they simulate collisions between cells (i.e. cells in these models can overlap) and thus are not mechanically accurate. Many published modelling studies, in addition to simulating cell movement and mechanical interactions, also include other assumptions about cell alignment, A and S motility engine performance and resulting cell orientation, slime trail following, collision resolution rules and others. These extra assumptions are sometimes intuitive, but often do not have a theoretical or experimental support and can be questionable. Furthermore, including these assumptions makes it difficult to differentiate what aspects of observed model behavior can be attributed purely to mechanical effects of cell-cell interactions and what aspects are the results obtained due to these extra assumptions.

1.3. THESIS SCOPE AND OUTLINE

The goal of the thesis was to formulate a more realistic and computationally efficient mechanical mass-spring model of a myxobacterium cell and study the importance of mechanical interactions between cells for the pattern formation in myxobacteria populations. In other words, the aim was to investigate what phenomena (patterns) in myxobacteria populations can be explained by using purely (bio)mechanical arguments.

The thesis is organized in five main studies. Models increasing in complexity are gradually introduced to evaluate the effects of important mechanical factors in formation of myxobacterial population patterns.

Chapter 2. Cell flexibility affects the alignment of model myxobacteria. The basic model was formulated and we investigated how cell bending stiffness affects cell alignment in the population in plane (two-dimensional space).

Chapter 3. Restriction of lateral movement facilitates the alignment of model myxobacteria population. Lateral restriction of cell movement due to contact with the substratum was introduced and it was investigated how this restriction affects cell alignment in the population.

Chapter 4. Effect of reversal time on cell movement patterns in model myxobacteria populations. It was studied how reversal or non-reversal of cells affects movement patterns in the populations.

Chapter 5. Short-range guiding can result in the formation of circular aggregates in myxobacteria populations. In this study, we introduces short-range guidance forces between the tail of one myxobacterium and the head of another, and investigated the resulting patterns.

Chapter 6. Three-dimensional simulations of myxobacteria movement. The model for cell movement was extended to three-dimensions. It was studied how three-dimensionality affects the results obtained in the previous chapters and how it could initiate the formation of fruiting bodies.

Supplementary movies of the thesis can be downloaded from
`http://www.biofilms.bt.tudelft.nl/`.

REFERENCES

[1] H. Reichenbach, *The ecology of the myxobacteria,* Environmental Microbiology **1**, 15–21 (1999).

[2] Y. Zhang, A. Ducret, J. Shaevitz, and T. Mignot, *From individual cell motility to collective behaviors: insights from a prokaryote, Myxococcus xanthus,* FEMS Microbiology Reviews **36**, 149 (2012).

[3] L. J. Shimkets, M. Dworkin, and H. Reichenbach, *The myxobacteria,* in *The Prokaryotes*, vol. 7, edited by M. Dworkin, S. Falkow, E. Rosenberg, K. H. Schleifer, and E. Stackebrandt (Springer, New York, 2006) pp. 31–115.

[4] B. Nan and D. R. Zusman, *Uncovering the mystery of gliding motility in the myxobacteria,* Annual Review of Genetics **45**, 21 (2011).

[5] D. Kaiser, *Coupling cell movement to multicellular development in myxobacteria,* Nature Reviews Microbiology **1**, 45 (2003).

[6] L. Jelsbak and L. Søgaard-Andersen, *Cell behavior and cell-cell communication during fruiting body morphogenesis in Myxococcus xanthus,* Journal of Microbiological Methods **55**, 829 (2003).

[7] W. Dawid, *Biology and global distribution of myxobacteria in soils,* FEMS Microbiology Reviews **24**, 403 (2000).

[8] M. Dworkin, *Cell-cell interactions in the myxobacteria,* Symp. Gen. Microbiol. **23**, 125–142 (1973).

[9] E. Rosenberg, K. H. Keller, and M. Dworkin, *Cell density-dependent growth of Myxococcus xanthus on casein,* Journal of Bacteriology **129**, 770 (1977).

[10] J. Henrichsen, *Bacterial surface translocation: a survey and a classification,* Bacteriological Reviews **36**, 478 (1972).

[11] D. Kaiser and C. Crosby, *Cell movement and its coordination in swarms of Myxococcus xanthus,* Cell Motility and the Cytoskeleton **3**, 227 (1983).

[12] L. Jelsbak and L. Søgaard-Andersen, *The cell surface-associated intercellular C-signal induces behavioral changes in individual Myxococcus xanthus cells during fruiting body morphogenesis,* Proceedings of the National Academy of Sciences of the United States of America **96**, 5031 (1999).

[13] Y. Wu, A. D. Kaiser, Y. Jiang, and M. S. Alber, *Periodic reversal of direction allows myxobacteria to swarm,* Proceedings of the National Academy of Sciences of the United States of America **106**, 1222 (2009).

[14] C. W. Wolgemuth, *Force and flexibility of flailing myxobacteria,* Biophysical Journal **89**, 945 (2005).

[15] M. Dworkin, *Lingering puzzles about myxobacteria,* Microbe **2**, 18–24 (2007).

[16] B. D. Blackhart and D. R. Zusman, *"Frizzy" genes of Myxococcus xanthus are involved in control of frequency of reversal of gliding motility,* Proceedings of the National Academy of Sciences of the United States of America **82**, 8767 (1985).

[17] L. Jelsbak and L. Søgaard-Andersen, *Pattern formation by a cell surface-associated morphogen in Myxococcus xanthus,* Proceedings of the National Academy of Sciences of the United States of America **99**, 2032 (2002).

[18] R. P. Burchard, *Trail following by gliding bacteria,* Journal of Bacteriology **152**, 495 (1982).

[19] M. Dworkin, *Tactic behavior of Myxococcus xanthus,* Journal of Bacteriology **154**, 452 (1983).

[20] R. Y. Stanier, *A note on elasticotaxis in myxobacteria,* Journal of Bacteriology **44**, 405 (1942).

[21] J. Hodgkin and D. Kaiser, *Genetics of gliding motility in Myxococcus xanthus (Myxobacterales): two gene systems control movement,* Molecular and General Genetics **171**, 177 (1979).

[22] H. Sun, D. R. Zusman, and W. Shi, *Type IV pilus of Myxococcus xanthus is a motility apparatus controlled by the frz chemosensory system,* Current Biology **10**, 1143 (2000).

[23] Y. Li, H. Sun, X. Ma, A. Lu, R. Lux, D. Zusman, and W. Shi, *Extracellular polysaccharides mediate pilus retraction during social motility of Myxococcus xanthus,* Proceedings of the National Academy of Sciences of the United States of America **100**, 5443 (2003).

[24] C. Wolgemuth, E. Hoiczyk, D. Kaiser, and G. Oster, *How myxobacteria glide,* Current Biology **12**, 369 (2002).

[25] T. Mignot, J. W. Shaevitz, P. L. Hartzell, and D. R. Zusman, *Evidence that focal adhesion complexes power bacterial gliding motility,* Science **315**, 853 (2007).

[26] M. A. Wozniak, K. Modzelewska, L. Kwong, and P. J. Keely, *Focal adhesion regulation of cell behavior,* Biochimica Et Biophysica Acta **1692**, 103 (2004).

[27] D. R. Zusman, A. E. Scott, Z. Yang, and J. R. Kirby, *Chemosensory pathways, motility and development in Myxococcus xanthus,* Nature Reviews Microbiology **5**, 862 (2007).

[28] K. A. O'Connor and D. R. Zusman, *Patterns of cellular interactions during fruiting-body formation in Myxococcus xanthus,* Journal of Bacteriology **171**, 6013 (1989).

[29] R. Welch and D. Kaiser, *Cell behavior in traveling wave patterns of myxobacteria,* Proceedings of the National Academy of Sciences of the United States of America **98**, 14907 (2001).

[30] O. A. Igoshin, A. Mogilner, R. D. Welch, D. Kaiser, and G. Oster, *Pattern formation and traveling waves in myxobacteria: theory and modeling,* Proceedings of the National Academy of Sciences of the United States of America **98**, 14913 (2001).

[31] A. Gallegos, B. Mazzag, and A. Mogilner, *Two continuum models for the spreading of myxobacteria swarms,* Bulletin of Mathematical Biology **68**, 837 (2006).

[32] M. S. Alber, M. A. Kiskowski, and Y. Jiang, *Two-stage aggregate formation via streams in myxobacteria,* Physical Review Letters **93**, 068102 (2004).

[33] M. A. Kiskowski, Y. Jiang, and M. S. Alber, *Role of streams in myxobacteria aggregate formation,* Physical Biology **1**, 173 (2004).

[34] O. Sozinova, Y. Jiang, D. Kaiser, and M. Alber, *A three-dimensional model of myxobacterial fruiting-body formation,* Proceedings of the National Academy of Sciences of the United States of America **103**, 17255 (2006).

[35] O. Sozinova, Y. Jiang, D. Kaiser, and M. Alber, *A three-dimensional model of myxobacterial aggregation by contact-mediated interactions,* Proceedings of the National Academy of Sciences of the United States of America **102**, 11308 (2005).

[36] Y. Wu, Y. Jiang, D. Kaiser, and M. Alber, *Social interactions in myxobacterial swarming,* PLoS Computational Biology **3**, e253 (2007).

[37] M. Hendrata, Z. Yang, R. Lux, and W. Shi, *Experimentally guided computational model discovers important elements for social behavior in myxobacteria,* PloS One **6**, e22169 (2011).

[38] U. Börner, A. Deutsch, and M. Bär, *A generalized discrete model linking rippling pattern formation and individual cell reversal statistics in colonies of myxobacteria,* Physical Biology **3**, 138 (2006).

[39] U. Börner, A. Deutsch, H. Reichenbach, and M. Bär, *Rippling patterns in aggregates of myxobacteria arise from cell-cell collisions,* Physical Review Letters **89**, 078101 (2002).

[40] J. Starruß, T. Bley, L. Søgaard-Andersen, and A. Deutsch, *A new mechanism for collective migration in Myxococcus xanthus,* Journal of Statistical Physics **128**, 269 (2007).

[41] A. B. Holmes, S. Kalvala, and D. E. Whitworth, *Spatial simulations of myxobacterial development,* PLoS Computational Biology **6**, e1000686 (2010).

[42] F. Peruani, A. Deutsch, and M. Bär, *Nonequilibrium clustering of self-propelled rods,* Physical Review E **74**, 030904 (2006).

[43] F. Ginelli, F. Peruani, M. Bär, and H. Chaté, *Large-scale collective properties of self-propelled rods,* Physical Review Letters **104**, 184502 (2010).

[44] B. Nan, J. Chen, J. C. Neu, R. M. Berry, G. Oster, and D. R. Zusman, *Myxobacteria gliding motility requires cytoskeleton rotation powered by proton motive force,* Proceedings of the National Academy of Sciences **108**, 2498 (2011).

[45] O. A. Igoshin, A. Goldbeter, D. Kaiser, and G. Oster, *A biochemical oscillator explains several aspects of Myxococcus xanthus behavior during development,* Proceedings of the National Academy of Sciences of the United States of America **101**, 15760 (2004).

2

CELL FLEXIBILITY AFFECTS THE ALIGNMENT OF MODEL MYXOBACTERIA[1]

2.1. INTRODUCTION

Myxobacteria are social bacteria that exhibit a complex life cycle. When nutrients are available, myxobacteria cooperatively swarm and feed. Upon starvation they aggregate to form multicellular spore-filled fruiting bodies, whose structure in different species can vary from simple mounds to elaborate tree-like structures [2, 3]. Although significant insight into the morphogenesis of myxobacterial fruiting bodies has been made over the recent decades, mechanisms of their formation are not completely understood.

Swarming of myxobacteria and the formation of fruiting bodies depend on the movement of individual cells. Myxobacteria cells are flexible rods [4, 5] that move on a substratum by gliding, which is defined as the movement of a bacterium on a solid surface in the direction of the long axis of the cell without the aid of flagella [6]. Two gliding motility systems have been identified in *Myxococcus xanthus*, the most studied myxobacterium [7]. One type of motility, S motility, is known to be powered by the extension, adhesion and retraction of type IV pili from the leading pole of the cell [8]. The other type, A motility, is less understood. Two dominant hypotheses for A motility suggest that it might be powered by extrusion of slime from the rear of the cell (the "slime gun" model, [9]) or alternatively, by focal adhesion complexes that are fixed to the substratum along the whole length of the cell [10], similar to focal adhesions of eukaryotic cells [11]. Myxobacterial cells periodically reverse the direction of gliding, i.e. the leading pole after the reversal becomes the trailing pole [12].

[1] Published in *Biophysical Journal* **99**, 3129 (2010) [1].

Throughout their life cycle, multiple myxobacteria cells often align to form rafts, sheets, spirals, streams and traveling waves (ripples) [13–18]. Swarms and fruiting bodies are also formed by domains of aligned cells [15, 19]. It has been shown that alignment of *M. xanthus* cells is necessary for development of fruiting bodies to proceed, since it allows for transfer of membrane-bound C-signal, an essential regulator of *M. xanthus* development [20]. Organized arrays of aligned cells can form from initially randomly oriented cells within several hours [13, 21]. It is known that A motility alone is sufficient for domains of aligned cells to form [21], but mechanisms of cell alignment are not known. It has been suggested that myxobacteria align due to mechanical interactions between moving rod-shaped cells [21–23], and that cell flexibility facilitates reorientation of cells upon mechanical contact [24, 25]. However, these suggestions have not been based on experimental or theoretical evidence.

Numerous modeling studies addressed the question of myxobacterial development [22, 26, 27], but only few of them studied the importance of mechanical factors. It has been shown that stiff rods can locally align because of geometrical constraints [28], and that a population of self-propelled stiff rods can form clusters due to mechanical interactions [29]. In another study [30], a Cellular Potts model was used to show that cell flexibility affects cell clustering in a population of 100 non-reversing cells, but no prediction of measurable bending stiffness values was made. In this paper, by means of a computational mass-spring model, we study how the movement of a single flexible rod-shaped cell and the alignment of a population of 500 mechanically interacting cells depend on cell flexibility and A motility engine type. The model is formulated in terms of experimentally measurable mechanical parameters, such as engine force, bending stiffness and drag coefficient. We consider two A motility hypotheses that correspond to the "slime gun" and the focal adhesions models. The results of the study reveal the importance of cell bending stiffness on the gliding pattern of a "slime gun" powered cell and on the ability of a larger population of cells to align.

2.2. MODEL DESCRIPTION

To study the pattern of cell gliding and the alignment of a population of cells, we created a mass-spring model [31] of a flexible rod-shaped bacterium that moves on a substratum and interacts mechanically with other bacteria. In the model description that follows we represent vectors by boldface letters and magnitudes of the vectors by the same lightface letters.

Particles. A bacterium of length L and width W is modeled as an ordered array of N particles that are connected by linear and angular springs (Figure 2.1A). Every particle $i = 1, \ldots, N$ has a position $\boldsymbol{r}_i$, velocity $\boldsymbol{v}_i$ and is acted upon by various forces $\boldsymbol{F}_i$. Forces that act on a particle arise from linear and angular springs within the same bacterium, an engine that propels the bacterium, drag with the substratum and collisions between different bacteria or parts of the same bacterium.

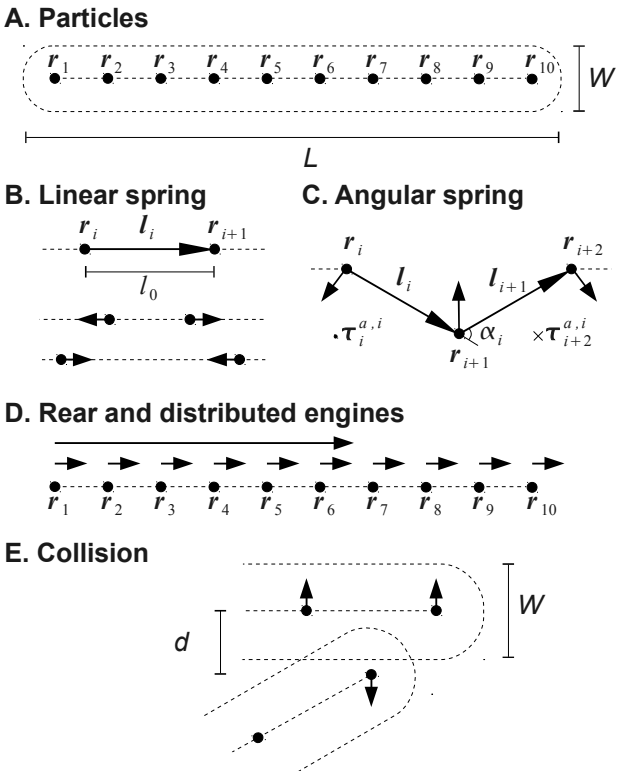

Figure 2.1: A mass-spring model of a flexible rod-shaped cell. Arrows without notation represent forces on particles. See text for explanation. (A) A bacterium of length L and width W comprised of $N = 10$ particles at positions $\boldsymbol{r}_1, \boldsymbol{r}_2, \ldots, \boldsymbol{r}_{10}$. (B) A linear spring i and the forces it produces on particles i and $i+1$. (C) An angular spring i and the forces it produces on particles i, $i+1$ and $i+2$. (D) Rear and distributed engine forces in a bacterium with $N = 10$ and $k^{\mathrm{e}} = -1$. (E) An example of forces of collision between two bacteria.

Linear springs. Linear springs keep adjacent particles of the same bacterium at a certain distance apart, resisting elongation or shortening of the bacterium (Figure 2.1B). A linear spring i connects every two adjacent particles i and $i+1$, and is defined by a vector $\boldsymbol{l}_i = \boldsymbol{r}_{i+1} - \boldsymbol{r}_i$, where $i = 1, \ldots, N-1$ and l_i is the length of the spring, an equilibrium length $l_0 = (L-W)/(N-1)$ and a stiffness k^{l}. The force exerted by the linear spring i on particle i is determined by Hooke's law, $\boldsymbol{F}_i^{\mathrm{l},i} = -k^{\mathrm{l}}(l_i - l_0)(\boldsymbol{l}_i / l_i)$. The same linear spring i exerts an opposite force $\boldsymbol{F}_{i+1}^{\mathrm{l},i} = -\boldsymbol{F}_i^{\mathrm{l},i}$ on the adjacent particle $i+1$. Moving and colliding myxobacteria cells do not shorten or elongate [32], therefore, the value of k^{l} was chosen to be large enough to model a cell that does not change its length markedly during simulations (Table 2.1).

Angular springs. Angular springs allow a bacterium to resist bending. An angular spring i connects every three adjacent particles i, $i+1$ and $i+2$, where $i = 1, \ldots, N-2$ (Figure 2.1C). The angular spring i has a stiffness k^{c} and exerts forces on all three parti-

cles so that the angle α_i between $\boldsymbol{l}_i$ and $\boldsymbol{l}_{i+1}$ decreases. When the three particles are aligned, i.e. when $\alpha_i = 0$, the angular spring does not exert any forces. The angular spring i produces two self-equilibrating torques with respect to $\boldsymbol{r}_{i+1}$: a torque $\boldsymbol{\tau}_i^{\mathrm{a},i}$ on particle i and a torque $\boldsymbol{\tau}_{i+2}^{\mathrm{a},i}$ on particle $i+2$. The magnitude of both torques is $\tau^{\mathrm{a},i} = k^{\mathrm{a}}\alpha_i$, the direction of $\boldsymbol{\tau}_i^{\mathrm{a},i}$ is $\hat{\boldsymbol{\tau}}_i^{\mathrm{a},i} = \boldsymbol{m}_i/m_i$, where $\boldsymbol{m}_i = \boldsymbol{l}_i \times \boldsymbol{l}_{i+1}$, and the direction of $\boldsymbol{\tau}_{i+2}^{\mathrm{a},i}$ is $\hat{\boldsymbol{\tau}}_{i+2}^{\mathrm{a},i} = -\hat{\boldsymbol{\tau}}_i^{\mathrm{a},i}$. The respective forces on the particles are $\boldsymbol{F}_i^{\mathrm{a},i} = (\tau^{\mathrm{a},i}/l_i^2)(\boldsymbol{l}_i \times \hat{\boldsymbol{\tau}}_i^{\mathrm{a},i})$, $\boldsymbol{F}_{i+2}^{\mathrm{a},i} = -(\tau^{\mathrm{a},i}/l_{i+1}^2)(\boldsymbol{l}_{i+1} \times \hat{\boldsymbol{\tau}}_{i+2}^{\mathrm{a},i})$ and $\boldsymbol{F}_{i+1}^{\mathrm{a},i} = -(\boldsymbol{F}_i^{\mathrm{a},i} + \boldsymbol{F}_{i+2}^{\mathrm{a},i})$. The system of three particles acted by an angular spring defined in this way satisfies the conservation of linear and angular momenta.

Engine forces. Since S motility is not necessary for the alignment of *M. xanthus* cells [21], we model only A motility. Two different A motility hypotheses are introduced in the model: (i) a distributed engine (analogous to the focal adhesions hypothesis), where a force is generated along the whole length of the cell, and (ii) a rear engine (analogous to the "slime-gun" hypothesis), where a force is generated at the trailing pole of the cell. Since a bacterium can reverse its direction of movement, an engine direction property k^{e} determines which pole of the bacterium is the leading or the trailing pole. k^{e} can take values -1 or 1; if $k^{\mathrm{e}} = 1$, the particle $i = 1$ is the leading pole and the particle $i = N$ is the trailing pole, while $k^{\mathrm{e}} = -1$ indicates the opposite case. The reversal of direction is modeled as a change in the value of k^{e}. Further, at every particle position $\boldsymbol{r}_i$ we define a unit vector $\hat{\boldsymbol{t}}_i$ tangent to the bacterial body. $\hat{\boldsymbol{t}}_i$ has the same direction as $-k^{\mathrm{e}}(\boldsymbol{l}_{i-1} + \boldsymbol{l}_i)$, if $i = 2, \ldots, N-1$, the direction of $-k^{\mathrm{e}}\boldsymbol{l}_i$ if $i = 1$ and the direction of $-k^{\mathrm{e}}\boldsymbol{l}_{i-1}$ if $i = N$. The distributed engine is then modelled by adding to every particle i of the bacterium a force $\boldsymbol{F}_i^{\mathrm{e}} = (F^{\mathrm{e}}/N)\hat{\boldsymbol{t}}_i$, where F^{e} is the magnitude of the engine force (Table 2.1), whereas a rear engine is modeled by adding a force $\boldsymbol{F}_i^{\mathrm{e}} = F^{\mathrm{e}}\hat{\boldsymbol{t}}_i$ to the trailing particle of the bacterium (Figure 2.1D). The magnitude of the A motility engine force is unknown; we use the value obtained by theoretical estimation of Wolgemuth *et al.* [9] (see Table 2.1). We also investigate how a change in the magnitude of the engine force affects the outcome of simulations.

Collision detection and response. A number of bacteria moving on a substratum or parts a bending bacterium can overlap, resulting in a collision. In such an event, we introduce forces that separate bacteria or their parts (Figure 2.1E). For collision detection and response, a bacterium $j = 1, \ldots, M$, where M is the number of bacteria in the population, is viewed as an array of line segments, whose ends are defined by particle positions. Each i-th line segment of a bacterium j is defined parametrically by $\boldsymbol{Q}_{ij}(P) = \boldsymbol{r}_{ij} + P(\boldsymbol{r}_{(i+1)j} - \boldsymbol{r}_{ij})$, where $0 \le P \le 1$ and $\boldsymbol{r}_{ij}$ indicates the position of a particle i in a bacterium j. If two line segments $\boldsymbol{Q}_{ij}$ and $\boldsymbol{Q}_{kl}$ are not adjacent segments on the same bacterium (i.e. if the segments do not share the same endpoint), a collision occurs if the distance between them becomes smaller than the bacterial width W. Thus, for each such pair of segments we find the points $\boldsymbol{Q}_{ij}(P_1)$ and $\boldsymbol{Q}_{kl}(P_2)$ on those segments that are separated by the smallest distance d, where $\boldsymbol{d} = \boldsymbol{Q}_{ij}(P_1) - \boldsymbol{Q}_{kl}(P_2)$ [33]. If $d < W$,

we introduce interaction forces to the particles at the ends of the segments to push the two segments apart: $\boldsymbol{F}^{\mathrm{c}}_{ij} = -(1-P_1)[k^{\mathrm{c}}(d-W)(\boldsymbol{d}/d)]$, $\boldsymbol{F}^{\mathrm{c}}_{(i+1)j} = -P_1[k^{\mathrm{c}}(d-W)(\boldsymbol{d}/d)]$, $\boldsymbol{F}^{\mathrm{c}}_{kl} = (1-P_2)[k^{\mathrm{c}}(d-W)(\boldsymbol{d}/d)]$ and $\boldsymbol{F}^{\mathrm{c}}_{(k+1)l} = P_2[k^{\mathrm{c}}(d-W)(\boldsymbol{d}/d)]$, where k^{c} is the collision stiffness. Parameter k^{c} is chosen freely to ensure that moving bacteria or parts of the same bacterium do not overlap markedly during the simulation (Table 2.1).

In addition, excessive bending of each angular spring i is limited by introducing interaction forces on particles $\boldsymbol{r}_i$ and $\boldsymbol{r}_{i+2}$. Since the length of a segment in our simulations does not effectively change due to stiff linear springs, the forces are introduced if the distance between the particles $\boldsymbol{r}_i$ and $\boldsymbol{r}_{i+2}$ become smaller than W, i.e. we find a vector $\boldsymbol{d} = \boldsymbol{r}_i - \boldsymbol{r}_{i+2}$ and introduce forces $\boldsymbol{F}^{\mathrm{c}}_i = -k^{\mathrm{c}}(d-W)(\boldsymbol{d}/d)$ and $\boldsymbol{F}^{\mathrm{c}}_{i+2} = k^{\mathrm{c}}(d-W)(\boldsymbol{d}/d)$ if $d < W$.

Drag forces and equations of motion. A myxobacterium on a substratum will often move in slime that is secreted by the cell itself and by other cells [34]. A bacterium moving at relatively slow speeds in viscous slime (i.e. at low Reynolds numbers) will be acted upon by Stokes drag force that is proportional to velocity of the bacterium. As predicted by the slender body theory, drag force on a cylinder-shaped myxobacterium would be twice as large in the direction normal to the bacterial body compared to the drag force in the direction parallel to the body [35]. We model this effect by considering anisotropic Stokes drag forces on separate particles. The direction tangential to the bacterium body is $\hat{\boldsymbol{t}}_i$ (see Engine forces), and the direction normal to bacterial body is $\hat{\boldsymbol{n}}_i$, found by rotating $\hat{\boldsymbol{t}}_i$ by $\pi/2$ in the plane made by $\boldsymbol{l}_i$ and $\boldsymbol{l}_{i+1}$. The drag force on a particle i in the direction tangent to the bacterial body is $\boldsymbol{F}^{\mathrm{d,t}}_i = -\zeta^{\mathrm{t}}\boldsymbol{v}^{\mathrm{t}}_i$, and the drag force in the direction normal to bacterial body is $\boldsymbol{F}^{\mathrm{d,n}}_i = -\zeta^{\mathrm{n}}\boldsymbol{v}^{\mathrm{n}}_i$, where superscripts t and n denote component vectors and a drag coefficient ζ in the direction of $\hat{\boldsymbol{t}}_i$ and $\hat{\boldsymbol{n}}_i$ respectively. The terminal (final) velocity of a particle, $\boldsymbol{v}^{\mathrm{f}}_i$, is the velocity at which the drag force will balance all the other forces acting on the particle: $\boldsymbol{v}^{\mathrm{f}}_i = \boldsymbol{v}^{\mathrm{f,t}}_i + \boldsymbol{v}^{\mathrm{f,n}}_i = (1/\zeta^{\mathrm{t}})\boldsymbol{F}^{\mathrm{t}}_i + (1/\zeta^{\mathrm{n}})\boldsymbol{F}^{\mathrm{n}}_i = (1/\zeta^{\mathrm{t}})(\hat{\boldsymbol{t}}_i \cdot \boldsymbol{F}_i)\hat{\boldsymbol{t}}_i + (1/\zeta^{\mathrm{n}})(\hat{\boldsymbol{n}}_i \cdot \boldsymbol{F}_i)\hat{\boldsymbol{n}}_i$, where $\boldsymbol{F}_i$ is the sum of the forces of all linear and angular springs, engine and contact forces that act on a particle i, $\boldsymbol{F}_i = \boldsymbol{F}^{\mathrm{l}}_i + \boldsymbol{F}^{\mathrm{a}}_i + \boldsymbol{F}^{\mathrm{e}}_i + \boldsymbol{F}^{\mathrm{c}}_i$, and $\zeta^{\mathrm{n}} = 2\zeta^{\mathrm{t}}$.

To our knowledge, the drag coefficient of a myxobacterium moving on a substratum has not been experimentally determined. Therefore, the value of ζ^{t} was chosen so that the terminal speed of a model bacterium powered by the engine force and moving in a straight line would be equal to the experimentally observed speed of *M. xanthus* v_b (Table 2.1), resulting in $\zeta^{\mathrm{t}} = (F^{\mathrm{e}}/N)/v_b$. Given the values of F^{e} and v_b, mass of a particle $m = \rho L\pi(W/2)^2/N$, found by approximating the shape of a bacterium by a cylinder with density ρ (Table 1), the value of ζ^{t} was found to be such that the bacterium reaches the terminal velocity in about 10^{-11} s. Since the timescale of myxobacteria movement is minutes, we assume in the model that inertia effects are negligible and that the velocity of a particle at each given time is $\boldsymbol{v}_i = \boldsymbol{v}^{\mathrm{f}}_i$, proportional to the sum of forces that act on it

Parameter	Value	Description
Model		
L	5 µm	Length of bacterium[1]
W	0.5 µm	Width of bacterium[1]
ρ	1000 kg·m^{-3}	Density of bacterium (approximately equal to the density of water)
N	10	Number of particles per bacterium
k^{l}	1×10^{-2} N·m^{-1}	Stiffness of a linear spring
k^{a}	1×10^{-15}– 1×10^{-18} N·m	Range of angular spring stiffnesses studied
k^{c}	6×10^{-4} N·m^{-1}	Stiffness of collision
F^{e}	100 pN	Engine force[2]
v_{b}	4 µm·min^{-1}	Speed of bacterial gliding[1]
T_{R} average	8.8 min	Average reversal time[1]
T_{R} standard deviation	2.1 min	Standard deviation of reversal time[1]
Solver		
$atol$	2.5×10^{-10} m	Absolute error tolerance[3]

Table 2.1: Parameter values used for simulations. [1]Wu *et al.* [27] [2]Wolgemuth *et al.* [9]. [3]An integration step is successful when error does not exceed atol [36].

(excluding drag). This leads to a system of differential equations

$$\frac{d\boldsymbol{r}_i(t)}{dt} = \boldsymbol{v}_i^{\mathrm{f}}(t) \tag{2.1}$$

for all bacteria j, describing the movement of all particles of all bacteria in the population.

In this study all bacteria move on a planar substratum (i.e. on the x-y plane). Therefore vectors $\boldsymbol{r}_i$ and $\boldsymbol{v}_i$ are two-dimensional and the system in Equation (2.1) translates into a system of $2 \times N \times M$ ordinary differential equations. We solve the system numerically with the Dormand-Prince fifth-order Runge-Kutta method [36] to obtain the positions of all particles in time. The algorithm was modified to include a maximum time step $W/(4v_b)$ in order to allow for collision detection. The parameter values used for simulations and error tolerance of the solver are listed in Table 2.1.

After each successful integration step, the direction of a bacterium is reversed if $t - t_{\mathrm{LR}} > T_{\mathrm{R}}$, where t is the current time of the simulation, t_{LR} is the time of the last reversal of the bacterium, and T_{R} is time interval until the next reversal. After a reversal, a new T_{R} value for the bacterium is sampled from a normal distribution with parameters following experimental measurements by Wu *et al.* [27].

Analysis of results. Every value of k^{a} was mapped to bending stiffness B of a bacterium viewed as a beam using the following procedure. A model bacterium was fixed at one end, a known force normal to the bacterial body was applied to the free end and its de-

flection was calculated. Bending stiffness was then found from $B = (F/\Delta z)((L-W)^3/3)$, where F is the magnitude of the applied force and Δz is the deflection of the free end [37].

The orientation of a bacterium j was defined as a vector pointing from the trailing particle to the leading particle of the bacterium, $\boldsymbol{o}_j = k^e(\boldsymbol{r}_{1j} - \boldsymbol{r}_{Nj})$. Alignment of a population of cells at time t was quantified by average orientation correlation (similar to the orientation correlation function used by Wu *et al.* [27]),

$$C(t) = (1/K)\sum_{j\neq k}^{K}[2cos^2\theta(\boldsymbol{o}_j(t),\boldsymbol{o}_k(t)) - 1],$$

where the sum is over all cell pairs, K is the number of cell pairs and $\theta(\boldsymbol{o}_j(t),\boldsymbol{o}_k(t))$ is the angle between the orientations of bacteria j and k at time t. Each term in the sum is equal to 1 if the two cells are aligned and equal to -1 if the orientations of the two cells are perpendicular. The ability of a cell j to maintain its orientation in time was quantified by orientation autocorrelation function, $C_j^a(\Delta t) = \sum_t[2cos^2\theta(\boldsymbol{o}_j(t),\boldsymbol{o}_j(t+\Delta t)) - 1$, where the sum is over all t values for which $t+\Delta t$ are defined. This function shows how well the orientation of the cell at time t is correlated with its orientation at time $t+\Delta t$.

2.3. RESULTS

In this study we investigated how flexibility of a rod-shaped cell affected i) the pattern of movement of a single cell powered by the rear and distributed engines, ii) the alignment of two colliding cells and iii) the alignment of a population of 500 mechanically interacting cells.

FLEXIBLE REAR-ENGINE POWERED CELLS EXHIBIT FLAILING BEHAVIOR

We first modeled gliding of a single cell on a substratum and studied how bending stiffness of the cell and the engine type affected the pattern of cell movement. The cell was initially placed with all its particles in a straight line, except for the trailing particle, which was offset from the long axis of the cell by 1% of cell width to introduce initial perturbation in engine direction. Cells with the distributed engine moved in a straight line independently of their bending stiffness (Movie 2.1 in Supplementary material). However, rear-powered cells moved in a straight line only for large bending stiffness values. For small bending stiffness values, shortly after the movement started, cells exhibited flailing behavior, i.e. complex snake-like movements (Figure 2.2, Movies 2.2 and 2.3) that were a result of cell bending caused by the engine force acting on the trailing pole of the cell. Very flexible cells with the rear engine were completely unable to produce directed movement (Movie 2.3). In a flailing cell, the trailing particle travels a longer distance than the leading particle. This observation allowed to estimate that the bending stiffness value below which a rear-engine cell exhibited flailing was $B_f = 2\times10^{-23}$ J·m (Figure 2.A.1A). In general, the value of B_f depends on the size of the engine force: a larger force is able to bend stiffer cells and is therefore expected to result in a larger value of B_f (Figure 2.A.1).

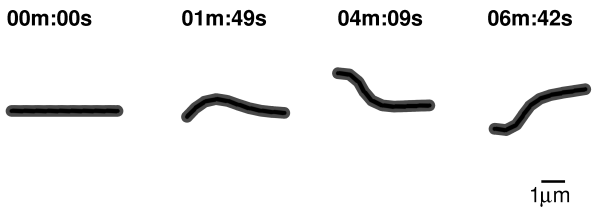

Figure 2.2: Shape and position of a rear-powered flailing cell at different times ($B = 1.2 \times 10^{-23}$ J·m).

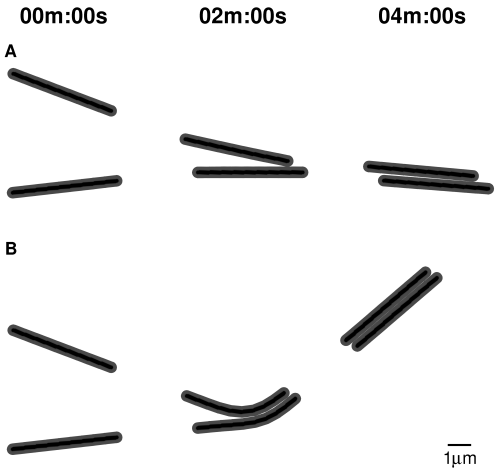

Figure 2.3: Positions and shapes of two colliding cells with distributed engine at different times. In (A) and (B) cells start from the same initial configuration. (A) Rigid cells, $B = 6.1 \times 10^{-22}$ J·m (B) Flexible cells, $B = 7.0 \times 10^{-25}$ J·m

TWO FLEXIBLE CELLS ALIGN BETTER UPON CONTACT THAN TWO RIGID CELLS

We next simulated a collision between two non-reversing cells and estimated how cell alignment after the collision depends on cell bending stiffness and the engine type. Two cells were initially placed on a substratum with random orientations and with their leading particles at random positions in a square with side L. Movements of the two cells were then simulated over an interval of 5 min. We studied a number of random initial configurations, each determined by initial positions and orientations of the cells. For each configuration we simulated movements of the cells for different bending stiffness values and two engine types. An example of the two cell collision for two different bending stiffness values is shown in Figure 2.3 and Movies 2.4 and 2.5.

We analyzed only those initial configurations that resulted in an effective collision between cells, i.e. the configurations where a collision between distributed engine cells produced a change in orientation of 5° or more of at least one cell for at least one bend-

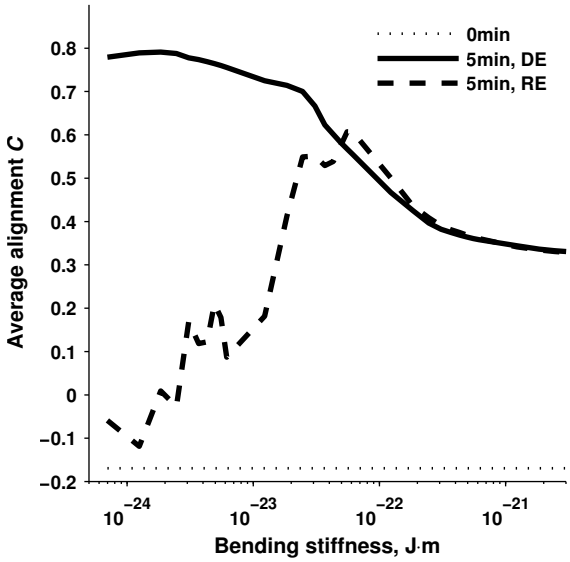

Figure 2.4: Average alignment C of two cells as a function of cell bending stiffness before the collision (dotted line), at 5 min for distributed engine cells (DE, solid line), at 5 min for rear engine cells (RE, dashed line). For each bending stiffness value, alignment C was averaged over 188 different initial configurations. Initial average alignment (dotted line) is negative because the initial configurations where the cells were well aligned did not produce effective collisions and were removed from the analysis (see text).

ing stiffness value. For cells with the distributed engine, the average alignment of the two cells due to collision increased as the bending stiffness of the cell decreased (Figure 2.4, solid line). The alignment of rear-powered cells due to collision depended on cell flexibility in a similar manner only above the value B_f (Figure 2.4, dashed line). Below B_f, rear-engine cells exhibited flailing behavior, continuously changed their orientation and therefore their ability to align was impaired. These results suggest that for non-flailing cells, flexibility helps two colliding cells to align. Similar results are obtained with different magnitudes of the engine force (Figure 2.A.2).

FLEXIBILITY INTERFERES WITH THE ALIGNMENT OF A POPULATION OF CELLS

The effect of cell flexibility on the alignment of a large population of cells was interestingly found to be opposite of that on the alignment of two colliding cells. We simulated movements of 500 reversing, mechanically interacting cells over a period of 4 hours and studied how the alignment of the population is affected by bending stiffness of the cell. The 500 cells were initially placed in a square computational domain with random positions and orientations (Figure 2.5A). The size of the domain was chosen so that the density of cells was $1/(\pi(L/2)^2) = 5 \times 10^6\,\mathrm{cm}^{-2}$. This density value allows for random distribution of cells within the domain and is physiologically relevant [38]. Periodic boundaries of the domain ensured that a (part of) bacterium leaving the domain entered it from the opposite side, keeping the density of bacteria in the domain constant.

Simulation results show that populations of rigid cells are well aligned at 4 hours (Fig-

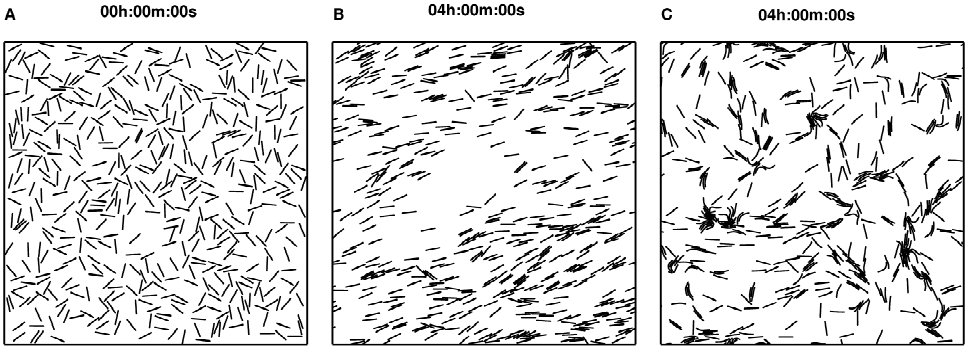

Figure 2.5: Spatial distribution of a population of 500 cells with the distributed engine at 0 h (A) and 4 h (B, C). Initially, the cells have random positions and orientations. The size of the domain is 100 µm, cell density in the domain is 5×10^6 cm^{-2}. (B) Rigid cells ($B = 6.1 \times 10^{-22}$ J·m). (C) Flexible cells ($B = 1.2 \times 10^{-23}$ J·m).

ure 2.5B) and the alignment is relatively stable (Fig. S3, Movie 2.6). In contrast, populations of flexible cells appear poorly aligned, although small temporary clusters consisting of tens of aligned cells are still visible (Figure 2.5C), Figure 2.A.3 and Movie 2.7). The alignment (average orientation correlation) of a population at 4 h for different cell bending stiffness values and two engine types is shown in Figure 2.6 (see also Figure 2.A.4 for variability between individual simulations). The average orientation correlation is close to zero (i.e. alignment is poor) for small bending stiffness values, but increases steeply to a plateau value as bending stiffness of the cell increases. In other words, flexibility impairs the ability of a population to align for cells both with the distributed and the rear engines. Below the bending stiffness value B_f a population of rear-powered cells is not expected to align well due to cell flailing, as the simulation results confirm (Figure 2.6). However, a population of rear-powered cells shows poor alignment for bending stiffness values as high as 7×10^{-23} J·m, the values for which a rear-powered cell does not flail. This suggests that flexibility interferes with the alignment of rear-powered cells directly, but not through the effect on the flailing motion of the cell.

We also found that the effect of cell flexibility on the alignment of the population is robust with respect to the initial configuration of cells. If all cells were initially aligned (Figure 2.A.5-A), they remained well aligned throughout the 4 h if the cells were rigid (Figure 2.A.5-B). However, a population of flexible cells rapidly lost its alignment (Figure 2.A.5-C, Movie 2.8). The average orientation correlation of a population at 4h as a function of the bending stiffness of the cell has a similar appearance to the one shown in Figure 2.6 (Figure 2.A.6).

In addition, to show that the effect of cell flexibility on the ability of a population to remain aligned is robust with respect to cell density in the domain, we simulated movements of 490 densely packed (cell density 4×10^7 cm^{-2}), initially aligned cells (Figure 2.7A). A population of rigid cells remained well aligned at 4 h (Figure 2.7B, Movie 2.9),

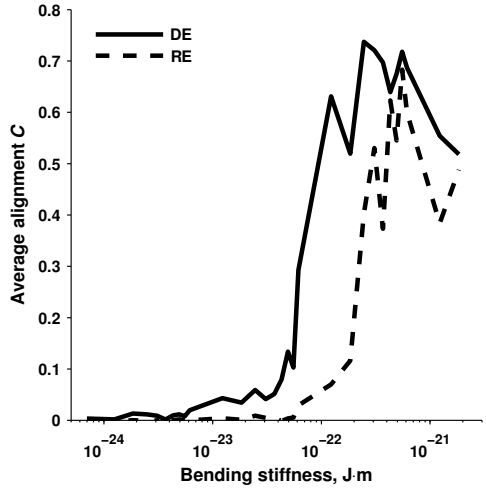

Figure 2.6: Alignment (average orientation correlation C) of a population at 4 h as a function of cell bending stiffness in the simulations where cells initially have random positions and orientations (Fig. 6). For each bending stiffness value, results of 3 simulations with different initial configurations of cells were averaged. Solid line - cells with distributed engine (DE), dashed line - cells with rear engine (RE).

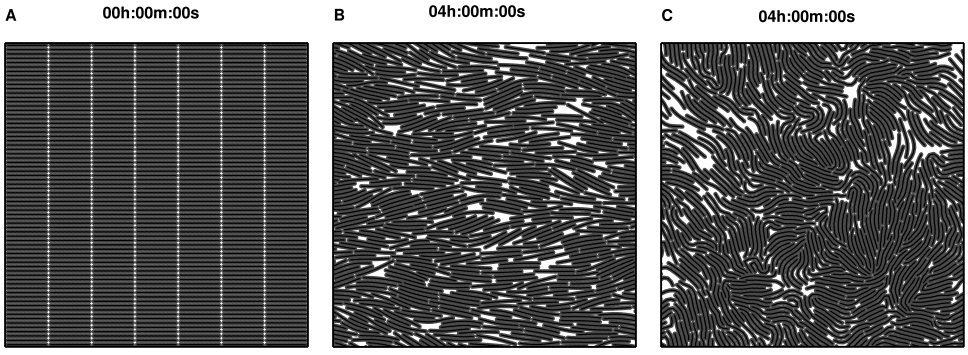

Figure 2.7: Spatial distribution of a population of 490 densely packed cells with the distributed engine at 0 h (A) and 4 h (B,C). Initially the cells are aligned. The size of the domain is 35 µm, cell density in the domain is 4×10^7 cm^{-2}. (B) Rigid cells ($B = 6.1 \times 10^{-22}$ J·m. (C) Flexible cells ($B = 1.2 \times 10^{-23}$ J·m.

but a population of flexible cells lost their alignment (Figure 2.7C, Movie 2.10, see also Figure 2.A.7).

FLEXIBLE CELLS ARE LESS LIKELY TO RETAIN THEIR ORIENTATION UPON CONTACT

To understand why the population of flexible cells is unable to align, although flexibility helps two colliding cells to align (Figure 2.4), we analyzed the ability of a cell to retain its orientation during multiple contacts with other cells in the population. For rigid cells,

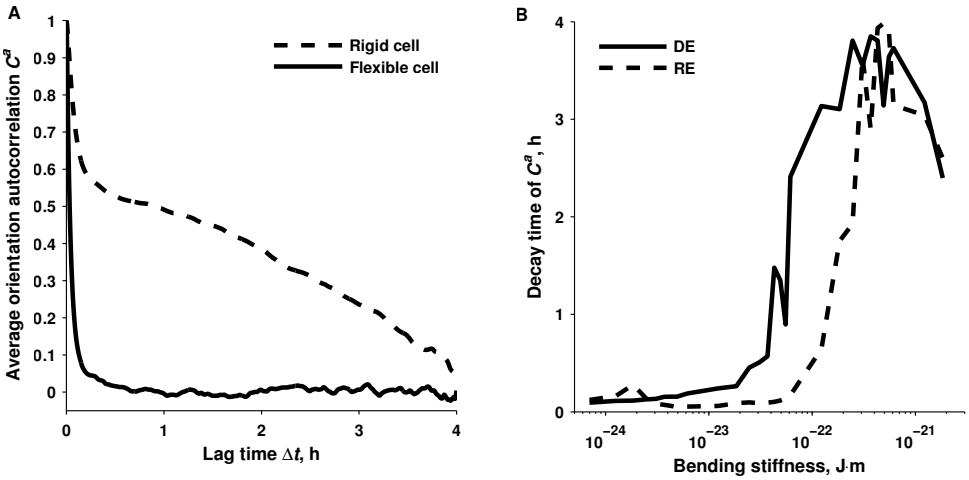

Figure 2.8: Ability of a cell to maintain its orientation upon mechanical interactions in a population of 500 cells with the distributed engine. Cell density in the domain is $5 \times 10^6\,\mathrm{cm}^{-2}$. (A) Average orientation autocorrelation function of flexible ($B = 1.2 \times 10^{-23}$ J·m) and rigid ($B = 6.1 \times 10^{-22}$ J·m) cells. (B) Decay time of average orientation autocorrelation function for different bending stiffness values. Decay time is defined as the time at which the orientation autocorrelation function value falls below 0.05. Solid line - cells with distributed engine (DE), dashed line - cells with rear engine (RE).

the orientation autocorrelation function C^a, that shows how well orientations of a cell at different time intervals are correlated (see Methods), maintains positive values for up to 4h, the length of the simulation. However, when cells are flexible, the values of C^a decay to nearly zero for time intervals larger than ~15 min (Figure 2.8A). Figure 2.8B shows that the decay time of C^a increases with increasing bending stiffness. In other words, as a cell becomes more flexible, it looses the ability to maintain its orientation for longer times. Conversely, rigid cells are more resistant to changes in their orientation upon mechanical interaction with other cells.

Figure 2.3 illustrates the mechanism of the inability of flexible cells to maintain their orientations upon contact. When two rigid cells that are almost aligned collide, they often adjust their orientations and continue to move in the directions similar to those before the contact (Figure 2.3A, Movie 2.4). However, if the cells are flexible, they bend upon contact and move in circular paths (Figure 2.3B, Movie 2.5). In both cases cells align well, however, circular motion of flexible cells results in large changes in their orientations during the collision.

The inability of flexible cells to maintain their orientations upon contact can explain why a larger population of flexible cells is not able to align. In a well aligned population of flexible cells, the cells would collide at small angles and would markedly change their orientation (similar to the situation in Figure 2.3B). The new orientations of the two cells would be very different from the dominant orientation of the remaining population. Thus, multiple collisions between flexible cells would result in the deterioration of alignment of an initially aligned population (Movies 2.8 and 2.10). Collisions between

rigid cells in a well aligned population would not change their orientation markedly (Figure 2.3A), thus keeping a population well aligned (Movie 2.9). This is further supported by the fact that for intermediate bending stiffness values (5×10^{-23}–5×10^{-22} J·m), both the alignment of the population of rear-powered cells and the ability of a rear-engine cell to maintain orientation are poorer than those of cells with the distributed engine (Figure 2.6 and Figure 2.8B). Poorer ability of a rear-engine cell to maintain orientation in comparison with a distributed engine cell can be explained by a larger torque that is applied by the rear engine force to the bent cell resulting in a faster cell rotation upon contact. Furthermore, an increase in the magnitude of the engine force results in larger bending stiffness values for which a population fails to align (Figure 2.A.8). Larger engine forces are able to bend stiffer cells, therefore their ability to maintain orientation is impaired.

2.4. DISCUSSION

In this study we created a mechanical mass-spring model of a flexible rod-shaped cell that glides on a substratum and showed that bending stiffness and engine type affected the pattern of cell gliding and the alignment of a population of 500 mechanically interacting cells.

Two motility systems have been described in *M. xanthus* [7]. Whereas the mechanism of S motility is known to involve the extension and retraction of type IV pili [8], the mechanism of A motility is debated [39, 40]. Among the most discussed hypotheses for A motility mechanism are the "slime gun" model, where the force is generated at the trailing pole of the cell by extrusion and swelling of polyelectrolyte gel [9], and the focal adhesions model, where the force is produced at the sites of adhesion with the substratum along the whole length of the cell [10]. Powered by the motility engine, a myxobacterium cell glides on a substratum along the long axis of the cell [32]. Our simulations suggest that a rear-engine (i.e. "slime-gun") powered cell would be able to travel in the direction of the long axis of the cell only when bending stiffness of the cell is above the value $B_f = 2 \times 10^{-23}$ J·m. Below that value, a cell would exhibit flailing, complex snake-like movements. Those movements would arise because the engine force acting on the trailing pole would bend the cell and produce torque that would rotate the cell. Flailing of *M. xanthus* has been observed experimentally when the leading pole of the cell is stuck [5, 10]. Our results show that a flexible rear-powered bacterium could exhibit flailing behavior even when the leading pole of a bacterium is free to move. Very flexible rear-engine cells would not be capable to produce any directed movement due to extensive flailing. In addition, we show that when engine forces are generated along the whole length of the cell, as the focal adhesions model of A motility proposes, a cell would be able to glide along the long axis of the cell independently of its bending stiffness. To our knowledge, bending stiffness of a myxobacterium cell has not been experimentally determined. Wolgemuth [41] theoretically estimated bending stiffness of *M. xanthus* to be $B = 3 \times 10^{-23}$ J·m by using experimental observations of the shape of a flailing cell [5]. Bending stiffness of a cell can also be estimated by assuming that the principal structural component of a cell is hollow-cylinder shaped cell wall. The bending

stiffness can then be found from $B = \pi E a^3 t$, where E is Young's modulus of the cell wall, a is the radius of the cylinder and t is the thickness of the cylinder wall (peptidoglycan) [37]. Given the values of $E = 0.25\,\text{MPa}$ [42], $t = 6.35\,\text{nm}$ (*Escherichia coli*) and $t = 2.41\,\text{nm}$ (*Pseudomonas aeruginosa*) [43], bending stiffness of a *M. xanthus* cell is estimated to be between $3.0 \times 10^{-23}\,\text{J·m}$ and $7.8 \times 10^{-23}\,\text{J·m}$. All estimated values are large enough to allow a slime-gun powered cell to produce directed movement, as predicted by our model. Furthermore, Kaiser and Crosby [14] observed that moving *M. xanthus* cells tend to glide with a small change in direction. In our model, such movement could be accounted for by a rear-engine powered cell with a bending stiffness value smaller but very close to B_f. It must also be emphasized that our determined value of B_f is dependent on the magnitude of the A motility engine force, which has not been experimentally measured, but only estimated theoretically [9]. To further investigate the conditions of cell flailing, the type of analysis performed by Wogemuth [41] could also be appropriate.

Myxobacteria often form various multicellular structures from aligned cells, such as multicellular rafts, swirls, streams or traveling waves [13–19]. The extent of alignment can vary from arrays of hundreds of aligned cells [13, 19, 21, 27] to the global alignment of the whole population during traveling wave formation [16]. It has been observed that a population of initially randomly oriented *M. xanthus* cells can form aligned domains within several hours [13, 21], although mechanisms of cell alignment are not well known. It is often assumed that cells align due to mechanical interactions between cells [21–23] and that flexibility facilitates cell reorientation upon collision [24]. Furthermore, slime trails that are left by gliding cells on a substratum and used by other gliding cells as tracks are thought to contribute to cell alignment [4, 18, 27, 34]. We show that a population of 500 randomly oriented reversing rigid cells (with bending stiffness values larger than $1 \times 10^{-22}\,\text{J·m}$ for distributed engine cells and larger than $5 \times 10^{-22}\,\text{J·m}$ for rear-engine cells), powered by A motility alone, without the need of S motility or slime trails, could align well within several hours only due to mechanical interactions between gliding cells. However, a population of flexible cells (with bending stiffness values smaller than $5 \times 10^{-23}\,\text{J·m}$ would not be able align, but would only produce small temporary clusters consisting of tens of aligned cells. Since random orientations of cells at the beginning of development might only be a laboratory condition, hardly ever seen in nature [15], we also found that alignment or non-alignment of a population is robust with respect to the initial configuration of cells and cell density. In other words, a population of initially aligned flexible cells, even when they are densely packed, would not be able to maintain the aligned state, whereas a population of rigid cells would stay well aligned. The inability of a larger population of flexible cells to align in our simulations is caused by the tendency of flexible cells to bend upon contact and move in circular paths (Figure 2.3B), resulting in large changes in the orientations of colliding cells. In contrast, rigid cells are more resistant to changes in their orientation upon collision. The ability of colliding cells to align while maximally preserving their orientations before the contact appears to be crucial in order for a population to align or remain aligned in our model. Overall, we conclude that cell flexibility can interfere with the formation of streams, traveling waves, domains of aligned cells within swarms or other structures from aligned

cells.

Marked bending and movement of myxobacteria cells in circular paths while in contact have been observed experimentally at low cell densities [44], suggesting poor ability of myxobacteria cells to maintain their orientations upon collisions. In addition, for the bending stiffness value of a *M. xanthus* cell theoretically estimated by Wolgemuth [41], our model predicts that a population of cells would not be able to align within several hours only as a result of mechanical interactions between cells. We therefore suggest that other factors, might play a role in the alignment of myxobacteria cells. Myxobacteria cells often move in slime secreted by other cells [34]. Viscous extracellular slime surrounding cells could increase their effective bending stiffness thus affecting their alignment and flailing behavior. It has also been proposed that focal adhesions (hypothesized to be a part of A motility engine) may act as attachment points between a cell and substratum. A cell would have extra bending stiffness due to the attachment [45].

Kaiser and Welch [25] proposed that cell flexibility helps myxobacteria to overcome "traffic jams" during fruiting body formation. This idea is consistent with our findings that flexibility allows cells to more easily change orientation upon mechanical interaction. In addition, our results suggest that the value of bending stiffness of myxobacteria could be a result of a trade-off: the ability of a population to efficiently align (e.g., to form streams and traveling waves) at the initial stages of fruiting body development would require a rigid cell, whereas flexible cells would be preferable to overcome "traffic jams" at later stages. Furthermore, myxobacteria cells might have evolved a mechanism to regulate their bending stiffness to serve for different purposes in the course of development. For example, the transition of myxobacteria from swarming, where cells are less aligned globally, to the rippling stage that shows a high degree of cell alignment could be a result of cell stiffening. Remarkably, cells of different species appear to have different flexibility [4], but the importance of this difference is unknown.

In conclusion, the proposed model shows that cell flexibility can be an important factor affecting both the movement of single myxobacteria cells and the alignment of cell populations. Experimental measurement of the important parameters of myxobacteria cells – bending stiffness, engine force and drag with the substratum – will allow to make more accurate predictions with the current model. In addition, our model does not consider possible cell-substratum binding forces due to focal adhesions. Although very little is known about the mechanics of focal adhesions, these binding forces could potentially affect cell collision dynamics. Furthermore, cells in our simulations move on a surface in a single layer, an assumption reasonable only for low density of cells. It would be important to investigate three-dimensional cell movement in multilayer populations.

2.A. SUPPLEMENTARY FIGURES

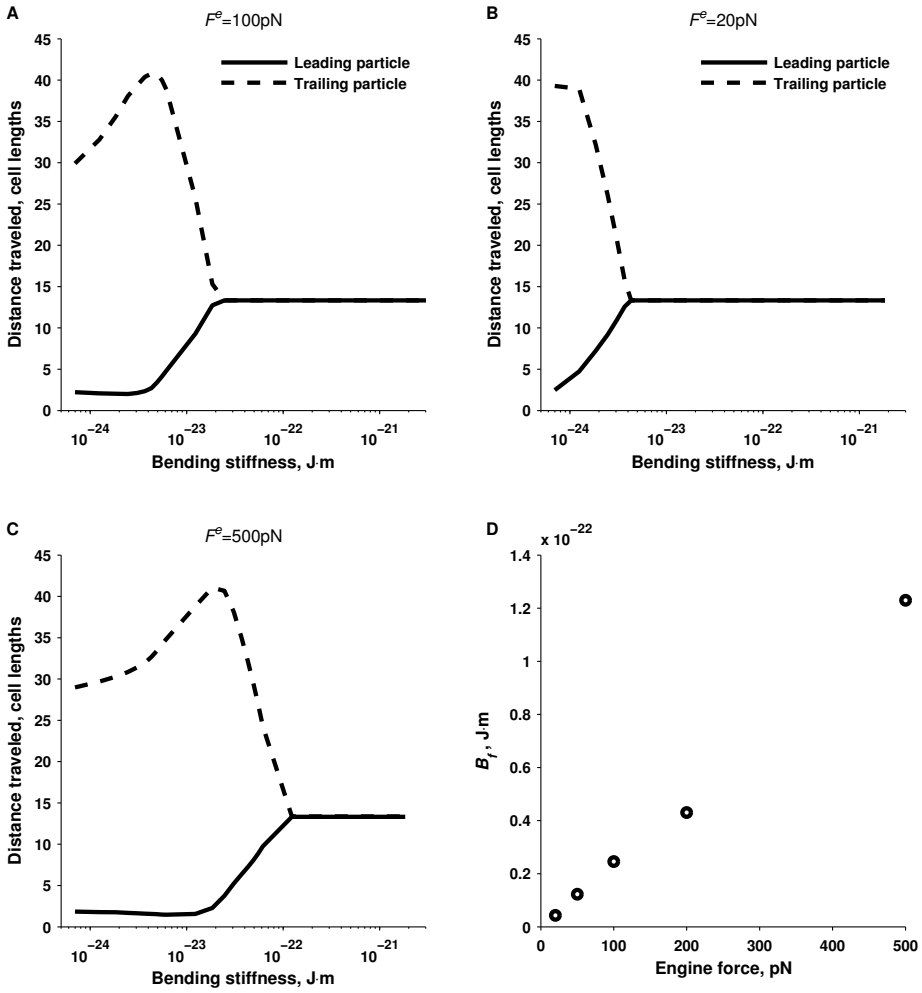

Figure 2.A.1: (A, B and C) Distance traveled over 1000 s by the leading particle s_l (solid line) and the trailing particle s_t (dashed line) of a rear-engine powered cell as a function of its bending stiffness. The bending stiffness value below which a cell exhibits flailing, B_f, is the value at which the two lines become separate and is defined as the largest value of B where $s_t/s_l > 1.05$. (A) The magnitude of the engine force $F^e = 100\,pN$. (B) $F^e = 20\,pN$. (C) $F^e = 500\,pN$. (D) B_f as a function of the engine force F^e.

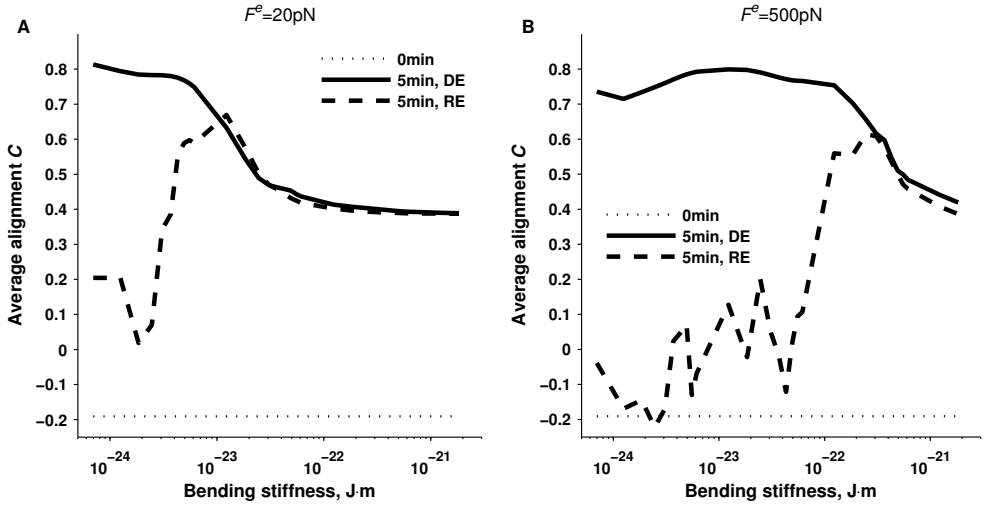

Figure 2.A.2: Average alignment C of two cells as a function of cell bending stiffness before the collision (dotted line), at 5 min for distributed engine cells (DE, solid line), at 5 min for rear engine cells (RE, dashed line). (A) $F^e = 20\,\text{pN}$. (B) $F^e = 500\,\text{pN}$. For each bending stiffness value, alignment C was averaged over 180 (A) and 185 (B) different initial configurations. Initial average alignment (dotted line) is negative because the initial configurations where the cells were well aligned did not produce effective collisions and were removed from the analysis (see text).

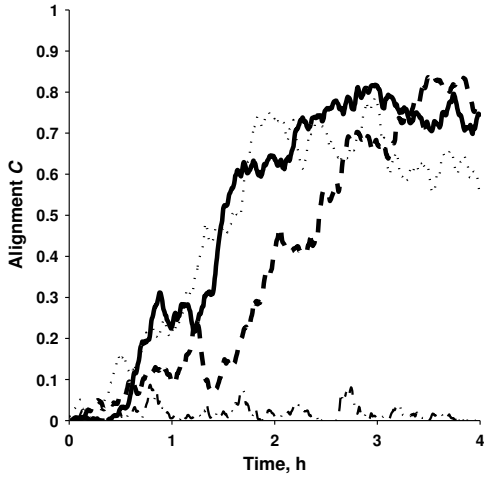

Figure 2.A.3: Alignment (average orientation correlation C) of a population as a function of time in the simulations where cells initially have random positions and orientations (see Figure 2.5). (Solid, dashed and dotted lines) Alignment dynamics of a population of rigid cells ($B = 6.1 \times 10^{-22}\,\text{J·m}$) for three different initial configurations of cells. (Dashed-dotted line) The dynamics of alignment of a population of flexible cells ($B = 1.2 \times 10^{-23}\,\text{J·m}$). In all examples cells are powered by the distributed engine.

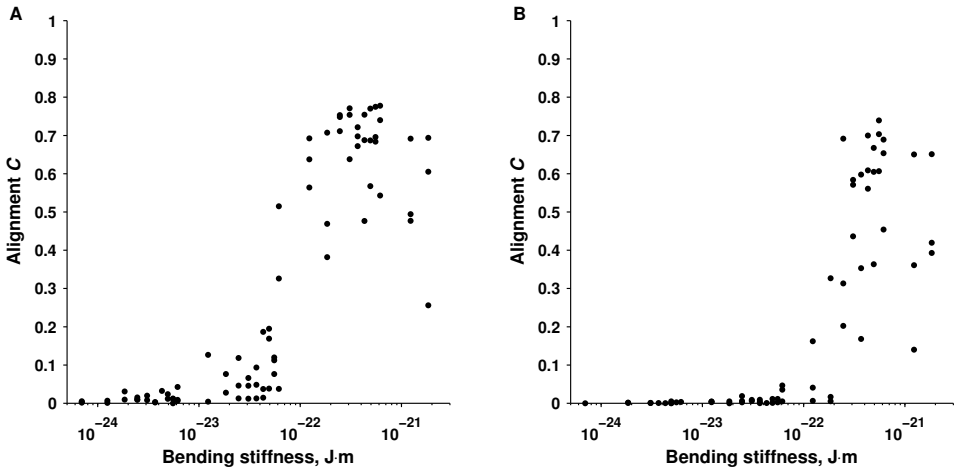

Figure 2.A.4: Alignment (average orientation correlation C) of a population at 4 h as a function of cell bending stiffness in the simulations where cells initially have random positions and orientations (Figure 2.5). One point represents a single simulation. Averaging all values obtained for a particular bending stiffness value results in Figure 2.6. (A) Cells with distributed engine. (B) Cells with rear engine.

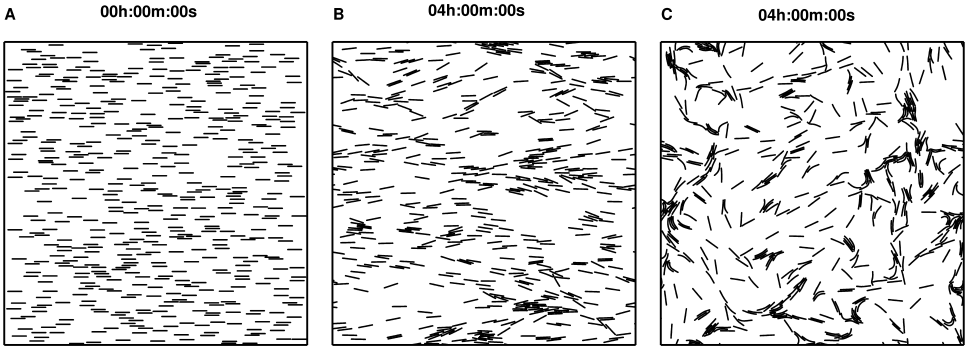

Figure 2.A.5: Spatial distribution of a population of 500 cells with the distributed engine at 0 h (A) and 4 h (B and C). Initially the cells are aligned but have random positions. The size of the domain is 100 µm, cell density in the domain is 5×10^6 cm^{-2}. (B) Rigid cells ($B = 6.1 \times 10^{-22}$ J·m). (C) Flexible cells ($B = 1.2 \times 10^{-23}$ J·m).

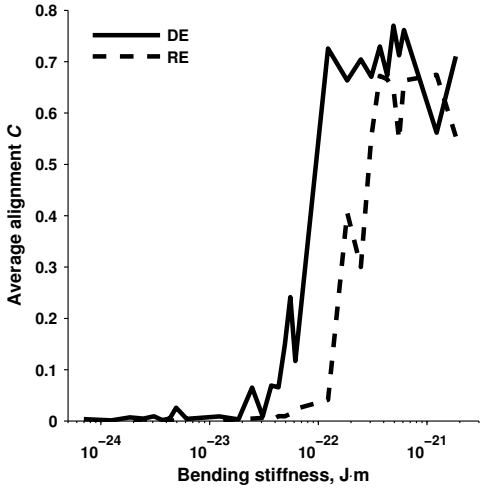

Figure 2.A.6: Alignment (average orientation correlation C) of a population at 4 h as a function of cell bending stiffness in the simulations where a population is initially aligned Figure 2.A.5. For each bending stiffness value, the results of 3 simulations with different initial configurations of cells were averaged. (Solid line) Cells with distributed engine (DE). (Dashed line) Cells with rear engine (RE).

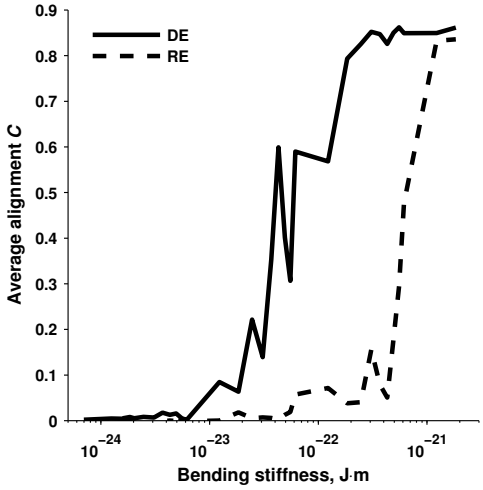

Figure 2.A.7: Alignment (average orientation correlation C) of a population at 4 h as a function of cell bending stiffness in the simulations where a population is initially aligned and densely packed (Figure 2.7). For each bending stiffness value, the results of 3 simulations with small random perturbation in the initial positions of cells were averaged. (Solid line) Cells with distributed engine (DE). (Dashed line) Cells with rear engine (RE).

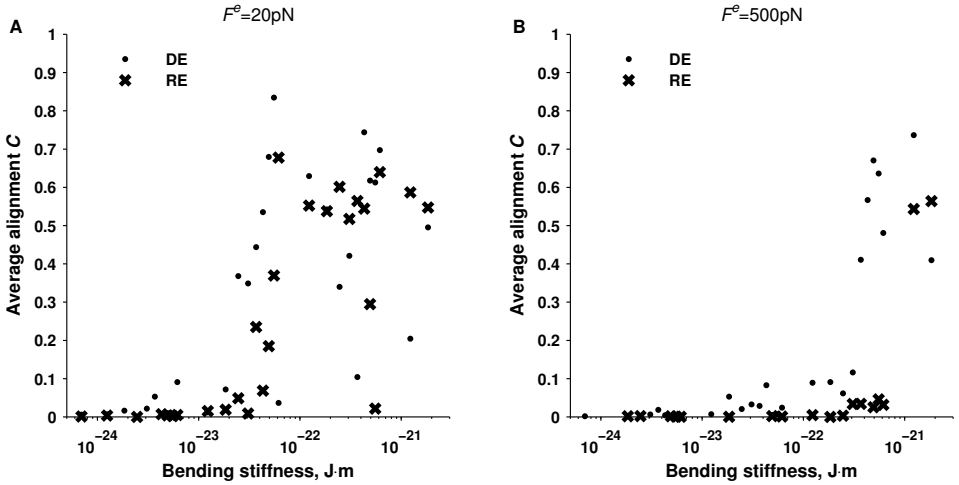

Figure 2.A.8: Alignment (average orientation correlation C) of a population at 4 h as a function of cell bending stiffness in the simulations where cells initially have random positions and orientations (Figure 2.5). One point represents a single simulation. (Dots) Cells with distributed engine (DE). (Crosses) Cells with rear engine (RE). (A) $F^e = 20\,\text{pN}$. (B) $F^e = 500\,\text{pN}$.

2.B. SUPPLEMENTARY MOVIES

Movie 2.1. Movement of a cell powered by the distributed engine ($B = 1.2 \times 10^{-23}\,\text{J·m}$).

Movie 2.2. Flailing movements of a rear-powered cell ($B = 1.2 \times 10^{-23}\,\text{J·m}$).

Movie 2.3. Flailing movements of a rear-powered cell ($B = 3.1 \times 10^{-24}\,\text{J·m}$).

Movie 2.4. A collision of two rigid cells ($B = 6.1 \times 10^{-22}\,\text{J·m}$) with distributed engine.

Movie 2.5. A collision of two flexible cells ($B = 7.0 \times 10^{-25}\,\text{J·m}$) with distributed engine.

Movie 2.6. Movements of 500 rigid ($B = 6.1 \times 10^{-22}\,\text{J·m}$), mechanically interacting cells with a distributed engine. Cells have random initial positions and orientations within the domain. The size of the domain is 100 µm, cell density in the domain is $5 \times 10^6\,\text{cm}^{-2}$.

Movie 2.7. Movements of 500 flexible ($B = 1.2 \times 10^{-23}\,\text{J·m}$), mechanically interacting cells with a distributed engine. Cells have random initial positions and orientations within the domain. The size of the domain is 100 µm, cell density in the domain is $5 \times 10^6\,\text{cm}^{-2}$.

Movie 2.8. Movements of 500 flexible ($B = 1.2 \times 10^{-23}\,\text{J·m}$), mechanically interacting cells with a distributed engine. Initially cells are aligned and have random positions. The size of the domain is 100 µm, cell density in the domain is $5 \times 10^6\,\text{cm}^{-2}$.

Movie 2.9. Movements of 490 densely packed rigid ($B = 6.1 \times 10^{-22}$ J·m), mechanically interacting cells with a distributed engine. Initially cells are aligned. The size of the domain is 35 µm, cell density in the domain is 4×10^7 cm^{-2}.

Movie 2.10. Movements of 490 densely packed flexible ($B = 1.2 \times 10^{-23}$ J·m), mechanically interacting cells with a distributed engine. Initially cells are aligned. The size of the domain is 35 µm, cell density in the domain is 4×10^7 cm^{-2}.

REFERENCES

[1] A. Janulevicius, M. C. van Loosdrecht, A. Simone, and C. Picioreanu, *Cell flexibility affects the alignment of model myxobacteria,* Biophysical Journal **99**, 3129 (2010).

[2] D. Kaiser, *Coupling cell movement to multicellular development in myxobacteria,* Nature Reviews Microbiology **1**, 45 (2003).

[3] L. J. Shimkets, M. Dworkin, and H. Reichenbach, *The myxobacteria,* in *The Prokaryotes*, vol. 7, edited by M. Dworkin, S. Falkow, E. Rosenberg, K. H. Schleifer, and E. Stackebrandt (Springer, New York, 2006) pp. 31–115.

[4] H. Reichenbach, H. H. Heunert, and H. Kuczka, *Schwarmentwicklung und Morphogenese bei Myxobakterien - Archangium, Myxococcus, Chondrococcus, Chondromyces,* Film C 893 (Institut für den Wissenschaftlichen Film, Göttingen, 1965).

[5] A. M. Spormann and A. D. Kaiser, *Gliding movements in Myxococcus xanthus,* Journal of Bacteriology **177**, 5846 (1995).

[6] J. Henrichsen, *Bacterial surface translocation: a survey and a classification,* Bacteriological Reviews **36**, 478 (1972).

[7] J. Hodgkin and D. Kaiser, *Genetics of gliding motility in Myxococcus xanthus (Myxobacterales): two gene systems control movement,* Molecular and General Genetics **171**, 177 (1979).

[8] H. Sun, D. R. Zusman, and W. Shi, *Type IV pilus of Myxococcus xanthus is a motility apparatus controlled by the frz chemosensory system,* Current Biology **10**, 1143 (2000).

[9] C. Wolgemuth, E. Hoiczyk, D. Kaiser, and G. Oster, *How myxobacteria glide,* Current Biology **12**, 369 (2002).

[10] T. Mignot, J. W. Shaevitz, P. L. Hartzell, and D. R. Zusman, *Evidence that focal adhesion complexes power bacterial gliding motility,* Science **315**, 853 (2007).

[11] M. A. Wozniak, K. Modzelewska, L. Kwong, and P. J. Keely, *Focal adhesion regulation of cell behavior,* Biochimica Et Biophysica Acta **1692**, 103 (2004).

[12] B. D. Blackhart and D. R. Zusman, *"Frizzy" genes of Myxococcus xanthus are involved in control of frequency of reversal of gliding motility,* Proceedings of the National Academy of Sciences of the United States of America **82**, 8767 (1985).

[13] L. Jelsbak and L. Søgaard-Andersen, *Cell behavior and cell-cell communication during fruiting body morphogenesis in Myxococcus xanthus,* Journal of Microbiological Methods **55**, 829 (2003).

[14] D. Kaiser and C. Crosby, *Cell movement and its coordination in swarms of Myxococcus xanthus,* Cell Motility and the Cytoskeleton **3**, 227 (1983).

[15] K. A. O'Connor and D. R. Zusman, *Patterns of cellular interactions during fruiting-body formation in Myxococcus xanthus,* Journal of Bacteriology **171**, 6013 (1989).

[16] B. Sager and D. Kaiser, *Intercellular c-signaling and the traveling waves of Myxococcus,* Genes & Development **8**, 2793 (1994).

[17] O. Sliusarenko, J. Neu, D. R. Zusman, and G. Oster, *Accordion waves in Myxococcus xanthus,* Proceedings of the National Academy of Sciences of the United States of America **103**, 1534 (2006).

[18] G. M. Vasquez, F. Qualls, and D. White, *Morphogenesis of Stigmatella aurantiaca fruiting bodies,* Journal of Bacteriology **163**, 515 (1985).

[19] A. E. Pelling, Y. Li, S. E. Cross, S. Castaneda, W. Shi, and J. K. Gimzewski, *Self-organized and highly ordered domain structures within swarms of Myxococcus xanthus,* Cell Motility and the Cytoskeleton **63**, 141 (2006).

[20] S. K. Kim and D. Kaiser, *Cell alignment required in differentiation of Myxococcus xanthus,* Science (New York, N.Y.) **249**, 926 (1990).

[21] D. Wall and D. Kaiser, *Alignment enhances the cell-to-cell transfer of pilus phenotype,* Proceedings of the National Academy of Sciences of the United States of America **95**, 3054 (1998).

[22] O. Sliusarenko, J. Chen, and G. Oster, *From biochemistry to morphogenesis in myxobacteria,* Bulletin of Mathematical Biology **68**, 1039 (2006).

[23] R. Welch and D. Kaiser, *Cell behavior in traveling wave patterns of myxobacteria,* Proceedings of the National Academy of Sciences of the United States of America **98**, 14907 (2001).

[24] D. Kaiser, *Bacterial swarming: a re-examination of cell-movement patterns,* Current Biology **17**, R561 (2007).

[25] D. Kaiser and R. Welch, *Dynamics of fruiting body morphogenesis,* Journal of Bacteriology **186**, 919 (2004).

[26] O. A. Igoshin, A. Mogilner, R. D. Welch, D. Kaiser, and G. Oster, *Pattern formation and traveling waves in myxobacteria: theory and modeling*, Proceedings of the National Academy of Sciences of the United States of America **98**, 14913 (2001).

[27] Y. Wu, A. D. Kaiser, Y. Jiang, and M. S. Alber, *Periodic reversal of direction allows myxobacteria to swarm*, Proceedings of the National Academy of Sciences of the United States of America **106**, 1222 (2009).

[28] Z. Csahók and A. Czirók, *Hydrodynamics of bacterial motion*, Physica A: Statistical and Theoretical Physics **243**, 304 (1997).

[29] F. Peruani, A. Deutsch, and M. Bär, *Nonequilibrium clustering of self-propelled rods*, Physical Review E **74**, 030904 (2006).

[30] J. Starruß, T. Bley, L. Søgaard-Andersen, and A. Deutsch, *A new mechanism for collective migration in Myxococcus xanthus*, Journal of Statistical Physics **128**, 269 (2007).

[31] D. H. Eberly and K. Shoemake, *Game Physics* (Morgan Kaufmann Publishers, San Francisco, 2003).

[32] H. Reichenbach, H. H. Heunert, and H. Kuczka, *Myxococcus spp. (Myxobacteriales) - Schwarmentwicklung und Bildung von Protocysten*, Film E 778 (Institut für den Wissenschaftlichen Film, Göttingen, 1965).

[33] C. Ericson, *Real-Time Collision Detection* (Morgan Kaufmann Publishers, San Francisco, 2005).

[34] R. P. Burchard, *Trail following by gliding bacteria*, Journal of Bacteriology **152**, 495 (1982).

[35] J. B. Keller and S. I. Rubinow, *Slender-body theory for slow viscous flow*, Journal of Fluid Mechanics Digital Archive **75**, 705 (1976).

[36] W. H. Press, S. A. Teukolsky, W. T. Vetterling, and B. P. Flannery, *Numerical recipes. The art of scientific computing*, third edition ed. (Cambridge University Press, Cambridge, 2007).

[37] J. M. Gere and S. P. Timoshenko, *Mechanics of Materials* (Kent Publishing, New York, 1984).

[38] L. J. Shimkets and M. Dworkin, *Excreted adenosine is a cell density signal for the initiation of fruiting body formation in Myxococcus xanthus*, Developmental Biology **84**, 51 (1981).

[39] T. Mignot, *The elusive engine in Myxococcus xanthus gliding motility*, Cellular and Molecular Life Sciences **64**, 2733 (2007).

[40] D. Kaiser, *Myxococcus - from single-cell polarity to complex multicellular patterns,* Annual Review of Genetics **42**, 109 (2008).

[41] C. W. Wolgemuth, *Force and flexibility of flailing myxobacteria,* Biophysical Journal **89**, 945 (2005).

[42] A. E. Pelling, Y. Li, W. Shi, and J. K. Gimzewski, *Nanoscale visualization and characterization of Myxococcus xanthus cells with atomic force microscopy,* Proceedings of the National Academy of Sciences of the United States of America **102**, 6484 (2005).

[43] V. R. F. Matias, A. Al-Amoudi, J. Dubochet, and T. J. Beveridge, *Cryo-transmission electron microscopy of frozen-hydrated sections of escherichia coli and pseudomonas aeruginosa,* Journal of Bacteriology **185**, 6112 (2003).

[44] H. Kühlwein, B. Schlicke, H. K. Galle, and H. H. Heunert, *Polyangium fuscum (Myxobacteriales) - Cystenkeimung und Schwarmentwicklung,* Film E 1582 (Institut für den Wissenschaftlichen Film, Göttingen, 1971).

[45] D. Kaiser, *Are there lateral as well as polar engines for A-motile gliding in myxobacteria?* Journal of Bacteriology **191**, 5336 (2009).

3

RESTRICTION OF LATERAL MOVEMENT FACILITATES THE ALIGNMENT OF MODEL MYXOBACTERIA POPULATION

3.1. INTRODUCTION

In Chapter 2, by means of a computational mass-spring model, it was shown that, given a myxobacterium cell is a flexible self-propelled rod gliding on a substratum in viscous slime and colliding with other rods, cell flexibility would affect the alignment of the whole cell population. It was found that a population of rigid cells aligns well, but cell flexibility impairs the alignment. It was predicted, that given a theoretically estimated bending stiffness value of *Myxococcus xanthus* cell of 3×10^{-23} J·m [1] and estimated motility engine force of 100 pN [2], a population of cells would show poor alignment, contradicting experimental observations [3]. The reasons for this discrepancy have not yet been understood.

In the model presented in Chapter 2, cell flexibility impaired the population alignment due to poor orientational stability of two colliding flexible cells. During collision cells would bend and travel in circular paths thus drastically changing the orientations they had before the collision (Figure 2.3B and 3.1A). One can sometimes observe similar behaviour of flexible colliding cells in experiments [4]. However, more often it can be seen that only the cell contacting with the leading pole would bend and turn, but the cell that is being pushed sideways would remain unbent and continue moving in the same direction [5] (also schematically drawn in Figure 3.1B). As a result the leading-pole contacting cell would align along the laterally contacting cell. These observations suggest that most of the cell body (except the leading tip) may not be able to move or be pushed

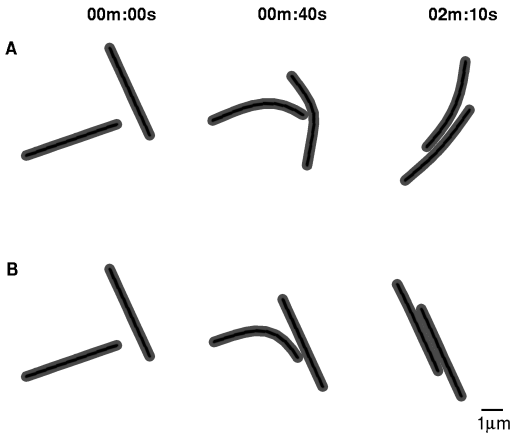

Figure 3.1: Shapes of two simulated cells at three moments during their collision, for bending stiffness $B = 3.1 \times 10^{-23}$ J·m. (A) Unrestricted cells. (B) Laterally restricted cells, $F_c = 200$ pN (see Model description).

by another cell in the lateral direction (the direction normal to bacterial body) and is restricted to move only in the forward direction (in the direction tangent to cell body). Only the leading tip of the cell in experimental videos appears to be free to move in any direction, thus bending upon collision and directing the turn, with the rest of cell body following the path traveled by the leading tip. Such movement in effect can be viewed as a cell moving on rails laid down by the leading pole. On the other hand, one can also observe lateral cell motion, either continuous or sudden jerks, when pushed sideways collectively by one or a group of cells [6, 7], as well as during cell flailing [1]. These observations suggest that a myxobacterium cell might be in two states, laterally restricted and unrestricted.

The mechanisms behind such lateral restriction are unclear. Focal adhesions, a part of proposed A-motility engine, could act as attachment points of the cell to the substrate [8], pushing the cell forward but restricting its lateral movement. The proposed two states of myxobacteria restriction would correspond to a cell attached to a substratum or detached. Alternatively, oriented polysaccharide chains in the slime that the cell secretes or the slime trails that a cell often follows [9] could create a larger drag in the lateral direction, thus restricting lateral movement of the cell.

In this study, by extending the previous mass-spring model in Chapter 2, we investigate the implications of lateral restriction of the cell movement to the alignment of a population of cells.

3.2. MODEL

To model a cell where only the leading tip (free part) can move laterally, but the rest of the cell body cannot (restricted part), we extended the model presented in Chapter 2 by assuming that the drag force in the direction normal to bacterial body in the restricted part is very large.

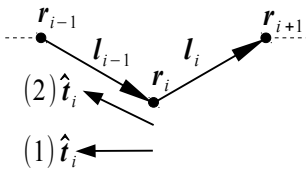

Figure 3.2: The direction tangent to bacterial body $\hat{\boldsymbol{t}}_i$ at particle position $\boldsymbol{r}_i$. In Chapter 2, $\hat{\boldsymbol{t}}_i$ was defined to point in the direction average between adjacent linear springs, $\boldsymbol{l}_i$ and $\boldsymbol{l}_{i+1}$, corrected for cell polarity, k^{e} (1). In this chapter, $\hat{\boldsymbol{t}}_i$ is defined to point to the particle in front of $\boldsymbol{r}_i$. In case of $k^{\mathrm{e}}=1$, it is the particle $\boldsymbol{r}_{i-1}$ (2).

Cell restriction. Using the notation from Chapter 2, if N_{f} is a number of particles in the free tip, for engine direction $k^{\mathrm{e}}=1$, the free tip would comprise particles $i=1,\ldots,N_{\mathrm{f}}$, while the remaining particles $i=N_{\mathrm{f}}+1,\ldots,N$ would form the restricted part. Conversely, in a cell with a reversed orientation, $k^{\mathrm{e}}=-1$, the free tip would comprise particles $i=N-N_{\mathrm{f}}+1,\ldots,N$. For particles in the free tip, the drag coefficient in the normal direction $\hat{\boldsymbol{n}}_i$ is $\zeta_i^{\mathrm{n}}=2\zeta^{\mathrm{t}}$ as in the original model, but for particles in the restricted part, we set an arbitrarily large number, $\zeta_i^{\mathrm{n}}=10^6\zeta^{\mathrm{t}}$.

In the present model, only the distributed engine is studied, given the recent evidence strongly supporting its existence [10]. Furthermore, in order for a bacterium to strictly follow the path laid by the leading pole and not to stall when the laterally restricted part travels a curved path, one needs the distributed engine force acting on a particle to point in the direction of the particle right in front of it (and not in the direction average between the segment in front of and behind the particle, as in the original model). Thus, for particles $i=2,\ldots,N-1$, the direction tangent to bacterial body $\hat{\boldsymbol{t}}_i$ is defined as the one of $-\boldsymbol{l}_{i-1}$ if $k^{\mathrm{e}}=1$ and as direction of $-\boldsymbol{l}_i$ if $k^{\mathrm{e}}=-1$ (Figure 3.2). For the cell ends, the directions are those of $-k^{\mathrm{e}}\boldsymbol{l}_i$ for particle $i=1$ and of $-k^{\mathrm{e}}\boldsymbol{l}_{i-1}$ for particle $i=N$. The normal direction $\hat{\boldsymbol{n}}_i$ is the tangential direction $\hat{\boldsymbol{t}}_i$ rotated by $\pi/2$.

A particle in the restricted part of the bacterium can become unrestricted (by setting its drag coefficient in the normal direction to $\zeta_i^{\mathrm{n}}=2\zeta_{\mathrm{i}}^{t}$) in two cases. First, following experimental observation where a group of cells is able to push a single cell laterally [7], a particle becomes unrestricted when the normal force acting on it exceeds a critical normal force, $F_i^{\mathrm{n}}>F_{\mathrm{c}}$. Second, in order to avoid stalling of bent cells due to discretization of a bacterium into a finite number of particles and linear segments, all particles comprising the angular spring i (i.e. particles i, $i+1$ and $i+2$) are unrestricted whenever it bends more than the critical angle, i.e. $\alpha_i>\alpha_{\mathrm{c}}=\pi/4$. As soon as the two conditions are not satisfied, a particle will become restricted again.

Collision response. The collision response algorithm presented in Chapter 2 was improved to avoid undesirable effects arising when contact forces are produced by adjacent segments, i.e. segments sharing the same endpoint. For example, in the situation shown in Figure 3.3A, contact forces between bacteria would be added twice, because according to the previous algorithm, segment *a* would be in contact with both segment *b* and *c*,

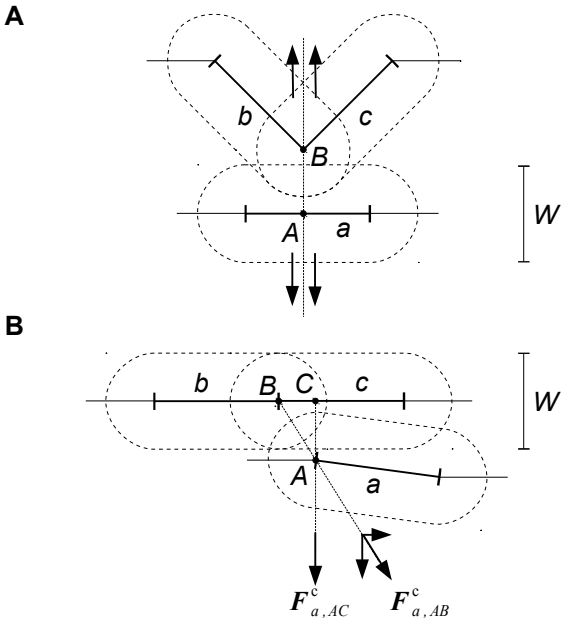

Figure 3.3: Issues of collision detection and response amended to the original model (Chapter 2). A. Double contact forces arise because two adjacent segments share the same endpoint. B. Friction forces arise when a segment is within contact distance with two adjacent segments, one of which makes contact with the end. $\boldsymbol{F}^{c}_{a,AC}$ is the collision force that acts on segment a due to segment c. $\boldsymbol{F}^{c}_{a,AB}$ is the collision force that acts on segment a due to segment c.

although there is only one contact point between bacteria. This implementation results in a contact twice as stiff compared to the contact where an end of the bacterium is involved. To avoid such unrealistic doubling, only one contact force is introduced in this situation. Because segments in a bacterium are ordered (i.e. the $P = 1$ end of one segment shares the same point with the $P = 0$ point of the next segment), contact forces are not introduced if, for the two segments $\boldsymbol{Q}_{ij}$ and $\boldsymbol{Q}_{kl}$, $P_1 = 0$ and $i \neq 1$ or $P_2 = 0$ and $k \neq 1$. The only exception to this rule arises when two adjacent segments on the same bacterium are not checked for collision, because they share a common point. Thus, when two contacting segments belong to the same bacterium and one of the segments is $i = 1$ with contact point $P = 0$ (a pole of the bacterium) and another segment is $i = 3$ with contact point $P = 0$, the collision forces are introduced.

Furthermore, in the situation depicted in Figure 3.3B, the end of segment *a* will be in contact with some non-end point of segment *c*, but also with the end of segment *b*. Contact between *a* and *b* would result not only in the desired normal contact forces on segments *a* and *b*, but also in forces in the tangential direction of bacteria. If bacteria moved in opposite directions, such friction forces would oppose relative movement of the two bacteria. Such situation can be especially relevant when bacteria are under large lateral stresses, that keeps them in the overlapped state. To overcome this undesirable ef-

fect, if the end of segment a makes a contact with the end of segment b, but also with the non-end point of segment c (adjacent to segment$b$),contact forces between a and b are not introduced. In situation of Figure 3.3B, this would leave only contact forces between segments a and c that are separating the two bacteria apart, the intended behavior.

Finally, in the improved algorithm, contact forces on particles $\boldsymbol{r}_i$ and $\boldsymbol{r}_{i+2}$ which were initially intended to limit an excessive bending for each angular spring in the original model in Chapter 2, were removed, because in case of $N > 3$ the algorithm is capable to resolve such excessive bending of angular springs without the need of this extra assumption.

Parameter values studied are the same as in Chapter 2, except for a stricter absolute tolerance $atol = 2.5 \times 10^{-13}$ m when integrating the ODE system of equations of motion (Equation (2.1)), T_R average set to 10 min and T_R standard deviation of $0.2T_R$. The number of particles in the free tip of a cell, N_f was chosen to be 3.

Analysis of results. We define the orientational stability of cells during two-cell collision simulations as $C_{t2} = (1/K)\sum_j [2\cos^2\theta(\boldsymbol{o}_j(t_i), \boldsymbol{o}_j(t_f)) - 1]$, where $\boldsymbol{o}_j(t_i)$ is the initial orientation of cell j, $\boldsymbol{o}_j(t_f)$ is the final orientation of cell j, and the number of cells is $K = 2$. Orientational stability, conceptually similar to orientation autocorrelation function presented in Chapter 2, shows how similar, on average, the initial and final orientation of the cell is during two-cell collision.

3.3. RESULTS

We explored the alignment of a model myxobacteria population of 500 cells for different values of cell bending stiffness, B, and critical lateral restriction force (i.e. the force necessary to overcome lateral restriction), F_c. It was found that lateral restriction has a marked effect on the alignment of a population of cells.

LATERAL RESTRICTION IMPROVES THE ALIGNMENT OF A POPULATION

Figure 3.4 shows the alignment of a population for different values of cell bending stiffness and critical lateral restriction force F_c. To determine whether lateral restriction affects the alignment of the population, a 2-sample t-test was performed to find points on the graph where the alignment of laterally restricted cells and non-restricted cells of the same bending stiffness is significantly different (Figure 3.4, stars). The results show that a population of laterally restricted cells with critical restriction force $F_c \geq 5\,\text{pN}$ aligns better than non-restricted cells for bending stiffness larger than $B = 1 \times 10^{-23}\,\text{J·m}$ (Figure 3.5, Movie 3.1 and 3.2). Alignment of laterally restricted cells with very small critical restriction force $F_c \leq 2\,\text{pN}$ does not differ from non-restricted cells. The alignment of cells with a high degree of lateral restriction $F_c = 200\,\text{pN}$ decreases again as the bending stiffness becomes very large $B > 1 \times 10^{-21}\,\text{J·m}$. The effect occurs because the rigid tip of the cell cannot bend and initiate cell turning. Combined with the inability of the rest of the cell body to move laterally, it results in the inability of a rigid cell to turn and resolve collisions and cell stalling upon collision (Movie 3.3 and 3.4). Interestingly, lateral

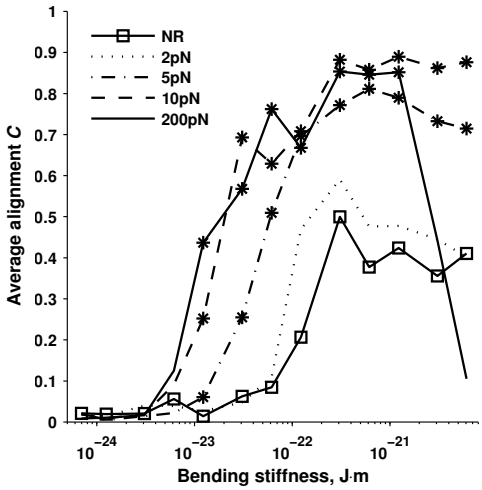

Figure 3.4: Alignment of a population of 500 cells at 4h for different values of cell bending stiffness and critical lateral restriction force F_c from 2 to 200pN. Every point is the average of 5 simulations with different random initial population configurations. Stars mark the points where the alignment is significantly different ($P < 0.05$) from the alignment of non-restricted cells (squares) of the same bending stiffness, as found by 2-sample t-test.

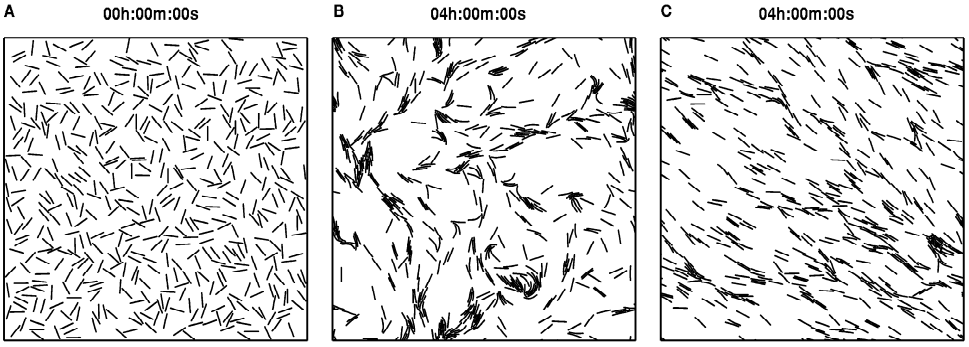

Figure 3.5: Spatial distribution of a population of 500 flexible cells ($B = 3 \times 10^{-23}$ J·m) at 0 h (A) and 4 h (B, C). Initially, the cells have random positions and orientations. The size of the domain is 100 µm, cell density in the domain is 5×10^6 cm^{-2}. (B) Unrestricted cells. (C) Laterally restricted ($F_c = 200$ pN) cells.

restriction has no effect on the alignment of very flexible cells 7×10^{-25}–6×10^{-24} J·m, which remained non-aligned in all studied conditions.

POPULATION OF FLEXIBLE CELLS ALIGNS BETTER DUE TO IMPROVED LOCAL ALIGNMENT OF LATERALLY RESTRICTED CELLS

Alignment or non-alignment of cells in the population depends on numerous two-cell and many-cell collisions during cell movement. In order to better understand how lat-

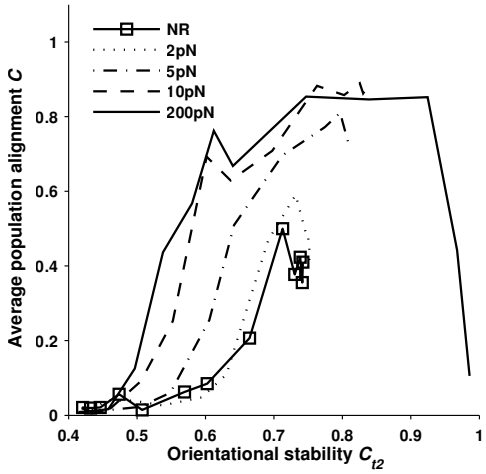

Figure 3.6: Average population alignment C as a function of orientational stability of cells during two cell collisions C_{t2} for different values of critical restriction force F_c from 2 to 200 pN. (NR) Non-restricted cells.

eral restriction of cells improves the alignment of the whole population, a series of two-cell simulation runs were performed as described in Chapter 2 and the ability of a population to align was correlated with the behavior of cells in two-cell collisions.

In Chapter 2 we showed, that non-restricted rigid cells are able to maintain their orientation for longer times, compared to flexible cells. This was suggested to be the reason for the better ability of the whole population to align, despite better local alignment of flexible cells during two-cell collisions. However, in that study, the conclusion was based on a temporal orientation correlation function of cells in a population (Figure 2.8). This raised the question about the cause and effect: is better orientational stability of cells the reason for the population alignment, or are cells more orientationally stable because the population happens to align due to other reasons? Figure 3.6 clarifies the issue: given a particular lateral restriction value, the population alignment C (defined in Chapter 2) increases as orientational stability of cells in two-cell collisions C_{t2} is improved due to increasing cell bending stiffness. It also shows that the ability of the population to align decreases when the orientational stability of cells becomes too large, consistent with our previous suggestion in Chapter 2. Further, Figure 3.6 shows that orientational stability of cells is not the single factor determining population alignment, because for the same value of orientational stability C_{t2} the alignment of the population can be very different for non-restricted and laterally restricted cells.

In a collision of two non-restricted rigid cells, their orientational stability does not depend on the initial site of contact on the cell: cells will change orientation by roughly the same small amount, regardless where the collision occurs (Figure 3.7). In contrast, contacts on most of the body of a flexible cell does not produce any change in orientation of that cell ($C_{t2} \rightarrow 1$), but the contact close to the leading tip (small value of the position in the cell) changes the orientation of the cell drastically (C_{t2} is between 0.5–

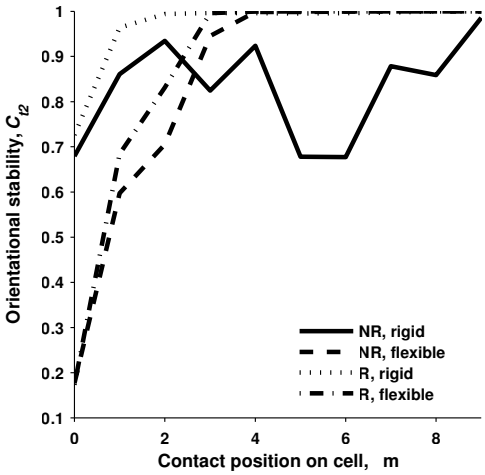

Figure 3.7: Orientational stability C_{t2} of cells during two-cell collision simulations as a function of the site of initial cell contact, expressed as a distance from the leading particle along the cell length. NR, non-restricted cells; R, restricted cells, $F_c = 20$ pN; Flexible cells, $B = 3 \times 10^{-24}$ J·m. Rigid cells, $B = 1 \times 10^{-21}$ J·m.

0.6). These results suggest that, in the model, poor orientational stability of a flexible cell, in comparison with the rigid one, is determined by collisions close to its leading pole. From Figure 3.7 it can be concluded, that in a head-to-lateral collision of flexible cells, the head-contacting cell would turn, but the laterally contacting cell would remain on its previous course. If contact points on both cells are close to their leading poles, both cells would move circularly and change orientations by a large amount, as shown in Figure 2.3B in Chapter 2. Lateral restriction appears to have a similar effect on cells as very large flexibility: for laterally restricted cells, any contact beyond the 3rd particle of a simulated myxobacterium cell (i.e. beyond the flexible tip) produces no lateral cell movement and thus no change in cell orientation (Figure 3.7, compare solid and dotted lines). Since C_{t2} profiles of non-restricted very flexible cells and all laterally restricted cells are similar, lateral restriction applied to very flexible cells has no effect on their movement, and thus on the alignment of cell population (Figure 3.4).

Simulation results were further analyzed to establish whether lateral restriction improves population alignment by improving cell orientational stability during two-cell collisions. For each bending stiffness value, it was analyzed whether better population alignment is correlated with the increased orientational stability during two-cell collisions. Remarkably, population alignment does correlate well ($\rho > 0.5$, $P < 0.001$) with orientational stability during two-cell collision only for large bending stiffness values ($B \geq 3 \times 10^{-22}$ J·m, Figure 3.8). However, for bending stiffness values where the improvement in the population alignment of laterally restricted cells is the most pronounced 1×10^{-23}–1×10^{-22} J·m, population alignment correlates very well with the better ability of two cells to align upon contact (Figure 3.8). In other words, cells with intermediate flexibilities align better locally when they are laterally restricted, and that appears to favor the alignment of the whole population. Figure 3.1 illustrates that laterally re-

stricted cells appear to align better (faster) than the non-restricted cells. For very rigid cells $B \geq 3 \times 10^{-21}$ J·m, the dependency of population alignment on C_{t2} and C_2 is non-linear; due to very high orientational stability of cells with $F_c = 200$ pN (data points maked with circles in Figure 3.8; see also Figure 3.4), cells are unable to resolve contacts and stall (Movie 3.4). Interestingly, if for these cell bending stiffness values, the results with $F_c = 200$ pN are removed from correlation analysis as an extreme case (i.e., if only the results with F_c ranging from 0 to 20 pN are included), population alignment increases with increasing orientational stability of cells, but decreases with increasing local alignment. It suggests that for very rigid cells, orientational stability and local alignment are inversely correlated (i.e. increasing orientational stability makes local alignment more difficult), and therefore, orientational stability appears to be the primary factor determining population alignment.

3.4. DISCUSSION

Visual observations of moving myxobacteria shows that during collisions, a cell often does not bend if pushed laterally in the middle of cell body, although it appears rather flexible when moving forward [5]. However, a previous study on the mechanical aspects of gliding myxobacteria (Chapter 2) indicated that colliding flexible rods would be able to produce a bend in a cell that is pushed sideways. This contradiction between visual observations and numerical model results suggests that there might be a mechanism in place to restrict the lateral movement of myxobacteria cells, and allow only forward movement of the cell. This mechanism could include focal adhesions that act as attachment points of the cell to the substrate, a part of proposed A-motility engine [8], or cell-secreted slime with oriented polysaccharide chains that could create an anisotropic drag. We have extended the mechanical model for gliding of myxobacteria presented in Chapter 2 to investigate the effect of lateral restriction of cellular movement on the alignment of a population of model myxobacteria, without assuming any particular mechanism for lateral restriction. The numerical results show, that lateral restriction improves the alignment of the population of cells. In Chapter 2 we predicted that given a theoretically estimated bending stiffness value of *M. xanthus*, $B = 3 \times 10^{-23}$ J·m [1], a population of non-restricted cells would not be able to align on the spatial scale observed in experiments (Movie 3.1). However, the results obtained in the current study indicate that a population of laterally restricted cells would show good alignment for this bending stiffness value, thus reconciling the model results with the experimental observations (Movie 3.2). Interestingly, for the intermediate bending stiffness values 1.2×10^{-23}–6.2×10^{-23} J·m, the improvement of alignment is correlated with better ability of two colliding cells to align (Figure 3.8), but not with their orientational stability. Overall, this study suggests that the restriction of lateral cell movement, whether due to attachment of cells to the substratum or other mechanisms, can serve as a way to increase the alignment of the population of cells. Our results predict that lateral restriction force should be at least 50–100 pN per cell to have an effect on the alignment of the population.

The simulations also show, that a flexible cell tip unrestricted in its movement is necessary for cell turning during the collision, with the rest of the cell body following the

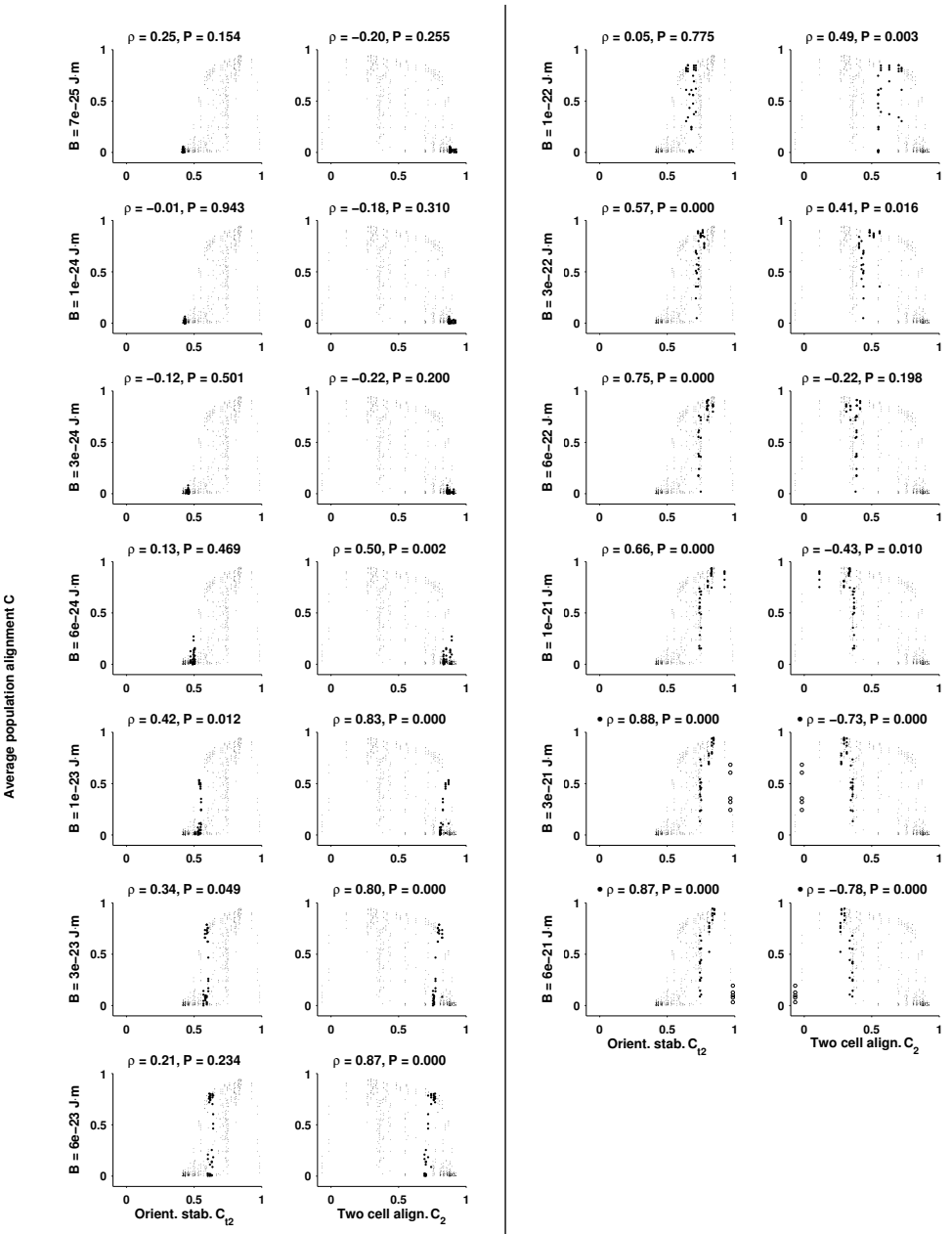

Figure 3.8: Average population alignment as a function of orientational stability and local alignment in two cell collision simulations. (Small dots, large dots and circles). Simulation results for all bending stiffness and F_c values. Each population simulation with a particular B and F_c value was repeated 5 times with different initial population configuration. (Large dots) Simulations of cells with a particular bending stiffness value (shown on the left of each plot) with different levels of lateral restriction. Correlation coefficient and P-value of the data is shown above the graph. (Circles) Simulations results for very rigid cells ($B = 3 \times 10^{-21}$ J·m and $B = 6 \times 10^{-21}$ J·m) with very high degree of lateral restriction $F_c = 200$ pN. These points were removed from linear correlation coefficient calculation.

path laid out by the leading pole. Rigid laterally-restricted cells are unable to turn and often stall upon collision. In other words, the simulations suggest that laterally restricted cells must be flexible enough to resolve contacts without stalling. To determine the extent of lateral restriction and its role in cell population dynamics, it would be important to experimentally measure the forces necessary to push the cell laterally. To better understand the mechanics of collisons, one could also observe a number of two cell collisions and determine how the cell alignment and orientational stability depends on the site of initial contact.

3.A. SUPPLEMENTARY MOVIES

Movie 3.1. Dynamics of a population of non-restricted flexible $B = 3 \times 10^{-23}\,\mathrm{J{\cdot}m}$ cells.

Movie 3.2. Dynamics of a population of laterally restricted ($F_c = 200\,\mathrm{pN}$) flexible ($B = 3 \times 10^{-23}\,\mathrm{J{\cdot}m}$) cells.

Movie 3.3. Dynamics of a population of non-restricted rigid ($B = 6 \times 10^{-21}\,\mathrm{J{\cdot}m}$) cells.

Movie 3.4. Dynamics of a population of laterally restricted ($F_c = 200\,\mathrm{pN}$) rigid ($B = 6 \times 10^{-21}\,\mathrm{J{\cdot}m}$) cells.

REFERENCES

[1] C. W. Wolgemuth, *Force and flexibility of flailing myxobacteria,* Biophysical Journal **89**, 945 (2005).

[2] C. Wolgemuth, E. Hoiczyk, D. Kaiser, and G. Oster, *How myxobacteria glide,* Current Biology **12**, 369 (2002).

[3] A. E. Pelling, Y. Li, S. E. Cross, S. Castaneda, W. Shi, and J. K. Gimzewski, *Self-organized and highly ordered domain structures within swarms of Myxococcus xanthus,* Cell Motility and the Cytoskeleton **63**, 141 (2006).

[4] H. Reichenbach, H. H. Heunert, and H. Kuczka, *Archangium violaceum (Myxobacteriales) - Schwarmentwicklung und Bildung von Protocysten,* Film E 777, 1:55-2:25 (Institut für den Wissenschaftlichen Film, Göttingen, 1968).

[5] K. Grimm, H. K. Galle, and H. H. Heunert, *Archangium violaceum (Myxobacteriales) - Bewegungsaktivität und Kolonieform,* Film E 1588, 3:00-3:15 (Institut für den Wissenschaftlichen Film, Göttingen, 1969).

[6] H. Reichenbach, H. H. Heunert, and H. Kuczka, *Chondromyces apiculatus (Myxobacteriales) - Schwarmentwicklung und Morphogenese,* Film E 779, 4:15-5:15 (Institut für den Wissenschaftlichen Film, Göttingen, 1965).

[7] H. Reichenbach, H. H. Heunert, and H. Kuczka, *Archangium violaceum (Myxobacteriales) - Schwarmentwicklung und Bildung von Protocysten*, Film E 777, 2:45-2:55 (Institut für den Wissenschaftlichen Film, Göttingen, 1968).

[8] D. Kaiser, *Are there lateral as well as polar engines for A-motile gliding in myxobacteria?* Journal of Bacteriology **191**, 5336 (2009).

[9] R. P. Burchard, *Trail following by gliding bacteria,* Journal of Bacteriology **152**, 495 (1982).

[10] B. Nan, J. Chen, J. C. Neu, R. M. Berry, G. Oster, and D. R. Zusman, *Myxobacteria gliding motility requires cytoskeleton rotation powered by proton motive force,* Proceedings of the National Academy of Sciences **108**, 2498 (2011).

4

EFFECT OF REVERSAL TIME ON CELL MOVEMENT PATTERNS IN MODEL MYXOBACTERIA POPULATIONS

4.1. INTRODUCTION

The pattern of myxobacterium cell movement consists of intervals of active gliding, stopping, and occasional reversals of direction [1, 2]. A cell reverses direction without turning, just by switching leading and trailing poles. Vegetative swarming cells reverse their direction of gliding once every 7-10 min, thus showing a typical oscillatory pattern of cell movement [3]. When exposed to starving conditions, myxobacteria begin to aggregate and form a fruiting body. During the course of development, gliding speed of cells and the duration of gliding intervals increase, while the duration of stop intervals and reversal frequency decrease. The net effect is that the distance traveled by the cell increases and at the final stages of fruiting body development the cells are moving essentially unidirectionally into the aggregation centers [2].

The biological function of myxobacteria cell reversing is not well understood. It has been suggested that reversals are necessary for net directed movement of swarms towards chemoattractants, by biasing the gliding intervals of cells into a particular direction (biased random walk) [4]. However, chemotaxis in individual myxobacteria cells remains controversial [5]. Coordinated cell reversals are observed during the formation of traveling waves (ripples), presumably as an efficient way to scavenge non-diffusable substances from the surface under starving conditions [6]. A computational study by Wu et al. suggests that reversal allows myxobacteria to swarm, because non-reversing cells block each other's movement and get stuck in traffic jams [7].

One of the systems regulating reversals in *Myxococcus xanthus* is the Frz ("frizzy") chemosensory system, homologous to the chemotaxis system of *E. coli* [8]. Different

Frz mutants can be either hypo-reversing (i.e. exhibit a decreased reversal frequency) or hyper-reversing (exhibit and increased reversal frequency). Colonies of hyper-reversing mutants (reversal time 1-2min) have a phenotype similar to colonies of non-motile cells, i.e. they are sharp-edged and non-swarming, because cells are continuously traveling back and forth with no net movement. Hypo-reversing mutants (reversal time 34min) are able to swarm, albeit slower than wild type cells, but are defective in fruiting body formation; instead of rounded well defined fruiting bodies, they form "frizzy" filaments [5, 9, 10]. Interestingly, no mutant that is still motile but completely unable to reverse has ever been isolated [7]. These studies suggest that cell reversals might be important not only during the vegetative swarming phase, but also during the developmental process.

In this study, by means of a computational mass-spring model developed in Chapter 2, we study how cell reversals affect the patterns formed in the population of cells that glide on a substratum and mechanically interact.

4.2. MODEL AND METHODS

Model parameters. The model used for the simulations is presented Chapter 2, with the modification of collision response algorithm described in Chapter 3. Simulations were performed with i) high (4×10^7 cm^{-2}) and low (5×10^6 cm^{-2}) population density of 1000 cells with $N = 10$ particles per cell and ii) low density populations of 1000 and 10000 cells with $N = 2$ particles per cell (perfectly rigid rods) were performed. When not noted otherwise, the simulations were performed with collision stiffness $k^c = 10^{-2}$ N·m^{-1}. The variable under study was the reversal time T_R. The standard deviation of T_R was chosen to be $0.2T_R$. For simplicity, cell stops and the variations in cell speed were not considered. For high-density population simulations, the effect of collision stiffness k^c on cell movement was also studied. k^c controls how much cells can overlap during the contact. Five cell bending stiffness values B were considered: 7×10^{-25} J·m ("very flexible"), 6×10^{-24} J·m ("flexible"), 6×10^{-23} J·m ("rigid"), 6×10^{-22} J·m ("very rigid") and 6×10^{-21} J·m ("extremely rigid").

Cell movement pattern analysis. To analyze cell movement, four measures were used: average cell speed, global population alignment, average maximum cluster size and cluster stability. For all measures, the results of the first hour of the simulation were discarded to allow the population to reach a quasi-steady state, and the average measure for the rest of the simulation was calculated.

Average cell speed was calculated by averaging all speeds of all cells at every time point. In the results section, it is presented as normalized to equilibrium speed of a bacterium v_b. **Global population alignment** was quantified using the same measure C as in Chapter 2, except that the orientation of the cell was here defined as the orientation of the leading segment, i.e. $\boldsymbol{o}_j = \boldsymbol{r}_{1j} - \boldsymbol{r}_{2j}$ if $k_\mathbf{e} = 1$, and $\boldsymbol{o}_j = \boldsymbol{r}_{Nj} - \boldsymbol{r}_{(N-1)j}$ if $k_\mathbf{e} = -1$.

The extent of **cell clustering** in the population was evaluated as follows. Cell clusters were identified as in Starruß *et al.* [11]. A cluster can be defined as a group of tightly spaced cells that move roughly in the same direction. Thus, two cells were considered to belong to the same cluster, if the separation between them was smaller than $W/4$

(i. e. the smallest distance between all pairs of segments of both cells is smaller than $W + W/4$, with the periodic boundary taken into account) and the angle between their orientations does not exceed $\pi/6$. Applying these criteria iteratively for all cell pairs, all cells belonging to the same cluster are identified. At each time step of the simulation, all clusters are detected and a maximum cluster size at that time step is found. As a measure of cell clustering in this study, we use the average maximum cluster size during the period of 1 to 6 h of the simulation, normalized by the population size. One has to note that although a cluster is usually understood as a group of cells that is separated from other cell groups in space, the above criteria can also be applied to high cell density situations, where two adjacent groups of aligned cells can form separate clusters due to differences in cell orientations. Furthermore, the definition of a cluster does not imply that the whole cluster of cells must move in the same direction. Since only two adjacent cells in the cluster must be oriented similarly, a swirling stream of cells, for example, will satisfy the definition of a cluster too.

To evaluate **cluster stability**, one needs to track the progress of a cluster in time by identifying a particular cluster in two consecutive time steps, bearing in mind the complexity of how clusters can split or join together during the time step. A particular cluster was identified to be the same in two consecutive time steps with the following procedure. Consider a set of clusters $\mathbf{D}_1$ at time t and a set of clusters $\mathbf{D}_2$ at time $t + \Delta t$, where a cluster itself is a set of bacteria. For all individual pairs of clusters D_1 and D_2 (from $\mathbf{D}_1$ and $\mathbf{D}_2$ respectively), the cluster similarity measure n_i/n_u is computed, where n_i is the size of intersection between cluster D_1 and D_2, and n_u is the size of the union of the two clusters. The cluster similarity measure shows what fraction of the bacteria the two clusters share. If, for all clusters from $\mathbf{D}_2$, a cluster D_1 has the largest similarity measure with a cluster D_2, and cluster D_2 has the largest similarity measure with a cluster D_1 for all clusters of D_1, the cluster D_2 is considered to be the same as cluster D_1. If this is not the case, the cluster D_2 is designated as a newly formed cluster. In such a way the progress of a particular cluster in time can be tracked, until it dissipates or joins with other clusters. In the figures and movies presented here, each color represents a particular cluster tracked in this way. Finally, cluster stability is defined as the average time that a bacterium spends in one particular cluster, normalized by the simulation duration.

4.3. RESULTS

HIGH-DENSITY CELL POPULATIONS

First the simulations of a high density population are discussed, where cells are initially densely packed and aligned, but with either of the two randomly selected orientations along the alignment axis (i.e. either oriented towards +x or –x, Figure 4.1A). We studied how the patterns of population movement depend on whether cells are reversing or non-reversing (T_R), on cell bending stiffness (B) and contact stiffness between cells (k^c). Contact stiffness is expected to have a profound effect on cell movement in dense populations, because it controls how easily a cell can squeeze through small spaces in between other cells.

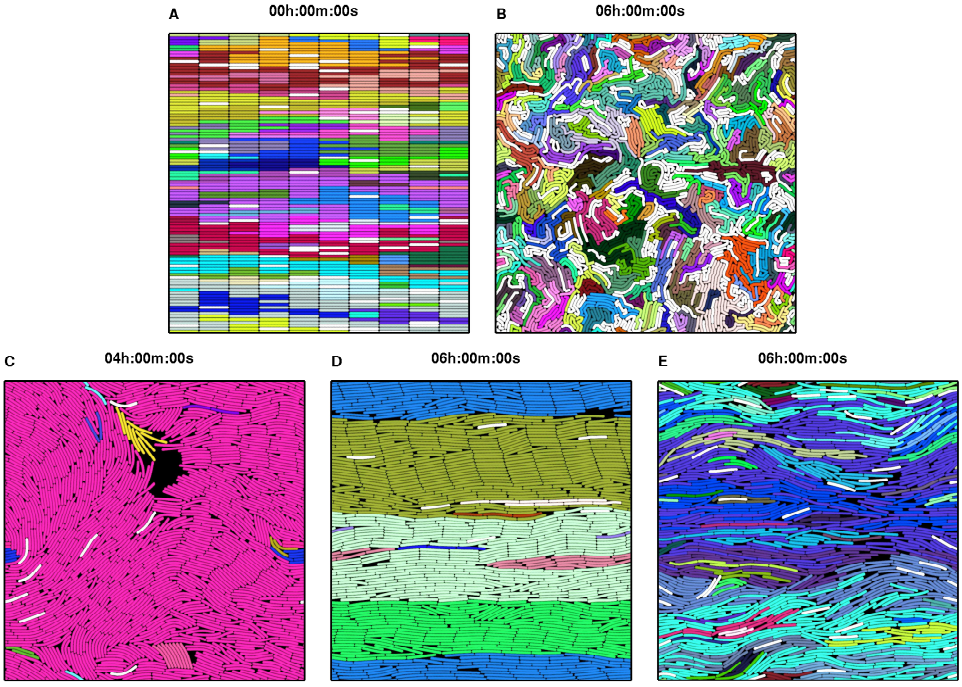

Figure 4.1: Cell patterns in high-density populations. Adjacent cells with the same color belongs to the same cluster, single cells (not belonging to any cluster) are shown in white. (A) Initial configuration. (B) A population of flexible non-reversing cells with hard contacts ($k^c = 0.01\,\mathrm{N{\cdot}m^{-1}}$) at $t = 6\,\mathrm{h}$. (C) A population of rigid non-reversing cells with hard contacts ($k^c = 0.01\,\mathrm{N{\cdot}m^{-1}}$) at $t = 4\,\mathrm{h}$. (D) A population of rigid non-reversing cells with soft contacts ($k^c = 0.002\,\mathrm{N{\cdot}m^{-1}}$) at $t = 6\,\mathrm{h}$. (E) A population of rigid reversing cells with soft contacts ($k^c = 0.002\,\mathrm{N{\cdot}m^{-1}}$) at $t = 6\,\mathrm{h}$.

Flexible cells and reversing cells move slower. Simulation results indicate that flexible cells, either non-reversing (Figure 4.2A) or reversing (Figure 4.2B), move slower than rigid cells. Figure 4.1B and Movie 4.1 illustrate that flexible cells do not have enough rigidity to pass each other and therefore entangle, blocking one another's path, whereas rigid cells are able to better maintain their linear shape, thus allowing cells to align side-by-side (Figure 4.2C and 4.2D, Movies 4.2 and 4.3, also shown in Chapter 2 for reversing cells only). Further, softer contacts between cells (smaller values of k^c) allow them to move faster, whereas stiff contacts slow down cell movement. This is understandable, because softer contacts allow for more overlap between cells and therefore cells are able to easier squeeze through the small spaces between other cells to continue moving. This is clearly visible by comparing Movies 4.2 - hard contacts, $k^c = 0.01\,\mathrm{N{\cdot}m^{-1}}$ - with Movie 4.3 - soft contacts, $k^c = 0.002\,\mathrm{N{\cdot}m^{-1}}$). Finally, on average, non-reversing cells move faster than the reversing cells, and this is especially notable for rigid and very rigid cells. We suggest that this is caused by the fact that non-reversing cells create more order, where

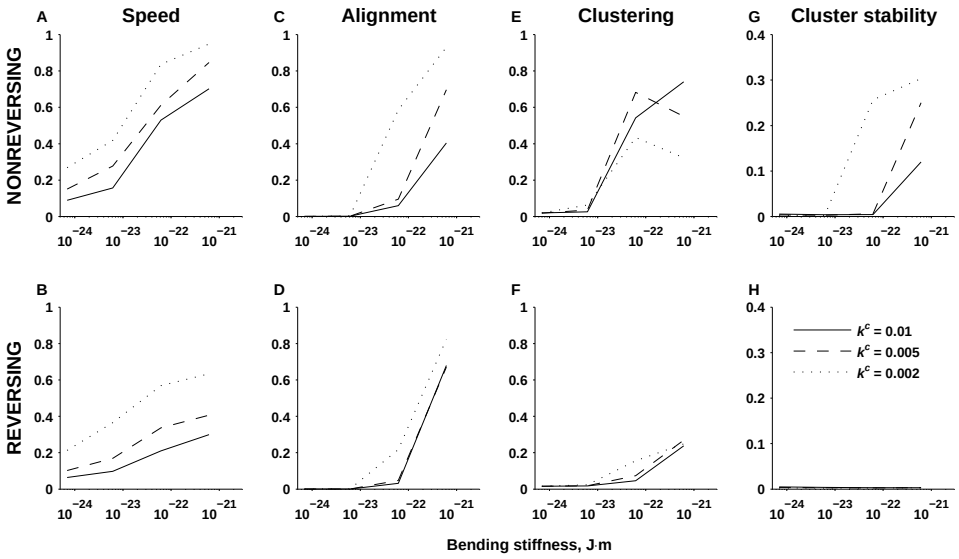

Figure 4.2: Speed, alignment, clustering and cluster stability in high-density populations of cells as a function of cell bending stiffness, contact softness and reversal or non-reversal. For every studied value of cell bending stiffness a measure average of 3 simulations with different initial cell configurations is plotted.

cells with similar orientations can move together in a similar direction, without blocking each other. Reversing cells, however, would break such an order and will often interfere with movement of other cells (compare Figure 4.1C and D - non-reversing cells - with Figure 4.1E - reversing cells - and the corresponding Movies 4.2 and 4.3 with 4.4).

Order created by non-reversing cells. Since very flexible and flexible cells ($B < 1 \times 10^{-23}$ J·m) (either reversible of non-reversible) barely move (Figure 4.2A,B), do not align (Figure 4.2C,D) or are incapable to produce any sizable clusters (Figure 4.2E,F), we will further discuss only cell alignment, clustering and cluster stability for rigid and very rigid cells.

It appears that **non-reversing cells with hard contacts** exhibit much better clustering behavior than reversing cells (Figure 4.2E, solid lines): the cell clustering is approaching 1, i.e. almost the whole population moving collectively (Figure 4.1C and Movie 4.2). Interestingly, the global alignment of the population in this case is relatively small (Figure 4.2C). Large clustering value with small global alignment is an indication of large non-linear cluster formation, i.e. swirls. However, the stability of those clusters is poor, as can be seen from Figure 4.2G, indicating temporary, constantly changing swirling behavior (Movie 4.2). Conversely, **non-reversing cells with soft contacts** (Figure 4.2, dotted lines) show medium clustering, but a large global alignment value (close to 1 for very

rigid cells), indicating that cells sorted themselves out into small parallel streams, moving in opposite directions (Figure 4.1D and Movie 4.3). Furthermore, the streams are persistent, as shown by a large cluster stability value (Figure 4.2G). It appears that cells with soft contacts moving in opposite directions can easily pass between other cells and therefore form and maintain oppositely moving streams. Cells with hard contacts, in contrast, are unable to easily pass one another, engage in a tug-of-war until the dominant direction wins and cells end up moving collectively as one large cluster (the clustering index close to 1) in roughly one direction (Movie 4.2). Cells with contacts of intermediate hardness ($k^c = 0.005\,\mathrm{N{\cdot}m^{-1}}$) show signs of both types of behavior (Movie 4.5). Overall, it appears that the decrease of contact stiffness increases global alignment of the population, decreases the size of clusters, but makes the clusters more stable. In other words, as the contact stiffness decreases, cells from non-linear swirling clusters gradually change into smaller, but more stable linear clusters.

Reversing cells form only small clusters regardless of the contact stiffness (small clustering values in Figure 4.2F). Nevertheless, high global alignment values are reached (Figure 4.2D). This behavior is similar to non-reversing cells with soft contacts (Figure 4.2 E and C), suggesting the presence of parallel streams. However, in contrast to non-reversing cells with soft contacts, the stability of clusters of reversing cells is almost zero (Figure 4.2H). This lack of cluster stability is expectable: since a cluster, by definition, is a group of cells traveling roughly in the same direction, for a stable cluster to exist, cells cannot reverse often, unless their reversal is coordinated. Because the reversal is random in this model, reversing cells would break existing clusters without allowing them to grow to a large size, resulting in less ordered system.

In summary, cells in the high-density simulations show four types of behavior: random cell movement without any observable order (all flexible and very flexible cells, Figure 4.1B and Movie 4.1), large non-linear (swirling) unstable clusters (rigid and very rigid non-reversing cells with large contact stiffness, Figure 4.1C and Movie 4.2), small parallel stable streams (rigid and very rigid non-reversing cells with small contact stiffness, Figure 4.1D and Movie 4.3) and small parallel unstable streams (rigid and very rigid reversing cells, Figure 4.1E and Movie 4.4).

LOW-DENSITY POPULATIONS OF CELLS

Optimum reversal time for global alignment. In the previous section, either non-reversing or reversing ($T_R = 10\,\mathrm{min}$) cells were studied. In order to examine how the population behavior changes for intermediate values of reversal times, a low-density simulation of 1000 cells with hard contacts were performed starting with a distribution of randomly oriented cells (Figure 4.3A). Consistent with the results of the previous section, very flexible and flexible cells are not only unable to globally align, but also cannot form large clusters for any reversal time value (Figure 4.4A). While the inability of flexible and very flexible cells for alignment or clustering in high density population can be explained by their poor mobility due to crowdedness, in low-density simulation cells on average move close to their equilibrium speed v_b. Therefore, the inability of these cells to form stable clusters can be explained by the same reason as their inability to align

(see Chapter 2). In order for clusters to be stable, cells in the cluster need to move with roughly the same orientation, whereas flexible contacting cells tend to change their orientation drastically, thus breaking the cluster (Movie 4.6).

Furthermore, all three types of rigid cells (rigid, very rigid and extremely rigid) show a narrow peak of *global alignment* values around reversal time of 5–10min (Figure 4.4A, Figure 4.3B, Movie 4.7). Interestingly, the optimal alignment range appears to depend on the cell bending stiffness, with very rigid cells showing best alignment. The decrease or increase of bending stiffness from a "very rigid" value results in impaired alignment, suggesting the existence of an optimum bending stiffness value for global cell alignment. *Clustering* increases steadily with the increasing cell reversal time, with non-reversing very rigid cells forming large clusters comprising most of the population in the computational domain (Figure 4.3C, Movie 4.8). Related to the very high clustering value, non-reversing cells also show large alignment values in addition to the narrow peak around $T_R = 10\,\text{min}$. For non-reversing cells, very rigid cells also appear to be optimal for cluster formation. This is consistent with our suggestion in Chapter 2, that in order for a population to align, a cell must have the ability to change its orientation, but not too much. Too small orientational stability will make the cells to "forget" their previous orientation upon contact. Too large an orientational stability (like the extremely rigid cells simulated) impairs their ability to "negotiate" a common orientation upon contact. For example, one can observe that even with very rigid cells, the clusters can turn and swirl, and slightly curved cells inside the clusters respond to change in cluster orientation (Figure 4.3C, Movie 4.8). Extremely rigid cells, however, cannot bend and external forces on a cluster would often break the cluster due to inability of cells to change their orientation and follow the changing cluster orientation (Figure 4.3D, Movie 4.9). Overall, the behavior of non-reversing cells in low-density populations is consistent with that of cells with hard contacts in high-density population, showing high clustering and medium alignment values.

Cell movement patterns on a larger spatial scale were also investigated in a low-density population of 10000 perfectly rigid cells (i.e. with $N = 2$ particles per cell). Initially the cells were distributed randomly on the substratum (Figure 4.3E). Reversing cells (T_R from 2 min to 15 min appear to form large domains of well aligned spatially segregated cells (Figure 4.3F-I, Movies 4.10-4.13), with growing empty spaces between the domains as the reversal time increases. Within the domain, cells appear to travel in both directions along the alignment axis. These patterns could not be observed in a small domain with very rigid cells (Figure 4.3B, Movie 4.7). At $T_R = 20\,\text{min}$, small clusters begin to form and the large scale alignment is lost (Figure 4.3J, Movie 4.14). Further increase in reversal time results in increasing cluster formation, as in a small domain (Figure 4.3K-L, Movie 4.15-4.16). Interestingly, the optimum reversal time value is shifted towards larger values, compared to a small domain, the maximum being at $T_R = 15\,\text{min}$ (Figure 4.4C, dashed line). The difference is not due the larger domain size, because 1000 perfectly rigid cells in a small domain also show the peak of $T_R = 15\,\text{min}$ (Figure 4.4C, solid line). The absolute value of the peak is smaller in a large domain due to larger number of cells involved. The only difference between the simulations is the number of segments per

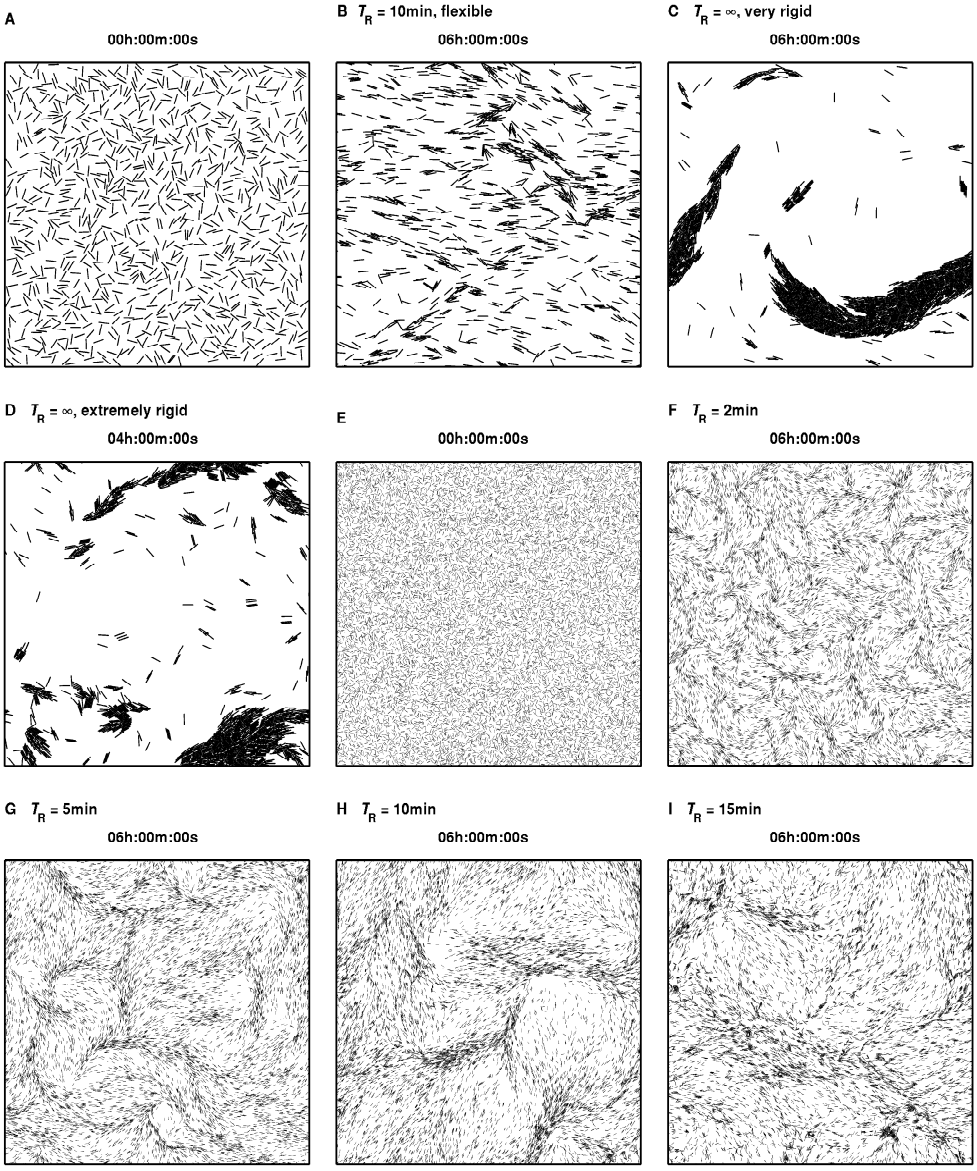

Figure 4.3: Cell patterns in low-density populations. (A-D) A population of 1000 very rigid cells. (A) initial configuration (B) Flexible reversing cells after 6h; (C,D) very rigid and extremely rigid non-reversing cells after 6h (E-L) A population of 10000 perfectly rigid rods. (E) Initial configuration. (F-K) Population configuration after 6h for increasing reversal times.

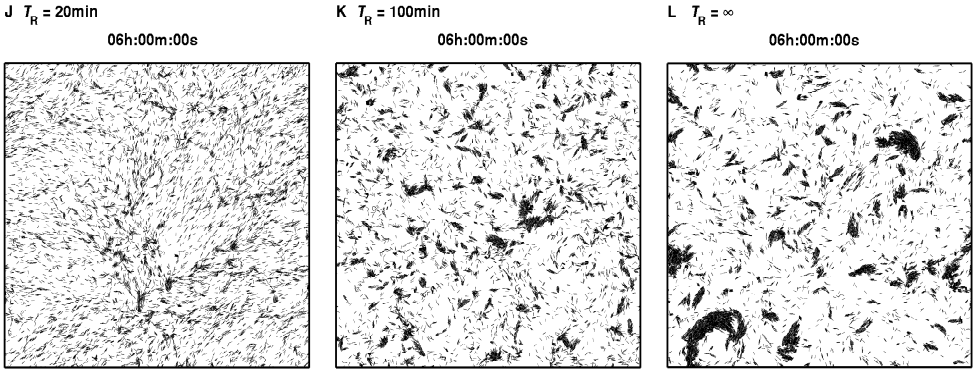

Figure 4.3: Continued.

cell: 9 segments for extremely rigid cells and only one segment for perfectly rigid cells. Using 9 segments per cell results in much larger number of contact points between cells (because contacts are resolved between segments in this model) compared to only one possible contact point between perfectly rigid cells. These results suggest that contact intensity between cells in the simulations also has an effect on cell alignment dynamics.

4.4. DISCUSSION

This study investigated how reversal or non-reversal of model myxobacteria cells affects the movement patterns of the whole population, for cells with different flexibility and contact softness.

A computational study by Wu *et al.* [7] suggests that in dense populations, non-reversing cells within a swarm get jammed and block each other's movement, while the reversal allows cells to swarm [7]. The results of our study show the opposite, i.e. that the non-reversing cells in dense populations move faster than the reversing cells, due to more order in non-reversing cell population. This effect is most prominent for rigid and very rigid cells (Figure 4.2). Within the range of parameters studied, complete stalling of cells was never observed. Experimentally observed increase of cell speeds during cell aggregation and fruiting body development [1, 2] is consistent with the increased order and less interference ("traffic jams") between cells that would result from cells switching from oscillatory to unidirectional movement. Furthermore, the most important factors affecting average cell speed in our study were cell flexibility and contact stiffness. Flexible cells entangled and blocked one another's movement, whereas rigidity increased their ability to squeeze through narrow spaces between other cells. Similarly, softer contacts allowed cells to overlap more thus leaving more space for movement and allowing cells to easier slip past one another. The reasons for differences in the conclusions reached in this study and those from Wu et al. are still unclear. One reason for the discrepancy could be that the study of Wu et al. simulated several thousands of cells in a different computa-

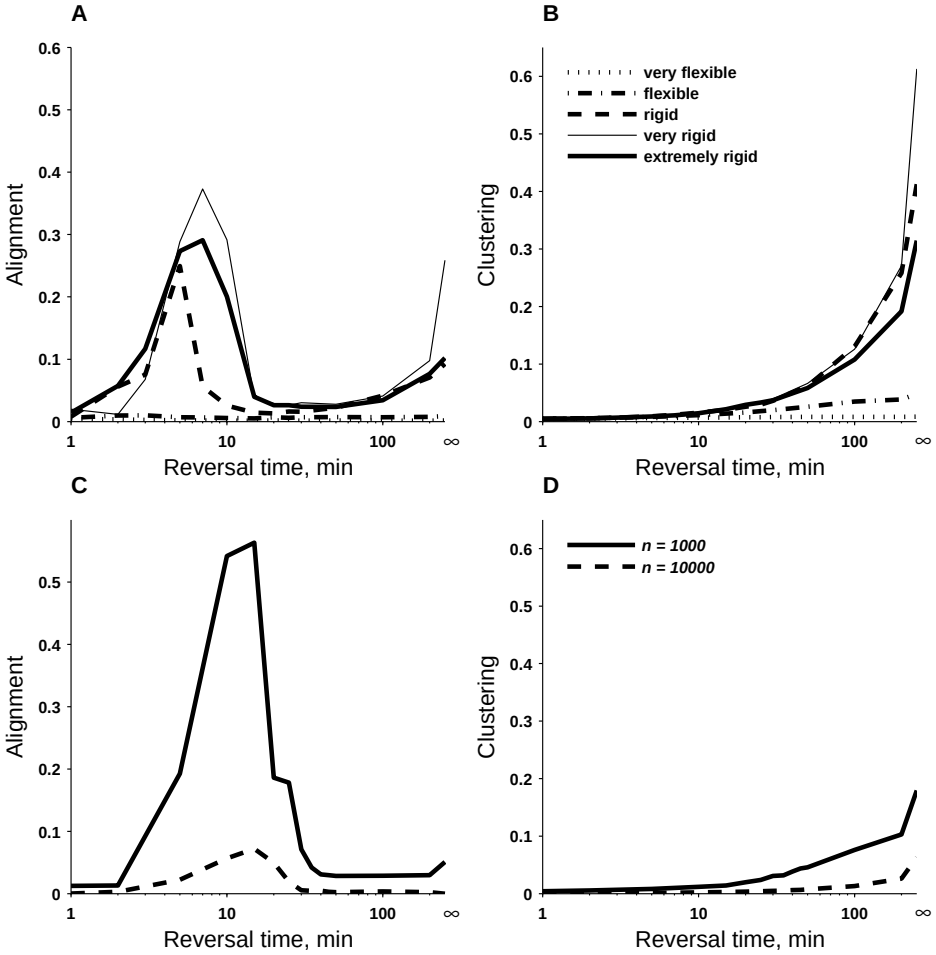

Figure 4.4: Alignment (A,C) and clustering (B,D) in low density populations. (A,B) $N = 10$ particles per cell, 1000 cells per domain. (C,D) $N = 2$ particles per cell (perfectly rigid rods), n is the population size, 1000 or 10000 cells. For every studied value of cell bending stiffness or reversal time, a measure average of 3 simulations with different initial cell configurations is plotted.

tional domain with smaller cell population density. More importantly, the study of Wu et al. used a different modelling approach (off-lattice node-based Monte-Carlo) and does not report on the bending stiffness of studied model cells. No animations of simulations are presented either; therefore a more detailed comparison of the dynamics of cells in the two studies is not possible.

An important parameter determining population dynamics is contact stiffness between cells, which controls how much two contacting cells can overlap. It is however not known exactly how hard the collisions between cells really are. Electron microscopy studies of myxobacteria cells in biofilms show that cell cross-sections are not round, but markedly deformed [12]. This suggests that cells can change their shape ("squeeze") upon mechanical contact with other cells, allowing easier passage of cells in dense populations, i.e. the contacts are presumably "soft".

In this study, non-reversing cells showed marked clustering, a behavior also observed in another computational study [11]. Cell rafts at the edges of swarms are often seen to split or join [13], behaviour also seen in our numerical simulations. Conversely, reversing cells showed little clustering, but good global population alignment, with a narrow optimum range of reversal times of 5–10 min. Noticeably, these optimum reversal times are almost the same as the experimentally observed cell reversal times in vegetative swarms [3]. The study of Wu *et al.* [7] similarly found that reversal facilitates the alignment of cells, and determined the optimal reversal time value for maximum swarm expansion to be within the range found in the present study. Moreover, it has been shown that cell alignment is necessary for C-signal transfer, essential for the development of *Myxococcus xanthus* to proceed [14]. Our results suggest that reversal of cells with a period of 5–10 min could be necessary to keep the population in the well-aligned state, allowing easy transfer of C-signal.

In the middle of the vegetative swarm, the cells are tightly packed, whereas at the edge of the swarm cell density is usually smaller, allowing the observation of movement of separate cell groups [7, 13]. The results in this study indicate that longer reversal times should result in larger clusters within the population. However, hypo-reversing Frz mutants (i.e. with increased reversal period) contain more single cells and fewer and smaller groups of cells at the edge of the swarming colony, compared to the wild type cells [9], inconsistent with the predictions of the current study. One has to note, however, that the present numerical model considered A-motility only, whereas S-motility is known to bring cells in groups [15]. Furthermore, hypo-reversing mutants exhibit slower swarming, which is inconsistent with the predicted larger cell speed of non-reversing cells. The reasons for this discrepancy are unknown.

During fruiting body development, cells travel collectively in streams to enter the nascent aggregates [16]. However, the mechanisms of stream formation are not well understood. Our simulation study showed that in dense populations of cells with soft contacts, adjacent, oppositely moving streams could form due to mechanical sorting of cells with similar orientation, with no additional mechanisms required. Interestingly, in the simulations one could also observe cells inside the streams that are oriented opposite to the majority of stream cells and being pushed by the stream against their engine direc-

tion (Movie 4.3). It would be interesting to experimentally investigate whether all cells in streams move accordingly to their polarity (engine force direction), and whether some of them are pushed along "against their will" by the surrounding cell mass. It is also a possibility that the observed increase in gliding speed of csgA cells mixed with wild type cells [2] could be a result of mechanical pushing of csgA cells by faster wild type cells. This study further suggests that experimentally observed change of a population pattern from aligned patches of cells in swarms [17] into elongated streams of cells can be due the observed increase of cell reversal period during fruiting body development [1, 2].

Finally, this study considered only independent, random reversals. There is evidence that cell reversal frequency depends on cell density [18]. Further, it has been observed that when two cells pass one another and come into contact, this encounter often results in one of the cells reversing [19]. Including such interactions into models might be important in order to better understand the role of cell reversals in myxobacteria pattern formation.

4.A. SUPPLEMENTARY MOVIES

Movie 4.1. Movement patterns of non-reversing, flexible cells with hard contacts ($k^{\mathrm{c}} = 0.01\,\mathrm{N{\cdot}m^{-1}}$) in a high-density population.

Movie 4.2. Movement patterns of non-reversing, very rigid cells with hard contacts ($k^{\mathrm{c}} = 0.01\,\mathrm{N{\cdot}m^{-1}}$) in a high-density population.

Movie 4.3. Movement patterns of non-reversing, very rigid cells with soft contacts ($k^{\mathrm{c}} = 0.002\,\mathrm{N{\cdot}m^{-1}}$) in a high-density population.

Movie 4.4. Movement patterns of reversing, very rigid cells with soft contacts ($k^{\mathrm{c}} = 0.002\,\mathrm{N{\cdot}m^{-1}}$) in a high-density population.

Movie 4.5. Movement patterns of non-reversing very rigid cells with $k^{\mathrm{c}} = 0.005\,\mathrm{N{\cdot}m^{-1}}$ in a high-density population.

Movie 4.6. Movement patterns of 1000 non-reversing flexible cells in a low density population.

Movie 4.7. Movement patterns of 1000 reversing very rigid cells in a low-density population.

Movie 4.8. Movement patterns of 1000 non-reversing very rigid cells in a low-density population.

Movie 4.9. Movement patterns of 1000 non-reversing extremely rigid cells in a low-density population.

Movie 4.10. Movement patterns of 10000 perfectly rigid cells, $T_R = 2\,\text{min}$.

Movie 4.11. Movement patterns of 10000 perfectly rigid cells, $T_R = 5\,\text{min}$.

Movie 4.12. Movement patterns of 10000 perfectly rigid cells, $T_R = 10\,\text{min}$.

Movie 4.13. Movement patterns of 10000 perfectly rigid cells, $T_R = 15\,\text{min}$.

Movie 4.14. Movement patterns of 10000 perfectly rigid cells, $T_R = 20\,\text{min}$.

Movie 4.15. Movement patterns of 10000 perfectly rigid cells, $T_R = 100\,\text{min}$.

Movie 4.16. Movement patterns of 10000 perfectly rigid cells, $T_R = \infty$.

REFERENCES

[1] L. Jelsbak and L. Søgaard-Andersen, *The cell surface-associated intercellular C-signal induces behavioral changes in individual Myxococcus xanthus cells during fruiting body morphogenesis,* Proceedings of the National Academy of Sciences of the United States of America **96**, 5031 (1999).

[2] L. Jelsbak and L. Søgaard-Andersen, *Pattern formation by a cell surface-associated morphogen in Myxococcus xanthus,* Proceedings of the National Academy of Sciences of the United States of America **99**, 2032 (2002).

[3] B. D. Blackhart and D. R. Zusman, *"Frizzy" genes of Myxococcus xanthus are involved in control of frequency of reversal of gliding motility,* Proceedings of the National Academy of Sciences of the United States of America **82**, 8767 (1985).

[4] D. B. Kearns and L. J. Shimkets, *Chemotaxis in a gliding bacterium,* Proceedings of the National Academy of Sciences of the United States of America **95**, 11957 (1998).

[5] C. Kaimer, J. E. Berleman, and D. R. Zusman, *Chemosensory signaling controls motility and subcellular polarity in Myxococcus xanthus,* Current Opinion in Microbiology **15**, 751 (2012).

[6] J. E. Berleman, T. Chumley, P. Cheung, and J. R. Kirby, *Rippling is a predatory behavior in Myxococcus xanthus,* Journal of Bacteriology **188**, 5888 (2006).

[7] Y. Wu, A. D. Kaiser, Y. Jiang, and M. S. Alber, *Periodic reversal of direction allows myxobacteria to swarm,* Proceedings of the National Academy of Sciences of the United States of America **106**, 1222 (2009).

[8] D. R. Zusman, A. E. Scott, Z. Yang, and J. R. Kirby, *Chemosensory pathways, motility and development in Myxococcus xanthus,* Nature Reviews Microbiology **5**, 862 (2007).

[9] V. H. Bustamante, I. Martínez-Flores, H. C. Vlamakis, and D. R. Zusman, *Analysis of the frz signal transduction system of Myxococcus xanthus shows the importance of the conserved c-terminal region of the cytoplasmic chemoreceptor FrzCD in sensing signals,* Molecular Microbiology **53**, 1501 (2004).

[10] D. R. Zusman, *"Frizzy" mutants: a new class of aggregation-defective developmental mutants of Myxococcus xanthus,* Journal of Bacteriology **150**, 1430 (1982).

[11] J. Starruß, T. Bley, L. Søgaard-Andersen, and A. Deutsch, *A new mechanism for collective migration in Myxococcus xanthus,* Journal of Statistical Physics **128**, 269 (2007).

[12] H. Palsdottir, J. P. Remis, C. Schaudinn, E. O'Toole, R. Lux, W. Shi, K. L. McDonald, J. W. Costerton, and M. Auer, *Three-dimensional macromolecular organization of cryofixed Myxococcus xanthus biofilms as revealed by electron microscopic tomography,* Journal of Bacteriology **191**, 2077 (2009).

[13] D. Kaiser and C. Crosby, *Cell movement and its coordination in swarms of Myxococcus xanthus,* Cell Motility and the Cytoskeleton **3**, 227 (1983).

[14] S. K. Kim and D. Kaiser, *Cell alignment required in differentiation of Myxococcus xanthus,* Science (New York, N.Y.) **249**, 926 (1990).

[15] J. Hodgkin and D. Kaiser, *Genetics of gliding motility in Myxococcus xanthus (Myxobacterales): two gene systems control movement,* Molecular and General Genetics **171**, 177 (1979).

[16] L. Jelsbak and L. Søgaard-Andersen, *Cell behavior and cell-cell communication during fruiting body morphogenesis in Myxococcus xanthus,* Journal of Microbiological Methods **55**, 829 (2003).

[17] A. E. Pelling, Y. Li, S. E. Cross, S. Castaneda, W. Shi, and J. K. Gimzewski, *Self-organized and highly ordered domain structures within swarms of Myxococcus xanthus,* Cell Motility and the Cytoskeleton **63**, 141 (2006).

[18] W. Shi, F. K. Ngok, and D. R. Zusman, *Cell density regulates cellular reversal frequency in Myxococcus xanthus,* Proceedings of the National Academy of Sciences of the United States of America **93**, 4142 (1996).

[19] E. M. F. Mauriello, D. P. Astling, O. Sliusarenko, and D. R. Zusman, *Localization of a bacterial cytoplasmic receptor is dynamic and changes with cell-cell contacts,* Proceedings of the National Academy of Sciences of the United States of America **106**, 4852 (2009).

5

SHORT-RANGE GUIDING CAN RESULT IN THE FORMATION OF CIRCULAR AGGREGATES IN MYXOBACTERIA POPULATIONS

5.1. INTRODUCTION

Myxobacteria are social bacteria that upon starvation form multicellular fruiting bodies whose shape in different species can range from simple mounds to elaborate tree-like structures consisting of 10^5–10^6 cells [1, 2]. The development of fruiting bodies depends on collective movement of cells in close contact with one another on a solid surface. After the movement of cells within the fruiting body has stopped, cells differentiate into dessication-resistant spores. Since collective cell motility during morphogenesis is also common in higher organisms [3], myxobacteria serve as a relatively simple model organism to study multicellular movement, organization and development.

During the course of development of myxobacteria, groups of cells moving in circular and/or spiral patterns form aggregation centers that later develop into fruiting bodies [4, 5]. Cell aggregates are dynamic, i.e. they can disperse, split, merge with other aggregates or they can stabilize and form a fruiting body [6]. Nascent cell aggregates grow as new cells enter in multicellular streams, where cells are aligned and move in concert [4, 5, 7]. Remarkably, circular and spiral patterns of cell movement are conspicuous during different stages of the morphogenesis of different species of myxobacteria and can be observed on different spatial scales from several cells to large streams (Figure 5.1) [8–16]. Several adjacent streams can move circularly within the fruiting body in opposite directions [17]. Spores in the fruiting body of *M. xanthus* have been shown to be organized in spiral patterns, presumably as a result of such movements [4].

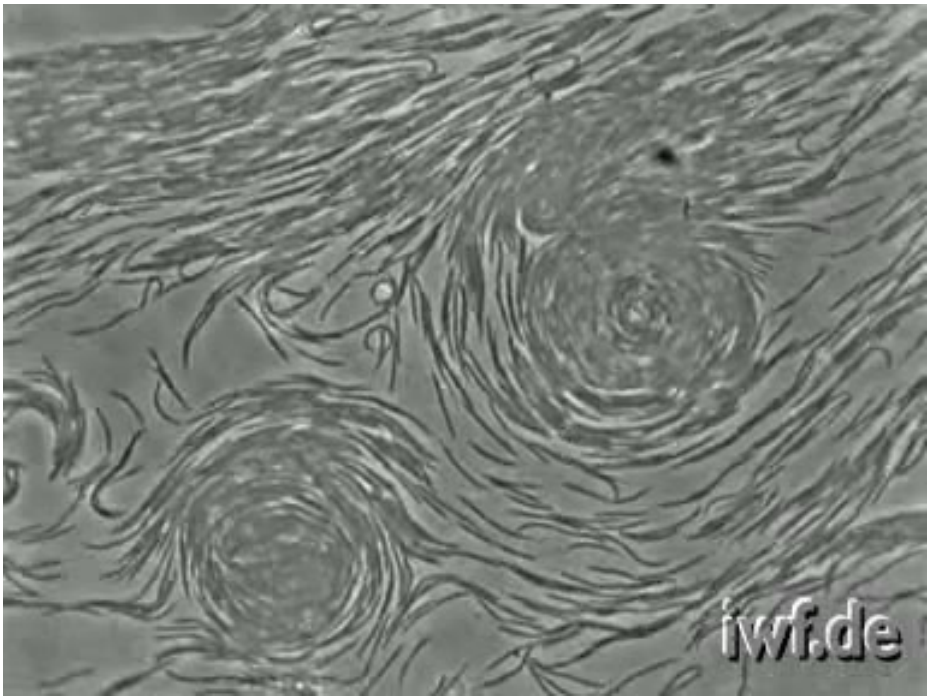

Figure 5.1: Circular aggregates during development of *Archangium violaceum.* Reproduced from Reichenbach *et al.* [18].

The mechanisms of stream and circular/spiral aggregate formation are not well understood. Circular aggregates can form by a stream of cells trapping itself [15]. Cells have been observed to travel long distances in streams and enter distant aggregates rather that the ones nearby, suggesting that aggregation is not caused by a long-range diffusible signal emitted from the aggregation centers [19]. Further, it has been shown that myxobacteria development is regulated by a C-signal that is passed from cell to cell through end-to-end contact [20]. These findings resulted in a hypothesis that myxobacteria aggregation and development depends on short-range contact mediated communication between cells, without the need of long-range signals. Recent studies on aggregate merging and dispersal dynamics further argues against the presence of long-range diffusible molecules to signal the aggregation process [6].

Vegetative cells in swarms reverse their direction of gliding approximately once every 10 min [21]. In the course of development, due to the C-signalling, the reversal frequency of cells is reduced, gliding speed is increased, making the cell movement essentially unidirectional (i.e. cells do not switch the leading and trailing pole anymore) at the final stages of development [22]. According to the conceptual model proposed by Sogaard-Andersen and Kaiser [23], streams form when moving cells come into end-to-end contact and their reversal frequencies decrease due to C-signalling, thus favoring movement of cells in roughly the same direction. However, the model does not address the question

of what keeps the cells in the chain. Moving cell masses and streams can turn and swirl [15], but cells appear to follow one another over long distances and not to escape the stream due to random fluctuations in cell orientation [24] or contacts with surrounding cells that would be expected to break the chain of cells. A guiding mechanism seems to be present for streams to be stable, i.e. for cells to continue following one another and move as one unit. One possible mechanism of such stability could be a long-range guiding system, other than a signal diffusing from aggregation centers. For example, at low cell population densities, cells are often observed to follow slime trails laid down by other cells [25]. This could establish a long-range order required to guide cells into aggregation centers. However, whether and how slime trails could persist in a very dense population, which is the usual state of myxobacteria communities, let alone in three-dimensions, is not clear. Alternatively, a cell could use short-range guiding mechanisms whereby guiding forces act only when cells are in contact or very close to one another. Possible hypothetical mechanisms for short-range guiding could include following the slime immediately extruded by another cell, a diffusible signal from a cell or physical adhesion between cells.

In this study, by means of a two-dimensional (2D) mass-spring model developed earlier (Chapter 2), we investigate how different types of short-range guiding interactions between the leading pole of one bacterium and the trailing pole of other bacterium, could affect the formation of patterns in myxobacteria population.

5.2. MODEL

To model short-range guiding interactions between cells, we use a mass-spring model previously described in Chapter 2 with changes to collision response presented in Chapter 3. In brief, a cell is modeled as an array of particles connected by linear and angular springs. Cells glide on a substratum powered by engine forces distributed along the whole length of a cell and change their direction of movement as a result of collisions with other cells. In addition to the features described in the basic model, here we introduce and study three kinds of short-range guiding forces (Figure 5.1). First (case a), adhesion between the leading pole ("head") of one cell and the trailing pole ("tail") of another cell is considered. Thereby, adhesion forces between a pair of line segments that connects the particles in the bacterium are introduced only when the head of one bacterium (for cell polarity for $k^{\mathrm{e}} = 1$, segment $\boldsymbol{Q}_{1j}$ with end point $P_1 = 0$, see Chapter 2) and the tail of another (or the same) bacterium (for cell polarity for $k^{\mathrm{e}} = 1$, segment $\boldsymbol{Q}_{(N-1)l}$ with end point $P_2 = 1$) are involved. Thus, when the smallest distance between two segments d (see Chapter 2) is $W < d < d_{\mathrm{g}}$, where d_{g} is a maximum guiding (adhesion in this case) distance and W is cell width, adhesion forces to respective head and tail particles of interacting bacteria were introduced (Figure 5.1, forces marked $\boldsymbol{F}^{\mathrm{g}}_{\mathrm{H}}$ and $\boldsymbol{F}^{\mathrm{g}}_{\mathrm{T}}$). The adhesion forces are described by the same 4 equations that govern collision response (Chapter 2), with $k^{\mathrm{g}} = F^{\mathrm{g}}_{\mathrm{max}}/d_{\mathrm{g}}$, where $F^{\mathrm{g}}_{\mathrm{max}}$ is the maximum guiding force (exerted when two segments are separated by distance d_{g}). Essentially, adhesion in the model is the collision response working in reverse, i. e. attracting cells when d becomes larger than W. As a result of these forces, the head of the trailing cell will tend to turn towards the

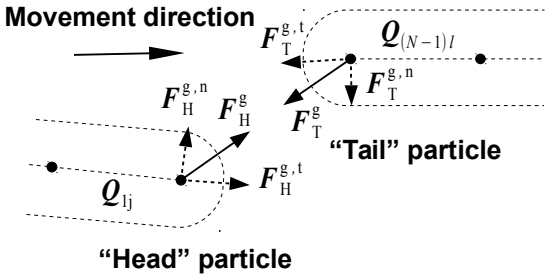

Figure 5.1: Short-range guidance forces in the model. For clarity, the distance between the head and tail of interacting bacteria is exaggerated. Numbering of segments is shown for the case of $k^e = 1$.

tail of the leading cell, when the distance between them is small enough, due to a normal component of adhesion force on the head particle ($\boldsymbol{F}_H^{g,n}$ in Figure 5.1). In addition, a component of adhesion force along the tangent of trailing bacterium body ($\boldsymbol{F}_H^{g,t}$ in Figure 5.1) will result in the increased speed of the trailing bacterium (i.e. the leading cell will pull the trailing cell forward). As the adhesion forces work in action-reaction pairs, the tail of the leading cell will also turn towards the head of the trailing cell and the speed of the leading cell will tend to decrease (due to normal and tangent component of adhesion force respectively, $\boldsymbol{F}_T^{g,n}$ and $\boldsymbol{F}_T^{g,t}$ in Figure 5.1). There will be no adhesion forces when the head of the trailing cell touches the tail of the leading cell (i.e. when $d = W$).

A second type of guiding force (case b) represents active following, whereby the force described by (a) is added only to the head of following cell, but not to the tail of leading cell (i.e. only $\boldsymbol{F}_H^g$ in Figure 5.1). It models the effect of a trailing cell being attracted to the tail of the leading cell, but having no effect on the movement of the leading cell.

In the third case (c), passive following (steering) is considered, when the force to head particle of the trailing cell is added only in the direction normal to bacteria body $\hat{\boldsymbol{n}}$ ($\boldsymbol{F}_H^{g,n}$ in Figure 5.1). By this, only the steering effect of the head of the trailing cell is modelled, i.e. turning the tip of the cell left or right, with respect to the normal trajectory of the cell.

The parameters used in the model are the same as in (Chapter 2), with the addition of extra parameters describing guiding forces. The value F_{max}^g was chosen to be 200 pN, unless stated otherwise, and $d_g = 2.5\mu$m (i.e. half of the bacterium width W). Since guidance forces not only steer the head of the cell, but can also speed up the cell (case a and b), the value of F_{max}^g was chosen in such a way that the speed-up due to the guiding force would be roughly within experimentally observed speed increase of myxobacteria during development, 1.5-2.5 times [22]. $F_{max}^g = 200$ pN results in 3-fold maximum increase of speed (100 pN engine force and maximum 200 pN guiding force results in maximal $3v_b$ speed). Four cell bending stiffness values B were studied in the simulations: 7×10^{-25} J·m, 6×10^{-24} J·m, 6×10^{-23} J·m and 6×10^{-22} J·m. In the text, we refer to those cell stiffnesses as "very flexible", "flexible", "rigid" and "very rigid" respectively. Further, as in Chapter 2, both low density (5×10^6 cm^{-2} and high-density (4×10^7 cm^{-2}) populations were studied. For low density population simulation, the collision stiffness

between cells was set as in Chapter 3 ($k^c = 0.01\,\mathrm{N{\cdot}m^{-1}}$). In high density populations, the collision stiffness had to be reduced to $k^c = 0.002\,\mathrm{N{\cdot}m^{-1}}$, because high collision stiffness blocks the movement of cells in a crowded environment (see Chapter 4).

To analyse cell movement, speeds and strain energies due to collisions between cells were shown for every line segment in the bacterium. Speed of a line segment was defined as an average speed of two particles at the ends of the segment. To find strain energies, for every two segments that overlap due to collision, i.e. if smallest distance between segments $d < W$ (Chapter 2), potential energy of the collision responce spring $(1/2)k^c(d-W)^2$ was calculated and one half of the value was added to both segments involved.

5.3. RESULTS

This study shows that guiding interactions between cells have a marked effect on the patterns observed in the model myxobacteria population.

Effect of guiding forces. Firstly, the effect of different types of guiding forces on cell movement patterns of a low-density population of non-reversing cells was studied. All cells were initially placed on a planar substratum with random positions and orientations (Figure 5.1A), and the movement of cells was simulated for 6 hours. A population of flexible non-guided cells at 6 hours forms clusters (Figure 5.1B and Movie 5.1), as also observed for non-reversing cells in Chapter 4. The presence of steering forces between cells (case c, passive following) resulted in occasional chains of cells between the clusters and small unstable circular structures that quickly dissipated (Figure 5.1C and Movie 5.2). However, cells with active following (case b) and head-to-tail adhesion (case a) formed stable rotating circular aggregates (Figure 5.1D and Movie 5.3, and Figure 5.1E and Movie 5.4 respectively). During the process of aggregate formation, streams of cells are first formed from randomly distributed cells. Streams collide with other streams, turn, move in circular trajectories, close upon themselves and trap the leading cells of the stream, with the rest of the cells starting to rotate around the trapped cells. The seed of rotation can also be formed by several cells swirling around a fixed point. Later, additional cells or entire streams join in to increase the size of the aggregate. Within the aggregate, cells appear to be arranged spirally, with new cells joining the free exposed tail of a cell at the edge of the aggregate. Decreasing the guiding force $F^g_{\max}$ from 200 pN to 100 pN made the population less likely to form stable rotating aggregates, resulting in a more dynamic system, where circular aggregates are smaller, can dissipate and streams can leave one aggregate and join another (case b, active following, Movie 5.5). Interestingly, when a cell at the edge of the aggregate leaves, it will often have a chain of follower cells behind it.

Effect of cell bending stiffness. Cluster sizes of non-guided cell populations appear to increase as the bending stiffness of the cell increases (Figure 5.2A-C, Figure 5.1B and Movies 5.6-5.8 and 5.1), i.e. stiffer cells result in larger more stable clusters. Similarly,

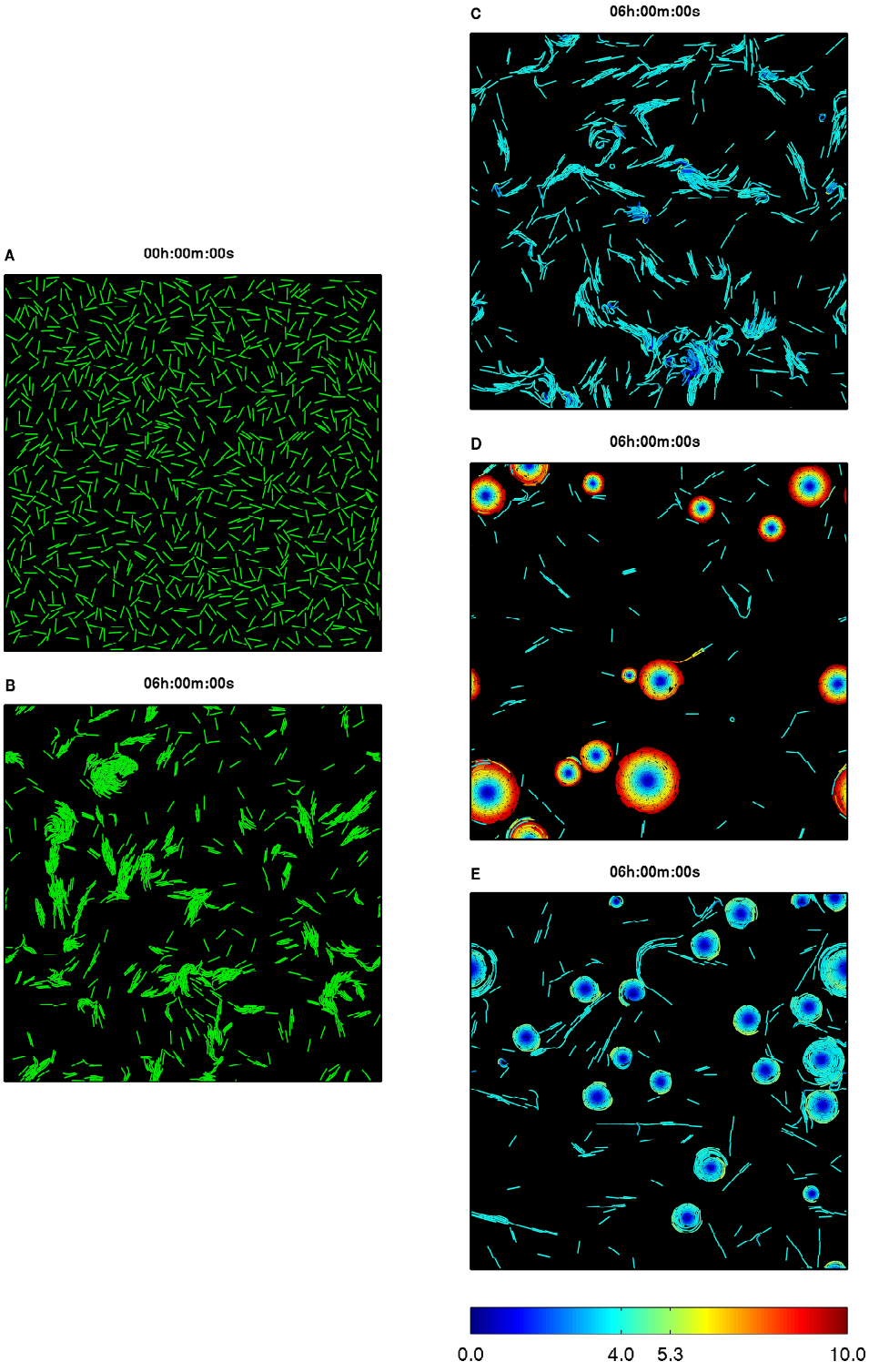

Figure 5.1: See next page.

Figure 5.1: Continued. The effects of short-range guidance on the patterns in the population of flexible cells. (A) Initial cell configuration. (B-E) Final configurations of a population at 6h: (B) non-guided cells, (C) cells with passive following, (D) cells with active following, (E) cells with head-to-tail adhesion. C-E also shows speeds of individual cells (colorbar at the bottom, $\mu m \cdot min^{-1}$).

the size of circular aggregates of cells with active following appears to increase as the bending stiffness of cells increase, and as a consequence, the number of aggregates in the computational domain decreases (Figure 5.2D-F, Figure 5.1D and Movie 5.9-5.11 and 5.3). Very flexible cells (Movie 5.9) form many small and stable circular aggregates due to their tendency to easier form a seed for a rotating aggregate. The size of these aggregates cannot increase, due to unavailability of free cells to join, because most of the cells are trapped in stable small aggregates (Figure 5.2D and Movie 5.9). Conversely, very stiff cells do not form circular aggregates (Figure 5.2F and Movie 5.11) because rigid cells cannot bend and are unlikely to generate a rotation seed or initiate the rotation of the entire stream.

Circular aggregates as rigid bodies. As the stable rotating aggregates form (Figure 5.2D and Movie 5.3), they appear to rotate as a rigid body, i.e. cells do not slide laterally within the aggregate, with cells in the center moving slower than cells at the edge of the aggregate. Furthermore, the speed of the cells at the edge of aggregates is larger than the speed of a freely moving bacterium, v_b, and appears not to depend on the aggregate size. As a consequence, because the speed of points at the edge of a rotating rigid body must be $v(R) = \omega R$, where R is the distance of the point from the rotation axis and ω is the angular speed, larger aggregates rotate with smaller angular speed, and the angular speed of a growing aggregate decreases. To validate this result, we created a continuous rigid body model of a rotating myxobacteria aggregate (see Appendix). The rigid body model predicts that the speed of the cells at the aggregate edge in the head-to-tail adhesion model (case c) should be $\omega R = v(R) = (4/3)v_b = 5.3 \mu m \cdot min^{-1}$, whereas in the active following (case b, given $F^g_{max} = 200\,pN$) maximum speed should be $\omega R = v(R) = 4v_b = 16 \mu m \cdot min^{-1}$, well in agreement with the simulation results (Figure 5.1D , Movie 5.3 and Figure 5.1E, Movie 5.4 respectively).

The finding that cells at the edge of a nascent rotating aggregate must move faster than their equilibrium speed can explain why large stable rotating aggregates do not form with only steering forces present. Since the guiding forces are short-range in this model, a trailing cell must continuously be within a short distance from a tail of a leading cell to be steered to travel in the trajectory of the leading cell. If a cell about to join an aggregate comes sufficiently close to the free exposed tail of a cell at the edge of the aggregate, it must increase its speed to continue being within a short range interaction distance to be steered to move in a circular path. Otherwise, the incoming cell is unable to catch up with the faster-moving cells at the edge of the aggregate and the distance between them increases until the guiding interaction is lost. Steering forces can only turn the head of the cell in the direction normal to the bacterium body, but cannot pull the cell in the direction of its movement to increase the speed. Conversely, head-to-tail

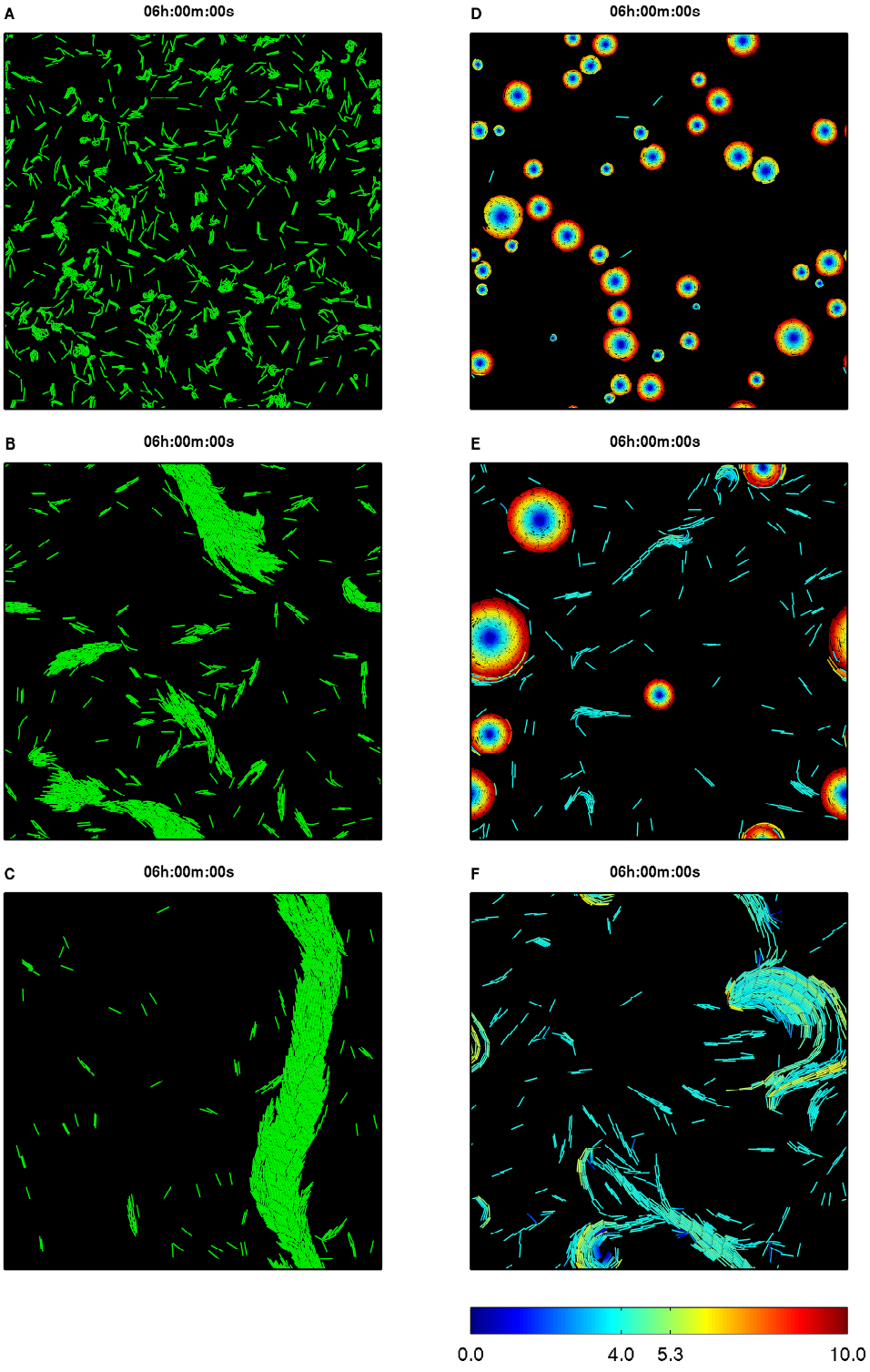

Figure 5.2: See next page.

Figure 5.2: Continued. Final configurations of a population at 6h. (A-C) non-guided cells. (D-F) cells with active following. (A,D) very flexible cells, (B,E) rigid cells, (C,F) very rigid cells. D-F also shows speeds of individual cells (colorbar at the bottom, $\mu m \cdot min^{-1}$).

adhesion and active following forces allow cells to speed up and catch up the tail of the leading cells and match their necessary speed to continue moving within short-range interaction distance, resulting in stable circular streams and rotating aggregates.

Stress inside circular aggregates. Overlaps between cells tend to be higher towards the center of rotating aggregates, which implies larger stresses that cells undergo due to being squeezed by surrounding cells. Figure 5.3 and Movies 5.12-5.15 show strain energies within the cells due to overlap between different bacteria (i.e. energies stored in the collision response springs). Whereas during cluster formation in non-guided populations of cells strain energies during the collision can reach temporary high values, inside the circular aggregates of guided cells high stresses are constant. This is consistent with the fact that in the core of the aggregate, cells move slower than their equilibrium speed, and thus the engine force of a cell is counteracted by pushing force from surrounding cells.

Robustness of circular aggregates. An interesting question is how robust the circular aggregates are with respect to their size and whether stable aggregates can form in populations of higher density. One can start a simulation where initially all cells in a population are arranged spirally to form a circular aggregate. Interestingly, pre-arranged aggregates of rigid and very rigid cells were relatively stable, although they did lose some cells (Movie 5.16 and 5.17). However, the aggregates of the same initial size made of flexible and very flexible cells (Movie 5.18 and 5.19) split after some time into several smaller aggregates and swirling streams (hollow aggregates). It appears that flexible cells under high stresses inside the aggregate can bend enough to start forming separate rotation seeds. This suggests the existence of a different optimum aggregate size for cells with different flexibility.

It was further explored whether the formation of circular aggregates is robust in high density populations. All cells were initially densely packed, aligned, but with random orientations. A population of non-guided cells for all bending stiffness values except for very rigid ones does not show any discernible characteristic movement pattern (Movie 5.20-5.22; see also Figure 4.1B in Chapter 4). Interestingly, very rigid cells were able to sort themselves into straight streams (Movie 5.23; see also Figure 4.1D in Chapter 4). However, in populations of flexible and very flexible cells with head-to-tail adhesion or active following there is a visible stable circular movement within the population (Figure 5.4A, Movie 5.24 and 5.25). Rigid and very rigid cells, however, sort into adjacent straight streams (Figure 5.4B, Movie 5.26 and 5.27), similar to the streams of rigid non-guided cells. While at low population density the size of the aggregates increases with cell rigidity, at high density rigid guided cells might not have formed the circular aggregates because the domain of simulation was too small. Interestingly, in populations with

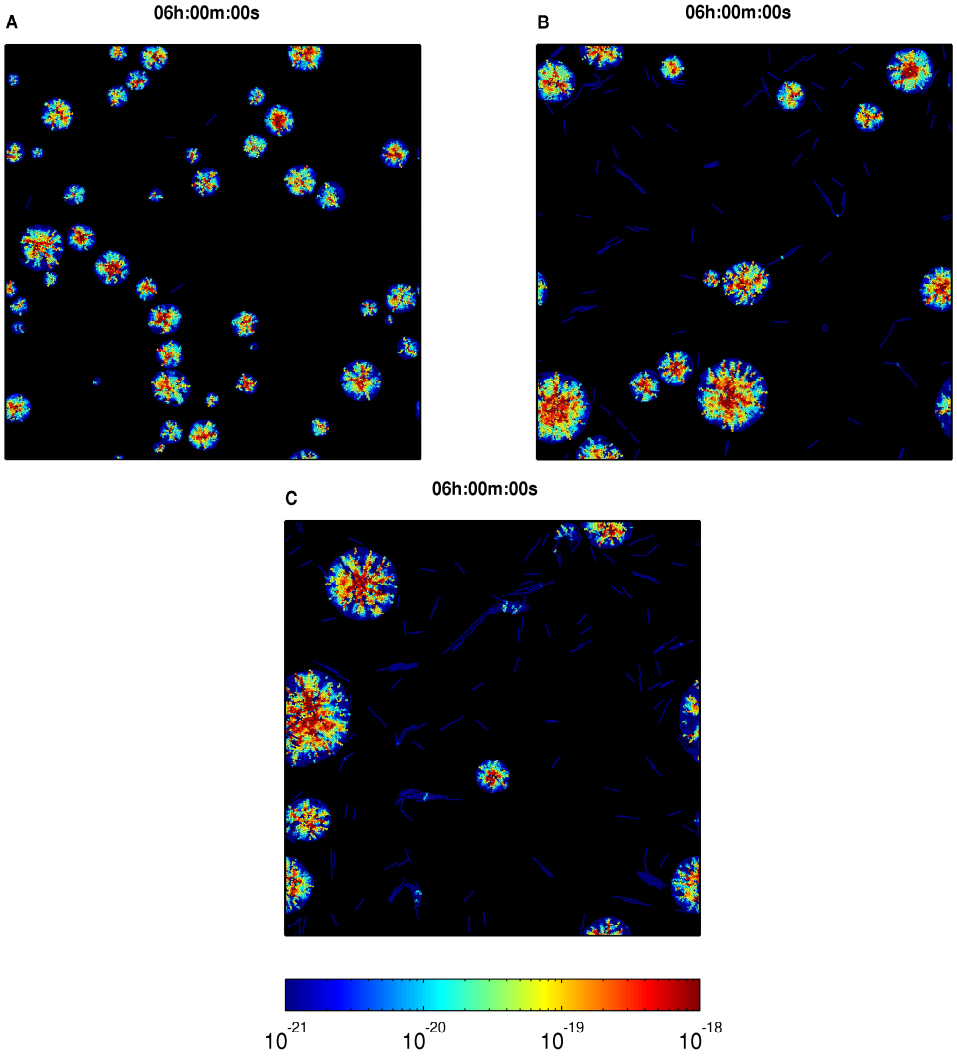

Figure 5.3: Strain energies due to cell overlap in circular aggregates of cells with active following (see colorbar at the bottom, J). (A) very flexible cells, (B) flexible cells, (C) rigid cells.

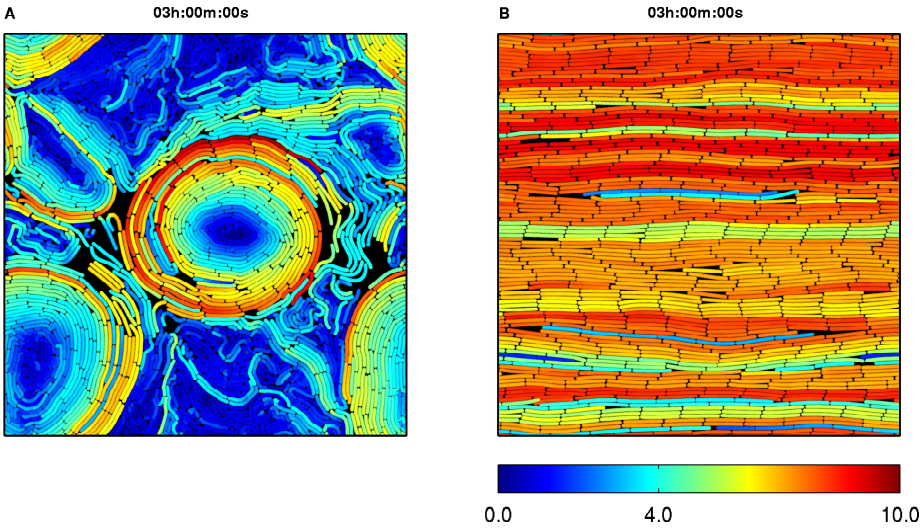

Figure 5.4: Patterns of cell movement in high-density populations at 3h. Color of cells shows their speed (colorbar at the bottom, μm). (A) Flexible cells. (B). Very rigid cells. Due to different speeds, streams travelling in opposite directions are visible. See also Movie 5.27.

active following, whole streams move with a speed larger than the equilibrium speed, because each cell is responding to the speed up of the cell in front of it by increasing its own speed. Due to the periodic boundary adopted in the model, it results in a self-sustained speedup of the whole stream.

Effect of cell reversal. Results presented so far have been obtained only with populations with non-reversing cells. In low population density conditions, reversing cells do not form circular aggregates even with guiding forces present (Movie 5.28-5.31). However, if in addition to guiding forces, cell reversals are suppressed when a head-to-tail interaction between cells takes place, circular aggregates do form (Movie 5.32-5.35). Non-guided cells with reversal suppression are also unable to form stable aggregates (Movie 5.36-5.39). These results suggest that both including guidance and suppressing reversal are necessary for stable rotating aggregates to form.

5.4. DISCUSSION

The mechanisms of myxobacteria aggregation during fruiting body formation are not well understood. The non-linear patterns of movement of myxobacteria cell masses and streams imply the existence of some sort of guiding mechanisms that keep the cells moving as one unit and directs them into aggregation centers [15]. It is not known whether these guiding mechanisms are long or short-range. In this study, by means of a mechanical mass-spring model, we demonstrate that short-range guiding interactions between head and tail of two myxobacteria cells in close contact are sufficient to produce stable

streams and circular/spiral aggregates in model myxobacteria populations.

Many features of cell movement that are present in our simulations are also observed in experimental videos. Multicellular cell masses (streams) in our simulations can travel in straight lines, or, when colliding with other streams or clusters of cells, can wave and swirl (Movie 5.5,[9]; Movie 5.5; [12, 15]. Circular aggregates in the simulations often form when a stream turns and closes upon itself, trapping the leading cells, a situation also observed in experimental movies (Movie 5.3; [15]. The simulated circular aggregates exhibit rotational movements (Movie 5.3). Similarly, circular and spiral movement is often observed in developing myxobacteria [10, 16]. In fact, the fruiting bodies often develop in places where such spiral aggregates initially form [4]. Additional streams of cells join the existing aggregates to increase their size (Movie 5.3, [22]. In the simulations, a circular aggregate sometimes forms from a rotation seed of several flexible cells (Movie 5.3, 5.9). Similar small rotating cell clusters been observed experimentally [8, 13, 26, 27]. Furthermore, smaller magnitudes of guiding forces results in more dynamic aggregate behaviour: the simulated streams can travel from one aggregation center to another, aggregates can dissipate, split or join with other aggregates (Movie 5.5). Our results show that the stability of large aggregates increases with increasing cell rigidity, whereas more flexible cells tend to form separate rotation seeds inside the aggregates due to easier bending and thus induce the splitting of a large aggregate (Movie 5.16-5.19). It has been experimentaly observed that the size of initial aggregates of different myxobacteria species differs [28]. Our results suggest that it might be the result of different bending stiffness of cells of different species. Finally, we also observed the formation of hollow aggregates and adjacent streams swirling inside aggregates in opposite directions (Movie 5.17, 5.18) [5, 17].

Interestingly, circular aggregates in our model rotate as rigid bodies, i.e. cells within the aggregate do not slide laterally past one another. As a consequence cells inside the aggregate move slower than the cells at the edge of the aggregate. Observation of experimental movies does not allow to tell conclusively whether this is the case in reality [10, 16]. Experimentally tagging part of the cells in the population with fluorescent markers could be used to determine whether aggregates rotate fully or partly as rigid bodies. Another experimentally testable prediction of the model is that cell speed at the edge of the aggregates is roughly the same and independent of the aggregate size. This means that smaller aggregates rotate with larger angular speeds, and the increase in aggregate size due to incoming streams will result in the decrease of the angular speed of aggregate rotation.

Interestingly, cells at the edge of the simulated aggregate, as well as the cells in the incoming streams, move with a speed larger than the equilibrium cell speed (Movie 5.3). Therefore, in order for stable rotating aggregates to be formed, short-range guiding interactions must act in such a way that the follower cell would both be steered left or right to follow the tail of the leader cell, and also would be capable of speeding up to catch up with the faster moving leader cell. Otherwise, since guiding interactions are short-range (half of cell width), a faster moving leader cell will “run away” from the follower cell and the guiding interaction will be lost. It has been shown that during development

the average speed of cells do increase due to interaction with other cells [22, 29], but unfortunately it was not reported how cell speed depends on its location within different structures within the developing population, such as spiral aggregates or streams.

To our knowledge, there is no experimental evidence about the existence of short-range guiding interactions between a head and a tail of two myxobacteria cells. The model proposed in this study does not imply any particular short-range guiding mechanism for myxobacteria aggregation, as long as the interaction would both steer the follower cell and also adjust its speed. One possibility could be mechanical adhesion force between a head and a tail of two myxobacteria. Alternatively, a follower cell could respond to a diffusible substance or slime secreted from the rear of the leader cells. For a short-range interaction, such a substance should diffuse slow enough, a distance comparable to cell width over minutes. For example, lipids could satisfy this requirement [6]. It has been shown that myxobacteria cells tend to follow slime trails produced by other myxobacteria [25]. For short-range guiding, a cell should follow only the new slime immediately secreted by the leader cells, but not the "old" slime. It has also been shown that myxobacteria development depends on contact mediated C-signalling [20]. C-signal is relayed by the end-to-end contact between cells [30], and one of its effects is to decrease the reversal frequency of the cell [22]. C-signal mutants are unable to aggregate or the aggregates that still form would quickly [31]. These results are consistent with C-signal acting as a part of guiding mechanism. In our simulations, weak guiding forces result in the formation of very dynamic aggregates that can easily disperse (Movie 5.5).

Although a real fruiting body develops in three dimensions, at the initial stages of aggregation, cells appear to move in independent monolayers that are stacked on top of one another [4, 31]. This observation justifies using a 2D-model in this study and explains how cell trapping would be possible when streams close upon themselves, without allowing cells to escape the aggregate by moving up. Further, the results show that there is mechanical stress accumulated inside circular aggregates. It has been observed experimentally that when a second layer forms on top of the original monolayer of M. xanthus cells, the cells leave the base layer from one point [31]. Our results suggest, that such phenomenon may be a result of mechanical stress inside those aggregates, where trapped cells are squeezed inside the aggregate and are pushed upwards when the stress becomes too high at some point inside the aggregate. Consistent with that idea is the observation that fruiting bodies develop at the places of traffic jams [32] or where spiral aggregates initially form [4].

Our study suggests the extension of the conceptual model whereby cell streams form when the reversal frequency of cells is reduced due to contact-mediated C-signalling as the two cells come into end-to-end contact. [23]. The suppression of cell reversals would then favour cell movement in roughly the same direction. However, that model does not address the question of what keeps cells in the chain even when the stream of cells turns. Our results show that cells with only suppressed reversals would not be able to form streams from initially randomly distributed reversing cells (Movie 5.36-5.39). Including active short-range guiding interactions in addition to reversal suppression allows to explain the formation of stable streams and circular aggregates from initially randomly

distributed population of reversing cells (Movie 5.32-5.35). Interestingly, in our simulations, densely packed, initially aligned rigid cells can mechanically sort into adjacent streams of cells moving in the same direction (Movie 5.23), but it is not clear whether this effect is due to a relatively small simulation domain. Furthermore, the bending stiffness of the myxobacterium cell have not been determined experimentally, but evidence for *Myxococcus xanthus* suggests that it is closer to the "flexible" value used in these simulations [33]. Guiding forces allows cells to form stable streams and circular aggregates independently of bending stiffness value and initial cell configuration.

5.A. A CONTINUOUS 2D RIGID BODY MODEL OF A CIRCULAR AGGREGATE

A circular aggregate is modeled as a rigid body with radius R rotating with constant angular speed ω. In a circular aggregate, bacteria are oriented normal to the radius of the aggregate and so are the engine force and velocity. In the mass-spring model, the magnitude of the engine force acting on one particle is $F_{\mathrm{p}}^{\mathrm{e}} = F^{\mathrm{e}} N^{-1}$. If the area of a bacterium per particle is $a = LWN^{-1}$, then, in a continuous model, the corresponding engine force on a small area element dA is $a^{-1} F_{\mathrm{p}}^{\mathrm{e}} dA$. The drag force acts in the opposite direction of velocity and has magnitude $a^{-1}\zeta^t v_i^t dA$.

In the head-to-tail adhesion model (case a), adhesion forces form action-reaction pair and are internal to the aggregate, while the engine force and the drag force acting on bacteria are the only external forces. Let us consider a circular sector of a small angle θ and its element between radii r and $r+dr$. The area of the element is $dA = \frac{1}{2}(r+dr)^2\theta - \frac{1}{2}r^2\theta = \frac{1}{2}\theta(2rdr + dr^2) \approx r\theta dr$. Torque produced by engine and drag forces on that element (assuming the engine force produces a counterclockwise rotation) is $d\tau = a^{-1}F_p^e dAr - a^{-1}\zeta^t v_i^t dAr = a^{-1}F_p^e r^2\theta dr - a^{-1}\zeta^t \omega r^3 \theta dr$. The total torque on the circular sector is

$$\int_0^R d\tau = a^{-1}\left(\frac{1}{3}F_p^e R^3\theta - \frac{1}{4}\zeta^t \omega R^4\theta\right).$$

Since the system is symmetric with respect to the rotation point and we assume the system in rotational equilibrium (rotating with constant ω), the total torque of the given circular sector must be zero, resulting in

$$\omega R = v(R) = \frac{4F_p^e}{3\zeta^t} = \frac{4}{3}v_b.$$

In other words, the continuous model predicts, that in the head-to-tail adhesion model, the speed of bacteria that are at distance R from the center (i.e. at the edge of the aggregate) should travel 4/3 their normal speed v_{b}.

In case of active following, guidance forces are added only to the trailing cell and do not form an action-reaction pair. Thus, the speedup forces become external to the system. The speedup force acts in the same direction as the engine force and the velocity. In the mass-spring model, the speedup force per particle on a bacterium can be between 0 and $F_{\mathrm{p}}^{\mathrm{g}} = F^{\mathrm{g}} N^{-1}$, depending on the distance between the tail of leading and the head of

following bacteria. In addition, the trailing cell can interact with tails of more than one bacterium at a time. Given each bacterium on average interacts with one tail, by adding all torques due to external forces, we estimate the maximum speed of cells at the edge of the aggregate (at distance R from the center) to be

$$\omega R = v(R) = \frac{4}{3}\frac{F_{\mathrm{p}}^{\mathrm{e}} + F_{\mathrm{p}}^{\mathrm{g}}}{\zeta^t} = \frac{4}{3} v_{\mathrm{b}}(1+k),$$

where

$$k = \frac{F_{\mathrm{p}}^{\mathrm{g}}}{F_{\mathrm{p}}^{\mathrm{e}}}.$$

5.B. SUPPLEMENTARY MOVIES

Movies 5.1-5.27 shows the dynamics of non-reversing cells.

Movie 5.1. A population of non-guided flexible cells.

Movie 5.2. A population of flexible cells with steering (passive following).

Movie 5.3. A population of flexible cells with active following.

Movie 5.4. A population of flexible cells with head-to-tail adhesion.

Movie 5.5. A population of flexible cells with active following, $F_{\mathrm{max}}^{\mathrm{g}} = 100\,\mathrm{pN}$.

Movie 5.6. A population of non-guided very flexible cells.

Movie 5.7. A population of non-guided rigid cells.

Movie 5.8. A population of non-guided very rigid cells.

Movie 5.9. A population of very flexible cells with active following.

Movie 5.10. A population of rigid cells with active following.

Movie 5.11. A population of very rigid cells with active following.

Movie 5.12. Strain energy of very flexible cells due to cell overlap (colorbar, J).

Movie 5.13. Strain energy of flexible cells due to cell overlap (colorbar, J).

Movie 5.14. Strain energy of rigid cells due to cell overlap (colorbar, J).

Movie 5.15. Strain energy of very rigid cells due to cell overlap (colorbar, J).

Movie 5.16. A population of very rigid cells with active following, initially spirally arranged.

Movie 5.17. A population of rigid cells with active following, initially spirally arranged.

Movie 5.18. A population of flexible cells with active following, initially spirally arranged.

Movie 5.19. A population of very flexible cells with active following, initially spirally arranged.

Movie 5.20. High-density population of non-guided very flexible cells.

Movie 5.21. High-density population of non-guided flexible cells.

Movie 5.22. High-density population of non-guided rigid cells.

Movie 5.23. High-density population of non-guided very rigid cells.

Movie 5.24. A dense population of very flexible cells with active following.

Movie 5.25. A dense population of flexible cells with active following.

Movie 5.26. High-density population of rigid cells with active following.

Movie 5.27. High-density population of very rigid cells with active following.

Movie 5.28. A population of reversing very flexible cells with active following.

Movie 5.29. A population of reversing flexible cells with active following.

Movie 5.30. A population of reversing rigid cells with active following.

Movie 5.31. A population of reversing very rigid cells with active following.

Movie 5.32. A population of reversing very flexible cells with active following and reversal suppression.

Movie 5.33. A population of reversing flexible cells with active following and reversal suppression.

Movie 5.34. A population of reversing rigid cells with active following and reversal sup-

pression.

Movie 5.35. A population of reversing very rigid cells with active following and reversal suppression.

Movie 5.36. Non-guided reversing very flexible cells with reversal suppression.

Movie 5.37. Non-guided reversing flexible cells with reversal suppression.

Movie 5.38. Non-guided reversing rigid cells with reversal suppression.

Movie 5.39. Non-guided reversing very rigid cells with reversal suppression.

REFERENCES

[1] D. Kaiser, *Coupling cell movement to multicellular development in myxobacteria,* Nature Reviews Microbiology **1**, 45 (2003).

[2] H. Reichenbach, *The ecology of the myxobacteria,* Environmental Microbiology **1**, 15–21 (1999).

[3] C. J. Weijer, *Collective cell migration in development,* Journal of Cell Science **122**, 3215 (2009).

[4] K. A. O'Connor and D. R. Zusman, *Patterns of cellular interactions during fruiting-body formation in Myxococcus xanthus,* Journal of Bacteriology **171**, 6013 (1989).

[5] G. M. Vasquez, F. Qualls, and D. White, *Morphogenesis of Stigmatella aurantiaca fruiting bodies,* Journal of Bacteriology **163**, 515 (1985).

[6] C. Xie, H. Zhang, L. J. Shimkets, and O. A. Igoshin, *Statistical image analysis reveals features affecting fates of Myxococcus xanthus developmental aggregates,* Proceedings of the National Academy of Sciences **108**, 5915 (2011).

[7] L. Jelsbak and L. Søgaard-Andersen, *Cell behavior and cell-cell communication during fruiting body morphogenesis in Myxococcus xanthus,* Journal of Microbiological Methods **55**, 829 (2003).

[8] K. Grimm, H. K. Galle, and H. H. Heunert, *Archangium violaceum (Myxobacteriales) - Bewegungsaktivität und Kolonieform,* Film E 1588, 3:10-3:30 (Institut für den Wissenschaftlichen Film, Göttingen, 1969).

[9] K. Grimm, H. K. Galle, and H. H. Heunert, *Archangium violaceum (Myxobacteriales) - Bewegungsaktivität und Kolonieform,* Film E 1588, 3:30-3:55 (Institut für den Wissenschaftlichen Film, Göttingen, 1969).

[10] K. Grimm, H. K. Galle, and H. H. Heunert, *Archangium violaceum (Myxobacteriales) - Bewegungsaktivität und Kolonieform,* Film E 1588, 3:55-4:35 (Institut für den Wissenschaftlichen Film, Göttingen, 1969).

[11] K. Grimm, H. K. Galle, and H. H. Heunert, *Archangium violaceum (Myxobacteriales) - Bewegungsaktivität und Kolonieform,* Film E 1588, 4:35-5:45 (Institut für den Wissenschaftlichen Film, Göttingen, 1969).

[12] H. Kühlwein, B. Schlicke, H. K. Galle, and H. H. Heunert, *Polyangium fuscum (Myxobacteriales) - Cystenkeimung und Schwarmentwicklung,* Film E 1582, 7:30-8:00 (Institut für den Wissenschaftlichen Film, Göttingen, 1971).

[13] H. Kühlwein, B. Schlicke, H. K. Galle, and H. H. Heunert, *Polyangium fuscum (Myxobacteriales) - Cystenkeimung und Schwarmentwicklung,* Film E 1582, 2:40-3:10 (Institut für den Wissenschaftlichen Film, Göttingen, 1971).

[14] H. Kühlwein, B. Schlicke, H. K. Galle, and H. H. Heunert, *Polyangium fuscum (Myxobacteriales) - Cystenkeimung und Schwarmentwicklung,* Film E 1582, 8:00-8:15 (Institut für den Wissenschaftlichen Film, Göttingen, 1971).

[15] H. Reichenbach, H. H. Heunert, and H. Kuczka, *Schwarmentwicklung und Morphogenese bei Myxobakterien - Archangium, Myxococcus, Chondrococcus, Chondromyces,* Film C 893, 13:40-14:20 (Institut für den Wissenschaftlichen Film, Göttingen, 1965).

[16] H. Reichenbach, H. H. Heunert, and H. Kuczka, *Archangium violaceum (Myxobacteriales) - Schwarmentwicklung und Bildung von Protocysten,* Film E 777, 4:55-5:15 (Institut für den Wissenschaftlichen Film, Göttingen, 1968).

[17] B. Sager and D. Kaiser, *Two cell-density domains within the Myxococcus xanthus fruiting body,* Proceedings of the National Academy of Sciences of the United States of America **90**, 3690 (1993).

[18] H. Reichenbach, H. H. Heunert, and H. Kuczka, *Archangium violaceum (Myxobacteriales) - Schwarmentwicklung und Bildung von Protocysten,* Film E 777 (Institut für den Wissenschaftlichen Film, Göttingen, 1968).

[19] L. Jelsbak and L. Søgaard-Andersen, *Pattern formation: fruiting body morphogenesis in Myxococcus xanthus,* Current Opinion in Microbiology **3**, 637 (2000).

[20] L. Søgaard-Andersen, *Cell polarity, intercellular signalling and morphogenetic cell movements in Myxococcus xanthus,* Current Opinion in Microbiology **7**, 587 (2004).

[21] B. D. Blackhart and D. R. Zusman, *"Frizzy" genes of Myxococcus xanthus are involved in control of frequency of reversal of gliding motility,* Proceedings of the National Academy of Sciences of the United States of America **82**, 8767 (1985).

[22] L. Jelsbak and L. Søgaard-Andersen, *Pattern formation by a cell surface-associated morphogen in Myxococcus xanthus,* Proceedings of the National Academy of Sciences of the United States of America **99**, 2032 (2002).

[23] L. Søgaard-Andersen and D. Kaiser, *C factor, a cell-surface-associated intercellular signaling protein, stimulates the cytoplasmic frz signal transduction system in Myxococcus xanthus,* Proceedings of the National Academy of Sciences of the United States of America **93**, 2675 (1996).

[24] D. Kaiser and C. Crosby, *Cell movement and its coordination in swarms of Myxococcus xanthus,* Cell Motility and the Cytoskeleton **3**, 227 (1983).

[25] R. P. Burchard, *Trail following by gliding bacteria,* Journal of Bacteriology **152**, 495 (1982).

[26] K. Grimm, H. K. Galle, and H. H. Heunert, *Archangium violaceum (Myxobacteriales) - Bewegungsaktivität und Kolonieform,* Film E 1588, 0:20-0:35 (Institut für den Wissenschaftlichen Film, Göttingen, 1969).

[27] K. Grimm, H. K. Galle, and H. H. Heunert, *Archangium violaceum (Myxobacteriales) - Bewegungsaktivität und Kolonieform,* Film E 1588, 1:45-1:55 (Institut für den Wissenschaftlichen Film, Göttingen, 1969).

[28] P. L. Grilione and J. Pangborn, *Scanning electron microscopy of fruiting body formation by myxobacteria,* Journal of Bacteriology **124**, 1558 (1975).

[29] L. Jelsbak and L. Søgaard-Andersen, *The cell surface-associated intercellular C-signal induces behavioral changes in individual Myxococcus xanthus cells during fruiting body morphogenesis,* Proceedings of the National Academy of Sciences of the United States of America **96**, 5031 (1999).

[30] S. K. Kim and D. Kaiser, *Cell alignment required in differentiation of Myxococcus xanthus,* Science (New York, N.Y.) **249**, 926 (1990).

[31] P. D. Curtis, R. G. Taylor, R. D. Welch, and L. J. Shimkets, *Spatial organization of Myxococcus xanthus during fruiting body formation,* Journal of Bacteriology **189**, 9126 (2007).

[32] R. Welch and D. Kaiser, *Cell behavior in traveling wave patterns of myxobacteria,* Proceedings of the National Academy of Sciences of the United States of America **98**, 14907 (2001).

[33] C. W. Wolgemuth, *Force and flexibility of flailing myxobacteria,* Biophysical Journal **89**, 945 (2005).

6

THREE-DIMENSIONAL PATTERN FORMATION BY MODEL MYXOBACTERIA

6.1. INTRODUCTION

So far in the previous chapters we studied myxobacteria movement in a plane (i.e., two-dimensionally, 2D). Experimental data show that at the initial stages of fruiting body development, myxobacteria cells move as 2D sheets [1, 2], thus 2D simulations are adequate for that situation. However, the process of building a fruiting body does occur in space (i.e., three-dimensionally, 3D) [3], therefore 3D models are necessary to fully understand myxobacteria development. *Myxococcus xanthus*, for example, builds a simple mound of cells, whereas *Chondromyces* forms a complex tree-like structure with sporangioles (Figure 1.4 in Chapter 1). Furthermore, similarly shaped fruiting bodies in different species can form by different paths. In *Chondromyces*, an undifferentiated cell mass secretes a slime stalk, raises the cells upwards with subsequent formation of sporangioles. In *Stigmatella aurantiaca*, a similarly shaped fruiting body is built by a mass of cells forming a structure of the shape and size similar to the final fruiting body and only later the cells withdraw from the stalk and sporangioles mature [4].

In this chapter, the model presented in Chapter 2 is extended for a 3D case. We investigated how the three-dimensionality affects the results observed in the previous chapters in comparison with simpler 2D models. The challenges associated with 3D simulations of myxobacteria movement are also discussed.

6.2. MODEL

The basic model used to study myxobacteria movement in 3D is the same as in Chapter 2, with all vectors (e.g., positions, directions, velocities, forces) here being three-

dimensional. However, several model adaptations are needed for the 3D case. If a particle comes closer than $W/2$ to the substratum (defined by the $z = 0$ plane), the substratum reaction force has to be added to the particle, $\boldsymbol{F}_i^{\mathrm{r}} = -k^{\mathrm{r}}(r_{\mathrm{z}} - (1/2)W)\hat{\boldsymbol{z}}$, where r_{z} is the z-component of particle position $\boldsymbol{r}_i$, k^{r} is substratum reaction stiffness and $\hat{\boldsymbol{z}}$ is unit vector in the +z direction.

In 3D, in order to fully describe the direction of particle motion, one needs two vectors normal to the tangent $\hat{\boldsymbol{t}}_i$, normal $\hat{\boldsymbol{n}}_{1i}$ and binormal $\hat{\boldsymbol{n}}_{2i}$, resulting in three orthogonal vectors. We assume that a drag coefficient in any direction normal to $\hat{\boldsymbol{t}}_i$ is ζ^{n}. Therefore two vectors $\hat{\boldsymbol{n}}_{1i}$ and $\hat{\boldsymbol{n}}_{2i}$ can be chosen randomly, as long as $\hat{\boldsymbol{t}}_i$, $\hat{\boldsymbol{n}}_{1i}$ and $\hat{\boldsymbol{n}}_{2i}$ are orthogonal. Mechanical torsion of a cell is not considered in this model. The final (terminal) velocity is then

$$\begin{aligned}\boldsymbol{v}_i^{\mathrm{f}} = \boldsymbol{v}_i^{\mathrm{f,t}} + \boldsymbol{v}_i^{\mathrm{f,n1}} + \boldsymbol{v}_i^{\mathrm{f,n2}} &= \frac{1}{\zeta^{\mathrm{t}}}\boldsymbol{F}_i^{\mathrm{t}} + \frac{1}{\zeta^{\mathrm{n}}}\boldsymbol{F}_i^{\mathrm{n1}} + \frac{1}{\zeta^{\mathrm{n}}}\boldsymbol{F}_i^{\mathrm{n2}} \\ &= \frac{1}{\zeta^{\mathrm{t}}}(\hat{\boldsymbol{t}}_i \cdot \boldsymbol{F}_i)\hat{\boldsymbol{t}}_i + \frac{1}{\zeta^{\mathrm{n}}}(\hat{\boldsymbol{n}}_{1i} \cdot \boldsymbol{F}_i)\hat{\boldsymbol{n}}_{1i} + \frac{1}{\zeta^{\mathrm{n}}}(\hat{\boldsymbol{n}}_{2i} \cdot \boldsymbol{F}_i)\hat{\boldsymbol{n}}_{2i}\end{aligned}$$

Keeping bacteria in the biofilm. Special attention should be paid to the vertical movement of cells, so that bacteria will not detach from the substratum and the biofilm when propelled by their motility engine. As in previous chapters, it has been assumed here that the myxobacterial engine is distributed along the bacterial body. Since the mechanics of the myxobacterial engine is not well understood, it was considered that a cell is able to propel itself within the slime, i.e. the distributed engine force pushes against the slime to propel the bacterium forward. Theoretically estimated engine force (the value used in the simulations, 100 pN) is orders of magnitude larger than the gravity force acting on a bacterium (10^{-2} pN). As a result, a cell could easily travel upward if oriented vertically within the slime in the model. Therefore, one needs to restrict vertical movement of cells by assuming that biofilm height is finite. A particle that is identified as being outside the biofilm does not propel itself (i.e. the engine force is not added to it) and is subjected to constant downward force that is analogous to the surface tension force of the slime, $\boldsymbol{F}_i^{\mathrm{s}} = -k^{\mathrm{s}}(F^{\mathrm{e}}/N)\hat{\boldsymbol{z}}$, where F^{e}/N is the engine force per particle, and k^{s} is the scaling factor. This force brings the escaped particle closer to the substratum and therefore back in contact with the rest of the population.

A particle is considered to be located within the biofilm if it is in direct or indirect contact with the substratum. A particle is considered in direct contact with the substratum if $r_{\mathrm{z}} < (1/2)W + d_{\mathrm{e}}$. A particle is regarded as being in indirect contact with the substratum if one can trace a way from the particle to the substratum via direct contacts through other particles. Suppose a particle A_1 is in direct contact with particle A_2, the partice A_2 is in direct contact with a particle A_3, and the particle A_3 is in direct contact with the substratum. Then particle A_1 will be in indirect contact with the substratum.

There is no limit on the number of intermediate particles between the particle in question and the substratum, however, in any contact chain $\rightarrow \mathrm{A}_3 \rightarrow \mathrm{A}_2 \rightarrow \mathrm{A}_1 \rightarrow$ particles A_1 and A_3 belonging to the same bacterium must be separated by at least two other particles in the bacterium. This rule is introduced to avoid the situations where due to

two bacteria being in close side-by-side contact, a contact chain can form where every other particle belongs to the same bacterium. In this case, two bacteria in side-by-side contact would be able to move vertically away from the biofilm as long as one (end) particle is within the indirect contact with the substratum.

Since the contacts in the model are detected segment-wise (see Chapter 2), a direct contact between the particles is determined using the following criteria. Suppose that the smallest distance between two segments $\boldsymbol{Q}_{ij}$ and $\boldsymbol{Q}_{kl}$ (that are eligible for collision detection) is smaller than $W + d_e$ (i.e. separation between cell boundaries determined by the collision distance is smaller than d_e). Then, if P_1 and P_2 are both between 0 and 1, then both particles of segment $\boldsymbol{Q}_{ij}$ are considered in direct contact with both particles of segment $\boldsymbol{Q}_{kl}$, i.e. particles i and $i+1$ are in direct contact with particles k and $k+1$. If for any segment $P = 0$, only particle i (or k) is in direct contact with the particles of the other segment, whereas if $P = 1$, only particle $i+1$ (or $k+1$) is in direct contact with the particles of the other segment.

The parameters used in the simulations are the same as in the previous chapters (see Table 2.1 in Chapter 2). Additional parameters for 3D simulations are the substratum reaction force constant $k^r = k^c$, the scaling factor for pseudo-surface tension force $k^s = 20$, maximum cell separation distance $d_e = 0.05\,\mu$m. Cell speed, population alignment, clustering and cluster stability were computed as in Chapter 4. Random high-density initial configuration of 3D population was obtained by placing the bacteria above the substratum with random 3D orientations and allowing them to be pushed towards the substratum due to pseudo surface tension force. Cell bending stiffness referred to as "very rigid", "rigid", "flexible" and "very flexible" are defined in Chapter 4.

6.3. RESULTS

Simulations have shown that model myxobacteria population dynamics in 3D have both similarities and differences compared with the 2D situation.

Cell alignment, clustering and speed. The alignment of a low-density 3D population of reversing cells has essentially the same dependency on bending stiffness as in 2D, as found in Chapters 2 and 3. Population alignment first increases as cell bending stiffness increases, and then slightly decreases for very rigid cells (Figure 6.1A). However, 3D populations show slightly better alignment than 2D populations for large cell bending stiffness values. Interestingly, the improved alignment is not the result of a better orientational stability of cells or improved cell alignment during two cell collisions in 3D, because for large bending stiffness values, the orientational stability and alignment in two-cell collision simulations are almost the same for 2D and 3D cases (Figure 6.1C and D). As similarly found for lateral restriction studied in Chapter 3, population alignment is well correlated with the orientational stability of cells during two-cell collisions in either 2D or 3D simulations. As the orientational stability increases due to increasing bending stiffness, the population alignment increases; for cells with orientational stability too large (very rigid cells), the population alignment drops (in other words, there is an optimum stiffness for alignment) (Figure 6.1B). However, the same orientational stability

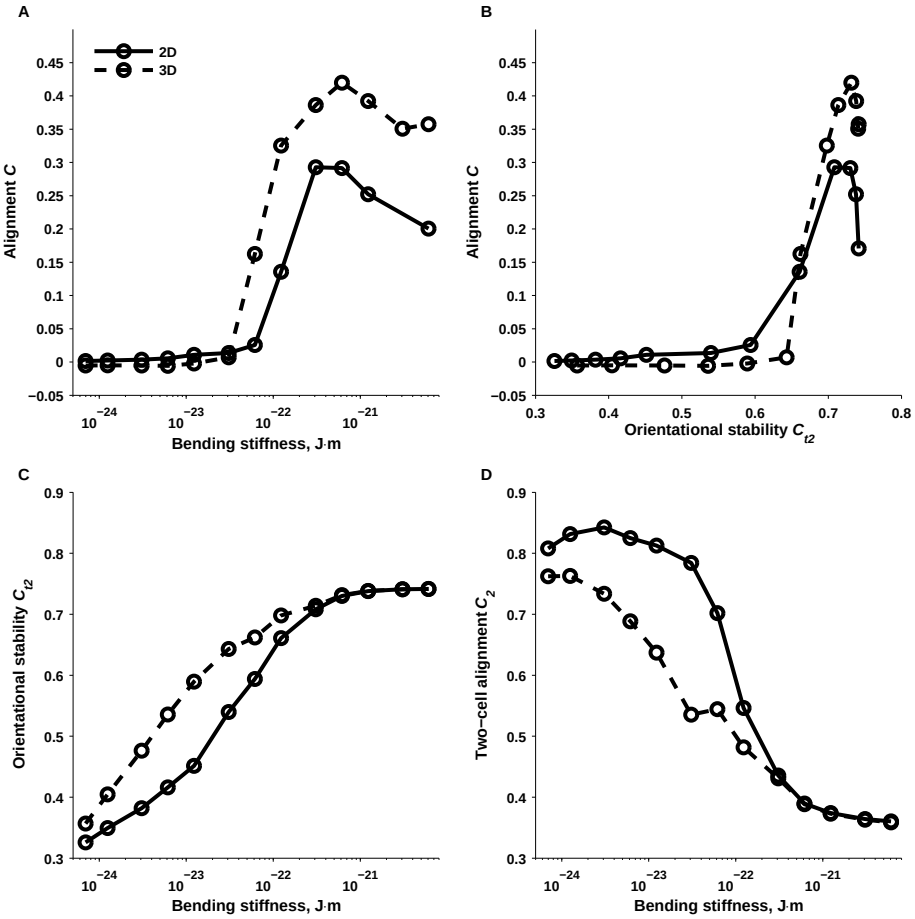

Figure 6.1: Cell alignment and orientational stability compared in 2D and 3D simulations. (A) Alignment of reversing cells. (B) Population alignment as a function of orientational stability of cells in two cell collision simulations. (C) Orientational stability in two cell collision simulations as a function of cell bending stiffness. (D) Cell alignment in two cell collision simulations as a function of cell bending stiffness.

values in 2D and 3D simulations can have a large difference in population alignment, further supporting the idea of Chapter 3 that orientational stability during two cell collisions is not the only factor affecting the population alignment in general, and that the improved alignment of 3D rigid cell populations might also be related to the outcome of the collisions of multiple cells in cell groups.

Similar orientational stability and cell alignment values during two rigid cell collisions for 2D and 3D cases (Figure 6.1C and D) also suggests that 3D rigid cell collision with cells initiated on the planar substratum proceeds in essentially the same way as the 2D collision. The 3D cells tend to remain on the substratum and not to move upwards during the collision, due to the downward pseudo surface tension force introduced in

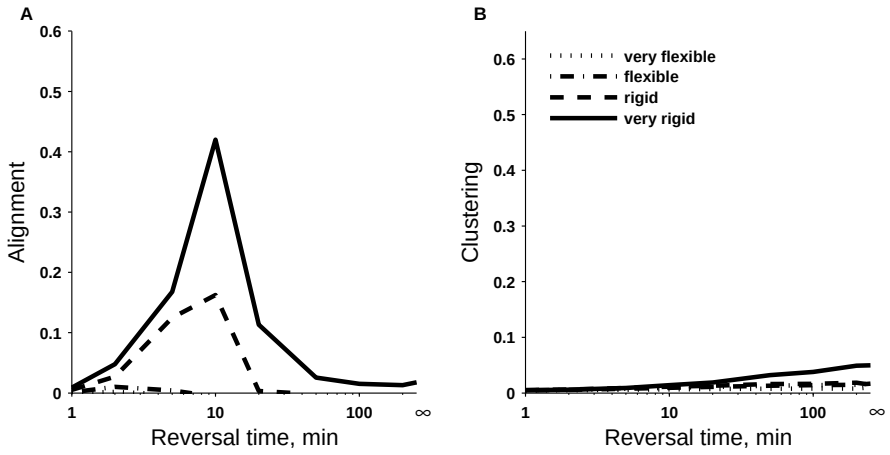

Figure 6.2: Alignment (A) and clustering (B) in a low-density 3D population as a function of reversal time.

the model. If, upon collision, the leading particle of a rigid cell is moving upwards, due to high cell rigidity other particles located in the middle part of a cell will be raised upwards too, thus losing contact with the substratum. As a result, a downwards pseudo surface tension force will be introduced that would oppose the movement of the whole cell upwards and return it back in contact with the substratum. The leading particle of a flexible cell, on the other hand, could move on top of another cell without other particles in the cell losing contact with the substratum. Therefore, a rigid cell in the model has a tendency to remain on the substratum until the forces pushing it upwards would counteract the surface tension force, a situation possible in multiple cell collisions within large clusters.

Comparably with the 2D simulations presented in Figure 4.4 of Chapter 4, a 3D population shows optimal alignment time for reversal times around the value of 10 min (Figure 6.2A). However, in contrast with 2D, a 3D population shows poor clustering for all reversal time values (Figure 6.2B). This can be explained by the fact that in clusters, stresses by surrounding cells can cause cells to rise on top of other cells and escape the cluster (Movie 6.1), a situation impossible in 2D. In dense 3D populations, due to this extra degree of freedom, the population is much less crowded than the 2D population and the speed of cells is almost independent of the bending stiffness or collision stiffness values (Figure 6.3A and B, compare to Figure 4.2 in Chapter 4). Similarly, population alignment and clustering are less dependent on contact stiffness value than in the 2D case (Figure 6.3C-F). One has to note, that although the clustering values are quite large for rigid and very rigid cells, the clusters are very short-lived for all contact stiffness values (Figure 6.3E-H, Movie 6.1).

Aggregates in population of guided cells. Remarkably, in simulations of low-density 3D populations of actively guided cells (case b, $F^{g}_{max} = 200\,pN$, see Methods of Chapter 5),

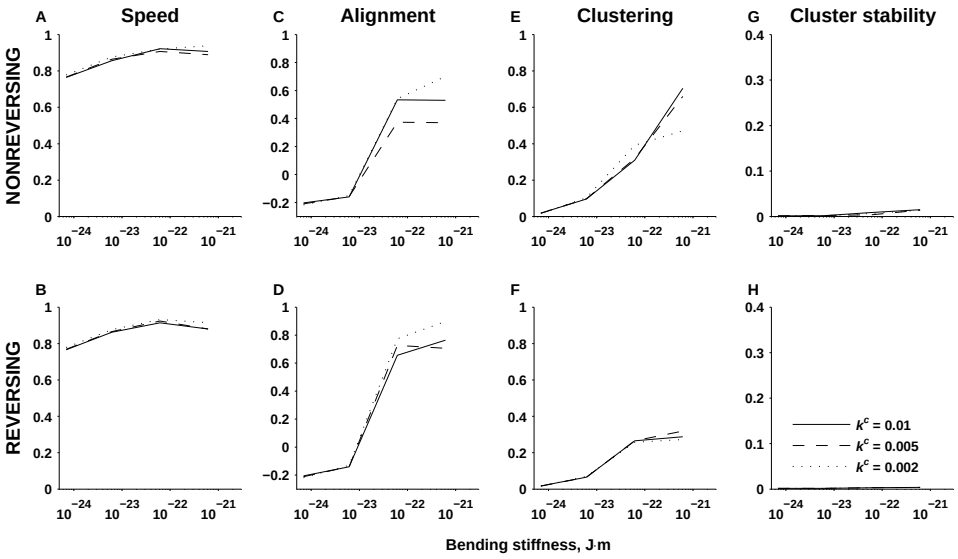

Figure 6.3: Speed of cells, alignment, clustering and cluster stability in high-density 3D populations as a function of cell bending stiffness.

stable circular aggregates do not form as in 2D (Figure 5.1 in Chapter 5). Very flexible and flexible cells form streams and exhibit swirling motion, but nascent circular aggregates are unstable and quickly dissipate (Movie 6.2 and 6.3). It appears that cells are able to escape the nascent circular aggregates by moving upwards and leaving the aggregate over its top, whereas in 2D the cells in the centre of the circular formation are trapped.

If cells are initially arranged in a spiral aggregate on a planar substratum (Figure 6.4A), the aggregate does not remain stable for any value of cell bending stiffness. This is in contrast to the 2D case, where the initial spiral aggregate of rigid and very rigid cells retained its shape during the whole simulation (Movies S16 and S17 in Chapter 5). In 3D, the cells leave the center of the aggregate (where the they are exposed to large stresses) by moving on top of it, coalesce into spiral streams and transform the aggregate into one or more rings of cells (hollow aggregates) that usually later dissipate (Figure 6.4B-F, Movie 6.4-6.7). Only the hollow aggregate formed by very rigid cells was stable for the duration of the simulation (Movie 6.4). Interestingly, during the formation of the hollow aggregate, flexible and very flexible cells formed temporary mounds of cells in the center of the initial aggregate (Figure 6.4C-D, Movie 6.6 and 6.7). Rings and mounds formed at places of large local cell density; as cells leave the central location, the formed structures disintegrate and do not form again. Interestingly, in case of full head-to-tail adhesion (case a in Chapter 4), neither rings of cells nor mounds form, but the spiral aggregate slowly disperses. The reasons for this are not understood, but may be related to overall

slower movement of cells compared to active following (see Chapter 4).

A five-fold increase of guidance force to $F^{g}_{max} = 1000\,pN$ (active following, case b, Chapter 5) did not make aggregates more stable, although the mounds formed by flexible and very flexible cells were larger (Movie 6.8-6.11). Cell aggregates splitting into two smaller formations were also observed (Movie 6.11, $t = 2\,h$). One has to note though, that at these magnitudes of guiding forces, cells in the simulations reach speeds up to an order of magnitude larger than equilibrium speed v_b, and this is biologically unrealistic. Nevertheless, these results suggest that the aggregates, rings and mounds in this model are unstable not due to insufficiently small guidance force sizes, but because of some other factors, possibly too low population density. It appears that the number of cells leaving the mounds is larger than the number of entering cells and therefore aggregates disperse.

Aggregates in high-density populations. Large density 3D populations with initially randomly distributed cells were also simulated. In the case of very flexible and flexible cells, dynamic mounds are continuously formed and dispersed (Figure 6.5 and Figure 6.6, Movie 6.12 and S13). Cells in mounds appear to move circularly or spirally. Interestingly, dynamic mounds keep forming throughout the duration of the simulation of very flexible cells (Figure 6.5, Movie 6.12), whereas flexible cells eventually form rope-like streams, with cells rotating spirally around the long axis of the stream (Figure 6.6, Movie 6.13). The formation of one stable stream is probably facilitated by the relatively small computational domain size. Since at low population densities dynamic mounds do not form, these results suggest that cell density might be a crucial factor in mound formation in this model. One can observe streams of cells come into and leave the dynamic mound, with cells in streams appearing to move spirally along the axis of the stream (Figure 6.6 at 40min and Movie 6.13).

6.4. DISCUSSION

In this chapter we studied how adding the third dimension to the bacterial movement affects the patterns created by myxobacteria populations and the results were compared with those obtained in the 2D simulations from the previous chapters.

Moving myxobacteria secrete slime and are enclosed in it to form a biofilm [5, 6]. Therefore, in contrast to 2D simulations, where cells move on a planar substratum, for 3D simulations it is necessary to take into account the biofilm boundary (its top surface) and contain the movement of cells within it. To achieve that, a set of rules were devised to introduce the effect of surface tension of the slime. According to these rules, whenever a cell loses contact with the substratum or with a group of cells that are in contact with the substratum, a force will push the cell downwards until such contact is re-established. This restricts vertical cell movement and does not allow cells “to float” in slime separately or in groups, without being connected to the substratum in some way.

The results show that the alignment of reversing, non-guided cells in 3D is essentially the same as in the 2D case, studied in Chapter 2. The alignment of rigid cells in 3D is slightly better than in 2D (Figure 6.1A). We have previously identified orientational stability of cells upon two-cell collisions as a factor affecting population alignment for

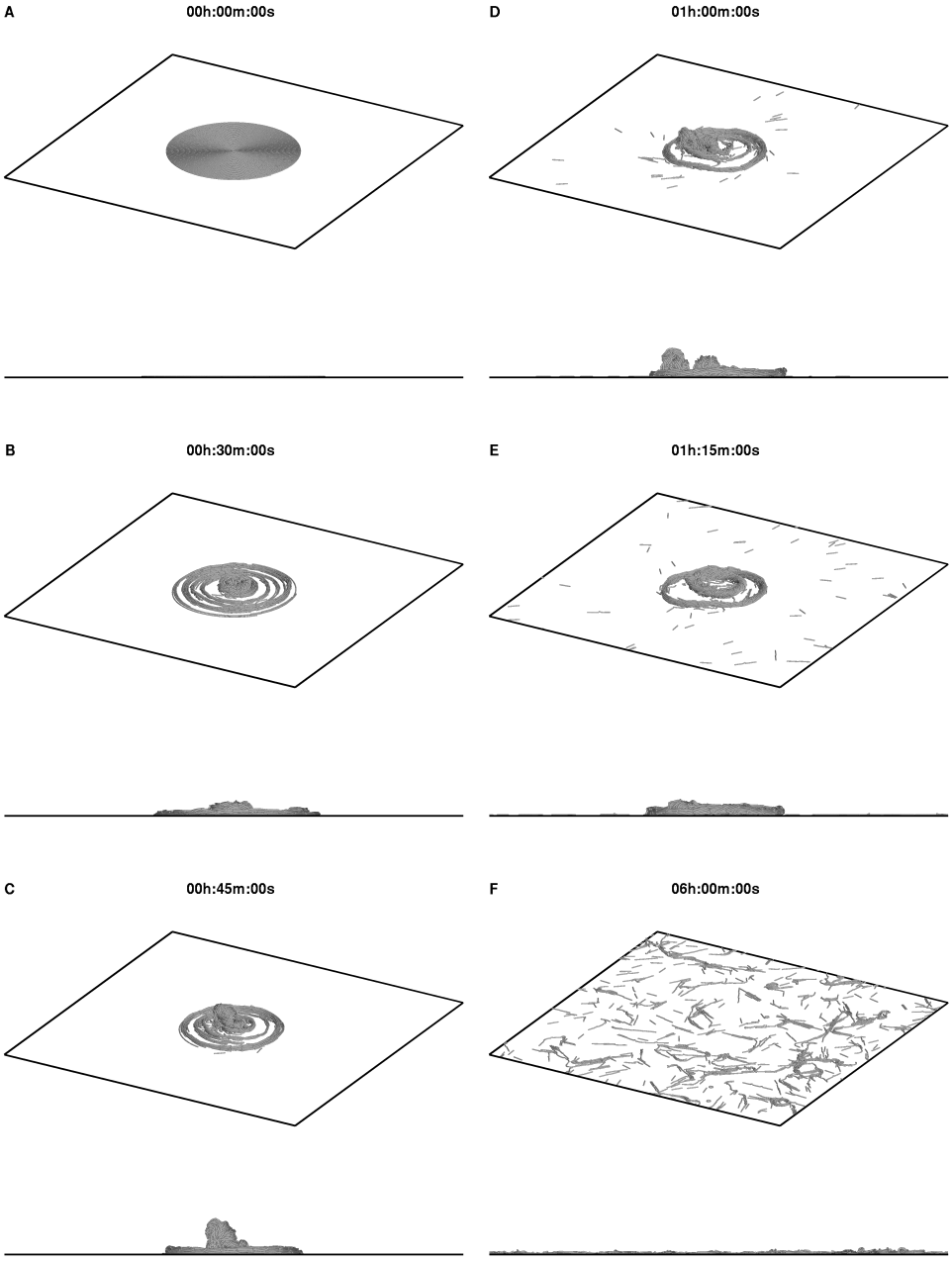

Figure 6.4: 3D population dynamics with initially spirally arranged very flexible cells with active following, $F^{g}_{\max} = 200\,\mathrm{pN}$. Perspective and front views of 3D population are shown.

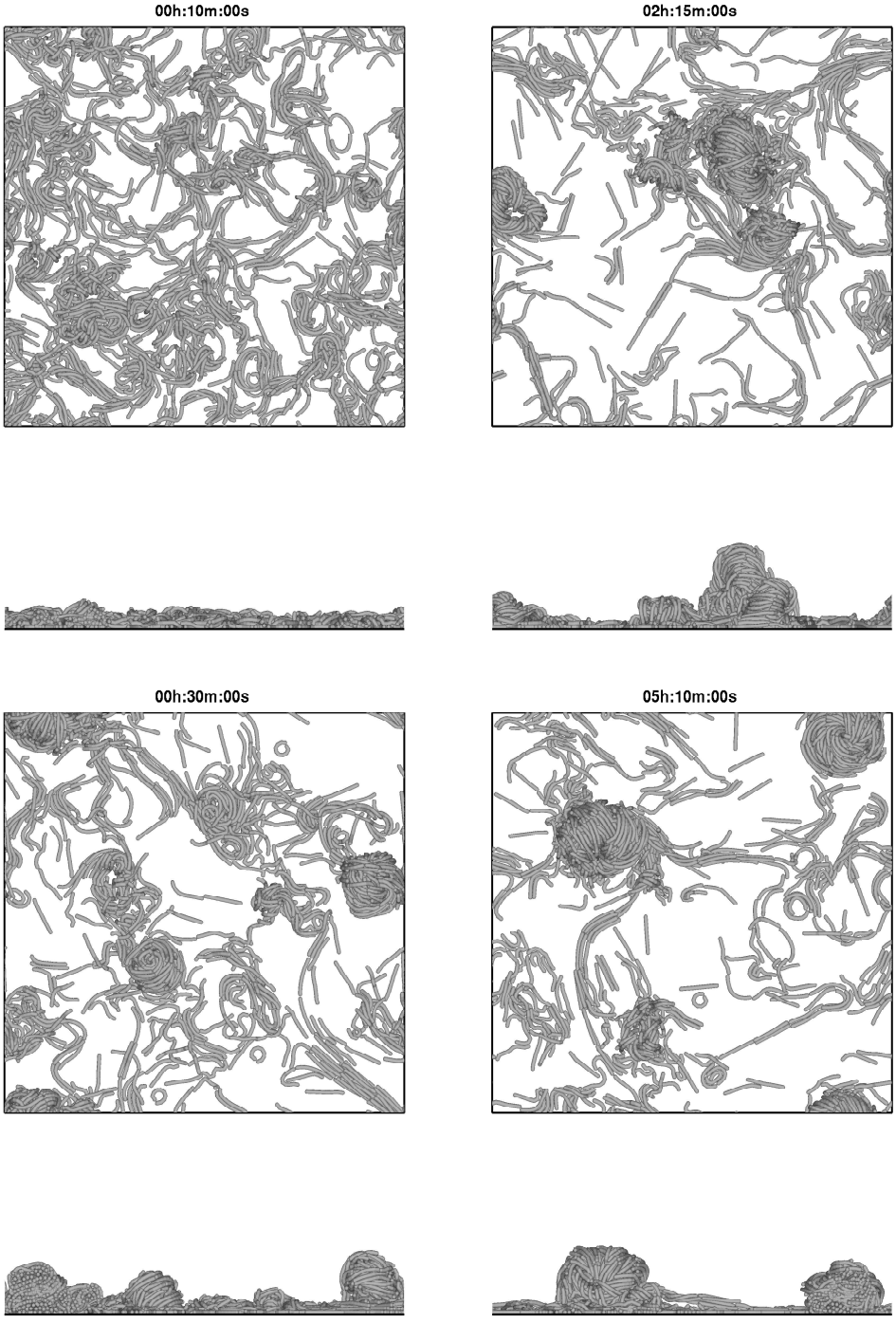

Figure 6.5: High density 3D population dynamics of initially randomly arranged very flexible cells with active following, $F^{g}_{max} = 200\,pN$.

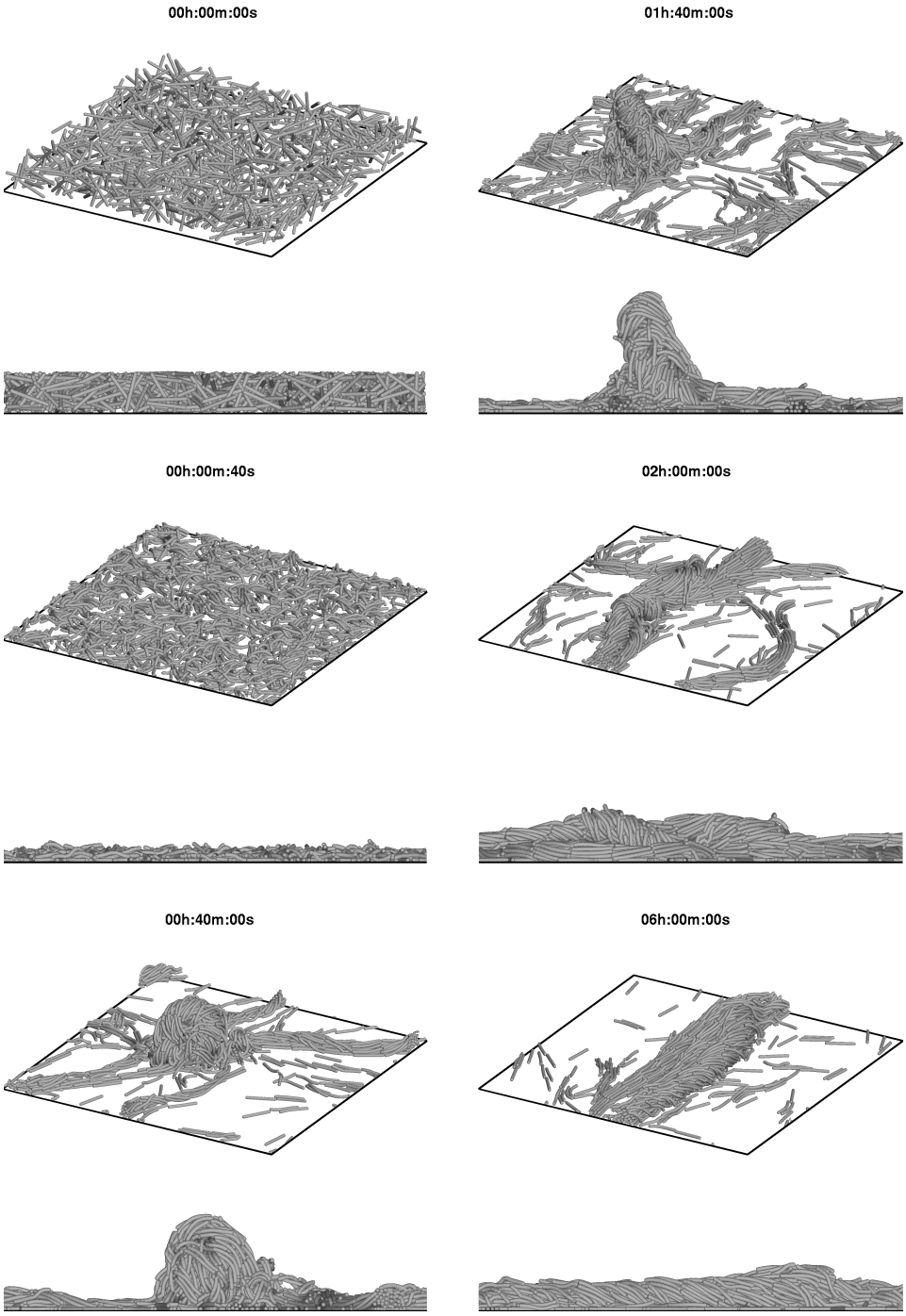

Figure 6.6: High density 3D population dynamics of initially randomly arranged flexible cells with active following, $F^{g}_{max} = 200\,pN$.

cells with different bending stiffness values (Chapter 2 and 3). However, although the population of rigid cells aligns better in 3D than in 2D, the orientational stability of rigid 3D cells in two-cell collision simulations are the same as in 2D. This suggests that other factors are responsible for the improved population alignment, possibly the way multiple cell collisions are resolved in the model. Similar situation was observed when cells with different lateral restriction forces were studied in Chapter 3. Further studies are necessary to fully understand how and why the population of reversing cells align in this model. Further, as in the 2D case, the 3D population aligns best with cell reversal time value around 10 min. However, cell clustering in 3D is dramatically worse than in 2D, because cells under stress inside the clusters are pushed upwards and are free to leave the cluster, a situation not possible in 2D simulations.

During the course of myxobacteria fruiting body development, a population of cells can form flat circular/spiral aggregates, and later in the development, spherical mounds [2, 7]. In Chapter 5 we showed that guiding interactions between the head and tail of two bacteria can result in the formation of stable circular aggregates in 2D. This study further demonstrates that in 3D, given a high cell density, guidance interactions between flexible cells (active cell following, see Chapter 4) can lead to the formation of spherical mounds, with cells inside these mounds moving circularly or spirally. The spherical mound with streams coming into and leaving it was observed in the simulations (Figure 6.6, Movie 6.13), as well as experimentally [8, 9]. Experimental observation also shows that cell aggregates in developing myxobacteria populations can be very dynamic; they can grow, disperse, split, join with other aggregates or stabilize and mature into a fruiting body [10]. Although the present model could explain the formation of spherical mounds, it cannot account for their stabilization. The mounds in the 3D model are very dynamic, unstable and always dissipate, in contrast to the 2D circular aggregates studied in Chapter 5. Since the 3D aggregates are also unstable when the guiding forces are increased 5-fold, the reason for such instability is unclear and could possibly be a not yet understood outcome of the assumptions of a 3D model. However, it was found that one important factor for mound formation in the model is cell density, because in low-density populations the mounds do not form at all. It has been shown that myxobacteria development requires high cell density populations [11]. It would be interesting to simulate even larger cell densities than those studied here (i.e. more cell layers) to investigate whether the aggregate stability will increase with increasing cell density. Furthermore, the results of this study and those of Chapter 5 suggest, that the transition between flat circular aggregate (2D) to spherical mound (3D) observed in experimental studies could occur when cells in a flat aggregate would acquire an extra degree of freedom of movement. For example, it could occur by loosening of the lateral adhesion of cells with the substratum or with other sheets of cells underneath, or, because mechanical stress in a planar aggregate becomes so large as to force cells to move out of the aggregate upwards. Our results suggest that experimental measurements of mechanical stress inside cell aggregates and forces of cell adhesion to substratum or between cells in different monolayers could further shed light on the process of morphogenesis in myxobacteria.

6.A. SUPPLEMENTARY MOVIES

Movie 6.1. Low density 3D population of non-guided, non-reversing very rigid cells.

Movie 6.2. Low density 3D population of actively guided (case b,$F^{\mathrm{g}}_{\mathrm{max}} = 200\,\mathrm{pN}$), non-reversing very flexible cells.

Movie 6.3. Low density 3D population of actively guided (case b, $F^{\mathrm{g}}_{\mathrm{max}} = 200\,\mathrm{pN}$), non-reversing flexible cells.

Movie 6.4. The population of very rigid, actively guided cells ($F^{\mathrm{g}}_{\mathrm{max}} = 200\,\mathrm{pN}$), initially spirally arranged.

Movie 6.5. The population of rigid, actively guided cells ($F^{\mathrm{g}}_{\mathrm{max}} = 200\,\mathrm{pN}$), initially spirally arranged.

Movie 6.6. The population of flexible, actively guided cells ($F^{\mathrm{g}}_{\mathrm{max}} = 200\,\mathrm{pN}$), initially spirally arranged.

Movie 6.7. The population of very flexible, actively guided cells ($F^{\mathrm{g}}_{\mathrm{max}} = 200\,\mathrm{pN}$), initially spirally arranged.

Movie 6.8. The population of very rigid, actively guided cells ($F^{\mathrm{g}}_{\mathrm{max}} = 1000\,\mathrm{pN}$), initially spirally arranged.

Movie 6.9. The population of rigid, actively guided cells ($F^{\mathrm{g}}_{\mathrm{max}} = 1000\,\mathrm{pN}$), initially spirally arranged.

Movie 6.10. The population of flexible, actively guided cells ($F^{\mathrm{g}}_{\mathrm{max}} = 1000\,\mathrm{pN}$), initially spirally arranged.

Movie 6.11. The population of very flexible, actively guided cells ($F^{\mathrm{g}}_{\mathrm{max}} = 1000\,\mathrm{pN}$), initially spirally arranged.

Movie 6.12. The high-density 3D population of actively guided very flexible cells ($F^{\mathrm{g}}_{\mathrm{max}} = 200\,\mathrm{pN}$).

Movie 6.13. The high-density 3D population of actively guided flexible cells ($F^{\mathrm{g}}_{\mathrm{max}} = 200\,\mathrm{pN}$).

REFERENCES

[1] P. D. Curtis, R. G. Taylor, R. D. Welch, and L. J. Shimkets, *Spatial organization of Myxococcus xanthus during fruiting body formation,* Journal of Bacteriology **189**,

9126 (2007).

[2] K. A. O'Connor and D. R. Zusman, *Patterns of cellular interactions during fruiting-body formation in Myxococcus xanthus,* Journal of Bacteriology **171**, 6013 (1989).

[3] H. Reichenbach, H. H. Heunert, and H. Kuczka, *Schwarmentwicklung und Morphogenese bei Myxobakterien - Archangium, Myxococcus, Chondrococcus, Chondromyces*, Film C 893, 14:55-17:35 (Institut für den Wissenschaftlichen Film, Göttingen, 1965).

[4] L. J. Shimkets, M. Dworkin, and H. Reichenbach, *The myxobacteria,* in *The Prokaryotes*, vol. 7, edited by M. Dworkin, S. Falkow, E. Rosenberg, K. H. Schleifer, and E. Stackebrandt (Springer, New York, 2006) pp. 31–115.

[5] P. L. Grilione and J. Pangborn, *Scanning electron microscopy of fruiting body formation by myxobacteria,* Journal of Bacteriology **124**, 1558 (1975).

[6] J. R. Lampky, *Ultrastructure of polyangium cellulosum,* Journal of Bacteriology **126**, 1278 (1976).

[7] G. M. Vasquez, F. Qualls, and D. White, *Morphogenesis of Stigmatella aurantiaca fruiting bodies,* Journal of Bacteriology **163**, 515 (1985).

[8] L. Jelsbak and L. Søgaard-Andersen, *Cell behavior and cell-cell communication during fruiting body morphogenesis in Myxococcus xanthus,* Journal of Microbiological Methods **55**, 829 (2003).

[9] H. Reichenbach, H. H. Heunert, and H. Kuczka, *Schwarmentwicklung und Morphogenese bei Myxobakterien - Archangium, Myxococcus, Chondrococcus, Chondromyces*, Film C 893, 14:22-14:55 (Institut für den Wissenschaftlichen Film, Göttingen, 1965).

[10] C. Xie, H. Zhang, L. J. Shimkets, and O. A. Igoshin, *Statistical image analysis reveals features affecting fates of Myxococcus xanthus developmental aggregates,* Proceedings of the National Academy of Sciences **108**, 5915 (2011).

[11] L. J. Shimkets and M. Dworkin, *Excreted adenosine is a cell density signal for the initiation of fruiting body formation in Myxococcus xanthus,* Developmental Biology **84**, 51 (1981).

7

OUTLOOK

Fruiting body formation of myxobacteria is a fascinating and yet not well understood example of biological morphogenesis. One can ask the question, how much of myxobacterial development is determined by physical (mechanical) properties of cells, and how important is the role of biological (biochemical, genetical) regulation during the process. Often, in numerical modelling studies of myxobacteria, in addition to simple mechanical interactions between cells, many other assumptions are included, among these slime trail following by individual cells, orienting effects of cells due to S-motility system, custom collision resolution rules etc. [1, 2]. A large number of assumptions makes these models rather complex. Very complex models are a less reliable tool for understanding biological systems, because they often involve a larger number of assumptions whose accuracy can be questioned (i.e. larger uncertainty). For example, one can observe that at small cell population density, cells tend to follow slime trails laid down by other cells [3]. However, it is not known how slime trails could be established and persist in a very dense population, where a particular spot on the substratum is constantly being overrun by different cells. Modelling studies that introduce a large number of assumptions, in addition, often do not distinguish which factors are necessary for the observed phenomena, and which ones could be dispensed with, thus obscuring the understanding of the crucial components of the system.

The approach of this thesis was to reduce the number of model assumptions to a minimum that would still allow us to obtain valuable insights into organization of myxobacteria populations. The goal of the thesis was to formulate a biomechanical model for a population of myxobacteria cells as interacting flexible self-propelled rods and investigate how much of the observed phenomena in myxobacteria populations could be explained only by mechanical interactions between cells. In the proposed model, the dominant mechanical force is gliding cells pushing one another upon mechanical contact. Another type of mechanical interaction introduced in the model was guiding forces between cells, whereby cells would tend to follow lagging poles (“tails”) of other cells

(Chapter 5). Reversal of cell movement was also studied as a mechanical property of a single moving cell (Chapter 4). Further, mechanical cell interaction with the environment was included: lateral restriction (e.g. due to interaction with substratum or slime, Chapter 3) and pseudo-surface tension force in 3D models due to biofilm boundary (Chapter 6).

This study shows that some of the experimentally observed formation of patterns and structures in myxobacteria populations during development could be accounted for with a rather simple set of mechanical interactions between cells. The most important results of the numerical model for myxobaterial populations developed in this thesis are summarized here:

- Global population *alignment* was observed in a population of reversing rigid cells. Cell flexibility impaired the alignment.
- Population *alignment* for flexible cells could be improved by lateral restriction of cells, e.g. by the contact with the substratum.
- Cell *clustering* was observed in a population of non-reversing cells.
- Cell reversal frequency was a major determinant of a population movement pattern (*alignment vs. clustering*). An optimal reversal time for global population *alignment* was found.
- *Stable streams* can arise by mechanical sorting of non-reversing cells with soft contacts in a dense population.
- *Unstable (temporary) swirls* can arise in dense populations of non-reversing rigid cells.
- *Stable streams and circular aggregates* arose in a 2D population with guiding forces between cells.
- *Stable streams and unstable mounds* of cells arose in 3D simulations of cells with guiding forces between cells.

Demonstrating that certain patterns and structures could be explained by a set of assumptions does not necessarily mean that these mechanisms are responsible for the observed phenomena in reality. However, modelling studies offer concrete ideas for experimental investigation to gather evidence in favour or against the proposed mechanisms. Furthermore, a number of experimental observations could not be accounted for in the current model (for example, the formation of complex *Chondromyces* tree-like fruiting body). Some of the obtained simulation results contradict the experimental data, for example, cluster sizes at the edge of swarms of reversing and non-reversing cells (Chapter 4), or stabilisation of 3D mounds was not obtained in the simulations (Chapter 6). Demonstrating that some phenomena cannot be explained by a set of assumptions using a wide range of parameter values suggests that the assumptions made in the model are incomplete and that additional mechanisms might be in place. Thus,

modelling studies emphasize what *can* and what *cannot* be explained by a certain set of assumptions, and help to direct future modelling research to focus on the factors that could explain the deviation between experimental observations and simulation results.

A number of follow-up studies would be interesting for future research.

- The findings of Chapter 4 that non-reversing cells in dense populations are more organized and thus move with higher speed are opposite to the results of Monte-Carlo simulations performed by Wu et. al [2], showing that non-reversing cells tend to form traffic jams and stall. To understand this difference, it could be useful to perform simulations with exactly the same conditions (population density, initial configuration etc.) as in Wu *et al.* [2] in order to have a more direct comparison of the results.

- Include more accurate *motility engine mechanics*. Currently, the model assumes that distributed engine pushes against slime and does not impact cells in the neighbourhood. Recent studies [4] show that A motility engine can transport beads on the surface of cells, suggesting that when cells are in contact, a motility engine of one cell could potentially push against neighbouring cells. Such additional mechanical interactions between cells would make cell movement dynamics more complex.

- Include *lateral adhesion* between cells and between cells and substratum. One can observe cell behaviour that would be consistent with adhesion between cells in experimental films [5]. In order to model lateral adhesion one needs to devise realistic rules of how the attraction force would work between two arbitrary line segments. In head-to-tail adhesion (Chapter 5), a "tail" of one bacterium and a "head" of another bacterium are involved, and one needs to represent attraction only between two points. A reverse collision response algorithm works fine for this purpose. However, for two line segments, one might need to introduce the attraction force not between the points that are located within the shortest distance on two line segments, but between the points located within the longest distance, but still within the critical adhesion distance. Including lateral adhesion forces, in addition to other phenomena, could possibly explain alignment of very flexible cells without the need of lateral restriction.

- Find a way to model a *biofilm boundary effect* in 3D simulations more realistically. Currently, the top biofilm boundary effect is simulated by introducing a pseudo-surface tension force if a cell detaches from the bulk of the population. It would be interesting to explicitly include slime in the model and track its configuration (as in Alpkvist *et al.* [6]). It would allow to introduce a more realistic slime surface tension force in the model and can potentially result in better understanding of 3D phenomena observed during the building of myxobacterial fruiting bodies.

- Include *cell division*. Starving myxobacteria during the process of fruiting body formation do not divide. However, in vegetative swarms, cells feed, grow and divide. It would be interesting to investigate how division of cells would affect cell

movement patterns in swarms. Modelling cell division and growth would present a certain computational challenge, because one needs to deal with model cells comprising a variable number of particles. A more computationally efficient but less accurate way to simulate a growing cell could be to vary the rest length of the springs connecting the particles in the bacterium.

Mechanical interactions between cells are ubiquitous not only in myxobacteria, but also in other motile bacteria forming biofilms, e.g. an opportunistic pathogen *Pseudomonas aeruginosa* [7]. Mechanical interactions would also be present in a growing colony of non-motile bacteria, because growing cells would push one another. The modelling approach developed in this thesis lays the foundation for a generalized mechanical model of biofilm formation including variable microorganism morphology (for example, with a mixed microbial population of cocci, bacilli and filamentous organisms). One of the main challenges associated with such a model would be the experimental evaluation of the intra- and inter-cellular forces that such a mechanical model involves (e.g., motility, adhesion, stiffness, drag, etc.). Therefore, the model presented here could be a useful tool to understand and guide experimental research of a wide range of bacterial biofilms.

REFERENCES

[1] A. B. Holmes, S. Kalvala, and D. E. Whitworth, *Spatial simulations of myxobacterial development,* PLoS Computational Biology **6**, e1000686 (2010).

[2] Y. Wu, A. D. Kaiser, Y. Jiang, and M. S. Alber, *Periodic reversal of direction allows myxobacteria to swarm,* Proceedings of the National Academy of Sciences of the United States of America **106**, 1222 (2009).

[3] R. P. Burchard, *Trail following by gliding bacteria,* Journal of Bacteriology **152**, 495 (1982).

[4] M. Sun, M. Wartel, E. Cascales, J. W. Shaevitz, and T. Mignot, *Motor-driven intracellular transport powers bacterial gliding motility,* Proceedings of the National Academy of Sciences of the United States of America **108**, 7559 (2011).

[5] H. Kühlwein, B. Schlicke, H. K. Galle, and H. H. Heunert, *Polyangium fuscum (Myxobacteriales) - Cystenkeimung und Schwarmentwicklung,* Film E 1582, 2:40-3:10 (Institut für den Wissenschaftlichen Film, Göttingen, 1971).

[6] E. Alpkvist, C. Picioreanu, M. C. M. van Loosdrecht, and A. Heyden, *Three-dimensional biofilm model with individual cells and continuum EPS matrix,* Biotechnology and Bioengineering **94**, 961 (2006).

[7] K. Zhao, B. S. Tseng, B. Beckerman, F. Jin, M. L. Gibiansky, J. J. Harrison, E. Luijten, M. R. Parsek, and G. C. L. Wong, *Psl trails guide exploration and microcolony formation in Pseudomonas aeruginosa biofilms,* Nature **497**, 388 (2013).

SUMMARY

Myxobacteria are social bacteria that are remarkable for their complex life cycle. In vegetative state, when nutrients are available, myxobacteria cooperatively swarm on a solid surface and feed. When exposed to starvation conditions, myxobacteria exhibit multicellular morphogenesis: 10^5–10^6 cells aggregate to form a fruiting body. Due to their unique life cycle, myxobacteria often serve as relatively simple model organism to study multicellular development and morphogenesis. Myxobacteria cells glide on a substratum, periodically reversing direction and interact with surrounding cells of a swarm. During developmental process, myxobacteria cells often form various patterns: clusters of cells, domains of aligned cells, circular aggregates and streams of cells traveling into the aggregates. The goal of the thesis was to formulate a computationally efficient mechanical mass-spring model of a myxobacterium cell and study the importance of mechanical interactions between cells for the pattern formation in myxobacteria populations. In Chapter 2, a basic model was formulated and it was investigated how cell flexibility affects cell alignment in the population in two-dimensions. The model was formulated in terms of experimentally measurable mechanical parameters, such as engine force, bending stiffness, and drag coefficient. It was shown, that a population of rigid cells can align well due to mechanical interactions between cells, but that cell flexibility impedes the alignment. Theoretical estimations of cell flexibility suggest that myxobacteria cells could be too flexible for the population to align due to mechanical interactions. Therefore, in Chapter 3 lateral restriction of cell movement due to contact with the substratum was introduced in the model. It was shown that lateral restriction can increase the ability of a population of flexible cells to align. In Chapter 4 it was studied how reversal period of cells affects population movement patterns. The results indicate that short reversal period results in domains of aligned cells, whereas long reversal period produces cell clusters. Furthermore, the model reveals that in densely packed populations, non-reversing cells can sort themselves due to mechanical interactions to produce streams of cells that travel in the same direction. Chapter 5 introduces short-range guidance forces between the trailing pole of one myxobacterium and the leading pole of another and investigates the resulting patterns. It is shown that certain types of short-range guiding interactions can explain the formation of circular aggregates. In Chapter 6, the model is extended to three-dimensions and simulation outcome is compared with the results obtained in the previous chapters. The three-dimensional model shows that guiding interactions as in Chapter 5 can initiate the formation of unstable mounds. Finally, the thesis Outlook discusses a series of directions in which the current model can be extended to further understand the importance of mechanical interactions between gliding cells on the development of myxobacteria.

SAMENVATTING

COMPUTATIONELE MODELLERING VAN PATROONVORMING DOOR MYXOBACTERIA

Myxobacteria zijn sociale bacteriën die opmerkelijk zijn voor hun complexe levenscyclus. In de vegetatieve toestand, wanneer voedingsstoffen beschikbaar zijn, zwermen myxobacteria coöperatief op een vast substraat en voeden zich aldaar. Bij blootstelling aan een tekort aan voedingsstoffen, vertonen myxobacteria meercellige morfogenese: 10^5–10^6 cellen aggregeren tot één vruchtlichaam. Vanwege hun unieke levenscyclus dienen myxobacteria dikwijls als relatief eenvoudig modelorganisme om meercellige ontwikkeling en morfogenese te bestuderen. Myxobacteria cellen schuiven en glijden op een substraat, waarbij zij periodiek omkeren en interactie hebben met omliggende cellen van een zwerm. Tijdens het ontwikkelingsproces vormen de cellen van myxobacteria vaak verschillende patronen: clusters van cellen, domeinen van gerichte cellen, circulaire aggregaten en stromen van cellen, die de aggregaten in en uit gaan. Het doel van dit proefschrift is om een rekenkundig efficiënt mechanisch massa-veer model van een mycobacterium cel te formuleren en een studie te doen naar het belang van mechanische interacties tussen cellen voor de patroonvorming in myxobacteria populaties. In hoofdstuk 2, is een basismodel geformuleerd en wordt gerapporteerd over het onderzoek hoe flexibiliteit van cellen het uitlijnen van die cellen in een populatie beïnvloeden in twee dimensies. Het model werd geformuleerd in termen van experimenteel meetbare mechanische parameters, zoals de motorkracht, buigstijfheid , en weerstandscoëfficiënt. Er werd aangetoond dat een populatie van stijve cellen zich goed kan uitlijnen door mechanische interacties tussen cellen, maar dat cel flexibiliteit de uitlijning belemmert. Theoretische schattingen van cel flexibiliteit suggereren dat myxobacteria cellen te flexibel zouden kunnen worden voor de populatie om zich uit te lijnen als gevolg van mechanische interacties. Daarom is in hoofdstuk 3 laterale beperking van celbeweging via contact met het substraat in het model ingevoerd. Er werd aangetoond, dat zijdelingse beperking het vermogen tot uitlijnen van een populatie van flexibele cellen kan verhogen. In hoofdstuk 4 werd onderzocht hoe de omkeerperiode van cellen de bewegingspatronen van een populatie beïnvloedt. De resultaten geven aan dat een korte omkeerperiode gebieden van uitgelijnde cellen oplevert, terwijl een lange omkeerperiode cel clusters produceert. Bovendien brengt het model naar buiten dat in dicht gepakte populaties, niet-reversibele cellen zich kunnen sorteren door mechanische interacties, waardoor stromen van cellen worden geproduceerd die in dezelfde richting bewegen. Hoofdstuk 5 introduceert de korte afstand sturingskrachten tussen de staart van een myxobacterium en de voorste uiteinde van een ander en onderzoekt de resulterende patronen. Er wordt aangetoond dat bepaalde vormen van korte afstand sturingsinteracties de vorming van cirkelvormige aggregaten kunnen verklaren. In hoofdstuk 6 is het model uitgebreid tot drie dimensies en worden simulatie resultaten vergeleken met de

resultaten van de voorgaande hoofdstukken. Het driedimensionale model laat zien dat de sturingsinteracties van hoofdstuk 5 de vorming van instabiele ophopingen kunnen initiëren. Tenslotte, hoofdstuk 7 bediscussieert een aantal richtingen waarin het huidige model kan worden uitgebreid om inzicht in het belang van mechanische interacties te verkrijgen.

CURRICULUM VITÆ

Albertas JANULEVICIUS

20-09-1976	Born in Vilnius, Lithuania.
1983–1994	Vilnius 50th Secondary School
1994–1998	B.Sc. in biology (specialized in molecular biology and biophysics), Vilnius University, Lithuania
1999–2001	M.Sc. in biophysics, Vilnius University, Lithuania
2002–2004	NUFFIC (Netherlands organisation for international cooperation in higher education) Huygens scholarship, visiting scientist at Neurons and Networks Group, Netherlands Institute for Brain Research, Amsterdam, The Netherlands
2007–	PhD student at Delft University of Technology, Department of Biotechnology (promotor prof. dr. ir. M.C.M. van Loosdrecht, co-promotor dr. ir. C. Picioreanu)